

Computational Fluid Dynamic Model Prediction of Focused Ultrasound-Enhanced Glymphatic Clearance

A

Thesis

Presented to

the faculty of the School of Engineering and Applied Science

University of Virginia

in partial fulfillment
of the requirements for the degree

Master of Science

by

Ryan Gladwell

May 2025

APPROVAL SHEET

This
Thesis
is submitted in partial fulfillment of the requirements
for the degree of
Master of Science

Author: Ryan Gladwell

This Thesis has been read and approved by the examining committee:

Advisor: Richard Price

Advisor:

Committee Member: Christopher Highley

Committee Member: John Lukens

Committee Member: Richard Price

Committee Member:

Committee Member:

Committee Member:

Accepted for the School of Engineering and Applied Science:



Jennifer L. West, School of Engineering and Applied Science

May 2025

Abstract	4
Graphical Abstract	5
Introduction	6
The Glymphatic System	6
Focused Ultrasound	10
FUS for Enhanced Glymphatic Clearance	11
Modeling the Glymphatic System	13
Methods	14
Assumptions	15
Results	16
Base Design	16
Clearance of Centralized Soluble Tracer (NO FUS)	17
Clearance of Centralized Tracer with FUS BBBO Applied on the Arterial Side (PAS FUS)	23
Clearance of Centralized Tracer with FUS BBBO Applied on the Venous Side (PVS FUS)	29
Clearance of Centralized Tracer with FUS BBBO Applied on the Whole Model (Whole FUS)	35
Centralized Tracer Model Comparisons	41
Distributed Tracer Model	43
Distributed Amyloid- β Model	46
Distributed α -Synuclein Model	50
Distributed Tracer FUS Model	54
Distributed Amyloid- β FUS Model	58
Distributed α -Synuclein FUS Model	62
Distributed Solute Model Comparisons	66
Distributed Solute Model Flux Comparisons	69
Discussion	71
The Effects of FUS	71
Different Solute Distributions	72
Different Solutes	72
Model Novelty and Limitations	75
Future Directions	76
Conclusion	79
References	80

Abstract

Focused Ultrasound (FUS) is the concentration of acoustic energy into a small region to produce therapeutic bioeffects via thermal or mechanical energy delivery. This technology has demonstrated ameliorative potential for a myriad of pathologies, including metastatic cancers, neurological motor disorders, and neurodegenerative diseases. FUS-induced blood-brain barrier opening (BBBO) has been shown to enhance glymphatic drainage, the brain-specific waste clearance pathway, and therefore represents a promising strategy for addressing the accumulation of neurotoxic solutes that is characteristic of many neurodegenerative diseases like Alzheimer's. It may also represent a compelling strategy to accelerate brain tumor antigen draining to meninges, which could trigger T cell priming, activation, and immunological tumor control. Here, we set out to define the biotransport mechanisms by which FUS produces a therapeutic effect on glymphatic drainage by engineering a 3D finite element COMSOL model of a single penetrating arteriole-venule vascular unit in the brain. This computational model, which takes *in vivo* literature values as inputs and produces flux and flow profiles as outputs, has produced insights into glymphatic waste clearance and FUS BBBO-mediated effects in the brain. Specifically, FUS BBBO causes spatially diverse changes that enhance the glymphatic system by increasing both convective and diffusive flux. This model can be used to optimize FUS parameterization and can increase clinician confidence in this emerging therapeutic.

Graphical Abstract

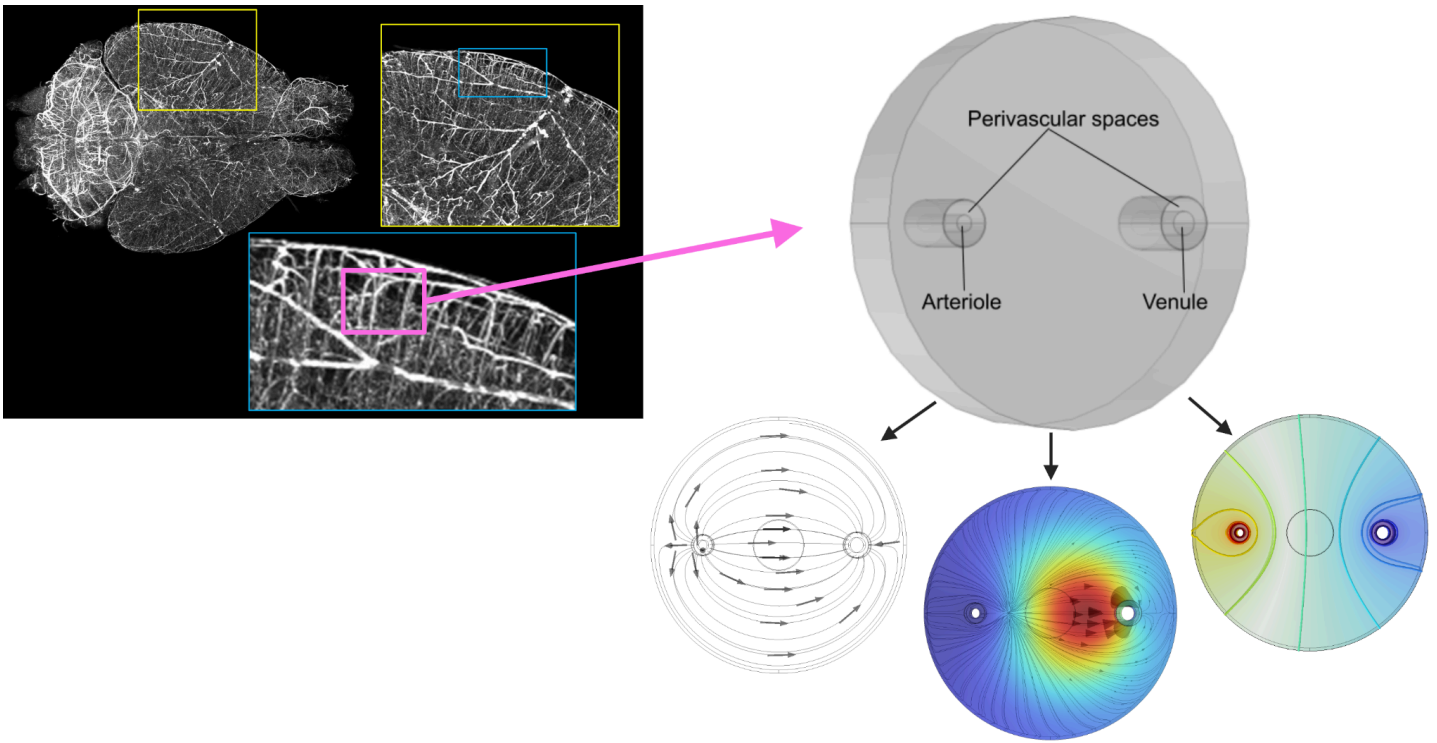


Figure 1. Graphical Abstract: *In vivo* parameter analysis enabled the creation of a computational model that can simulate flow velocity, concentration flux, and pressure gradients in the brain. Mouse brain microCT provided by the Wythe lab at the University of Virginia.

Introduction

The Glymphatic System

Any energetic cellular process generates by-products that, if not disposed of, can disrupt cellular, organ, and organismal homeostasis. Brain tissue is especially metabolically active. Consequently, the accumulation of pathological proteins is a hallmark etiology of many neurodegenerative disorders, such as the build-up of amyloid- β in Alzheimer's Disease (AD) or α -synuclein in Parkinson's Disease.

The brain is classically considered to be immune privileged.¹ Whereas the homeostasis of peripheral tissue is maintained via fluid and waste clearance performed by lymphatic vessels and circulating immune cells, the mammalian brain has internal systems of regulation that maintain the optimal environment.^{2,3} Two modalities accomplish this goal: active surveillance and phagocytosis by residential glial cells and passive maintenance through the glymphatic (glial-dependent lymphatic) system.

The glymphatic system differs from peripheral lymphatics in two main ways. First, the blood-brain barrier, a highly impermeable shield composed of epithelial and endothelial tight junctions, pericytes, and astrocytic endfeet, separates the vasculature and parenchyma. This barrier prevents the entry of potentially dangerous large molecules, facilitates endocytosis of essential nutrients, and mediates communication with the periphery. Second, no vessels in the brain uniquely function analogously to peripheral lymph vessels.⁴ Instead, the clearance of the large amount of neurotoxic waste generated by very metabolically active neural tissue depends on cerebrospinal fluid (CSF) flow through arterial perivascular spaces, into the parenchyma to mix with interstitial fluid and solutes, and back into venule perivascular spaces to drain out of the brain. Perivascular spaces, also known as Virchow-Robin spaces, are the periarterial (PAS), perivenous (PVS), and pericapillary spaces created by the gap between the astrocytic endfeet and the brain vasculature's endothelium. CSF flows through these spaces not only to clear waste, but also to supply glucose, lipids, and neuromodulators to the brain.^{5,6}

Indeed, CSF, a plasma ultrafiltrate, is critical for regulating many aspects of the brain environment, including buoyancy, nutrient distribution, and waste clearance. It is produced continuously in the choroid plexus, an epithelial-endothelial vascular convolute within the brain's ventricular system, at a rate of approximately 500 milliliters per day in humans.^{7,8} After production, CSF travels from the lateral ventricles to the third and fourth ventricles and arrives in the subarachnoid space and cisterns.⁹ It is from the subarachnoid spaces that CSF flows through perivascular spaces, following brain-penetrating arterioles and ascending venules (Fig 2).

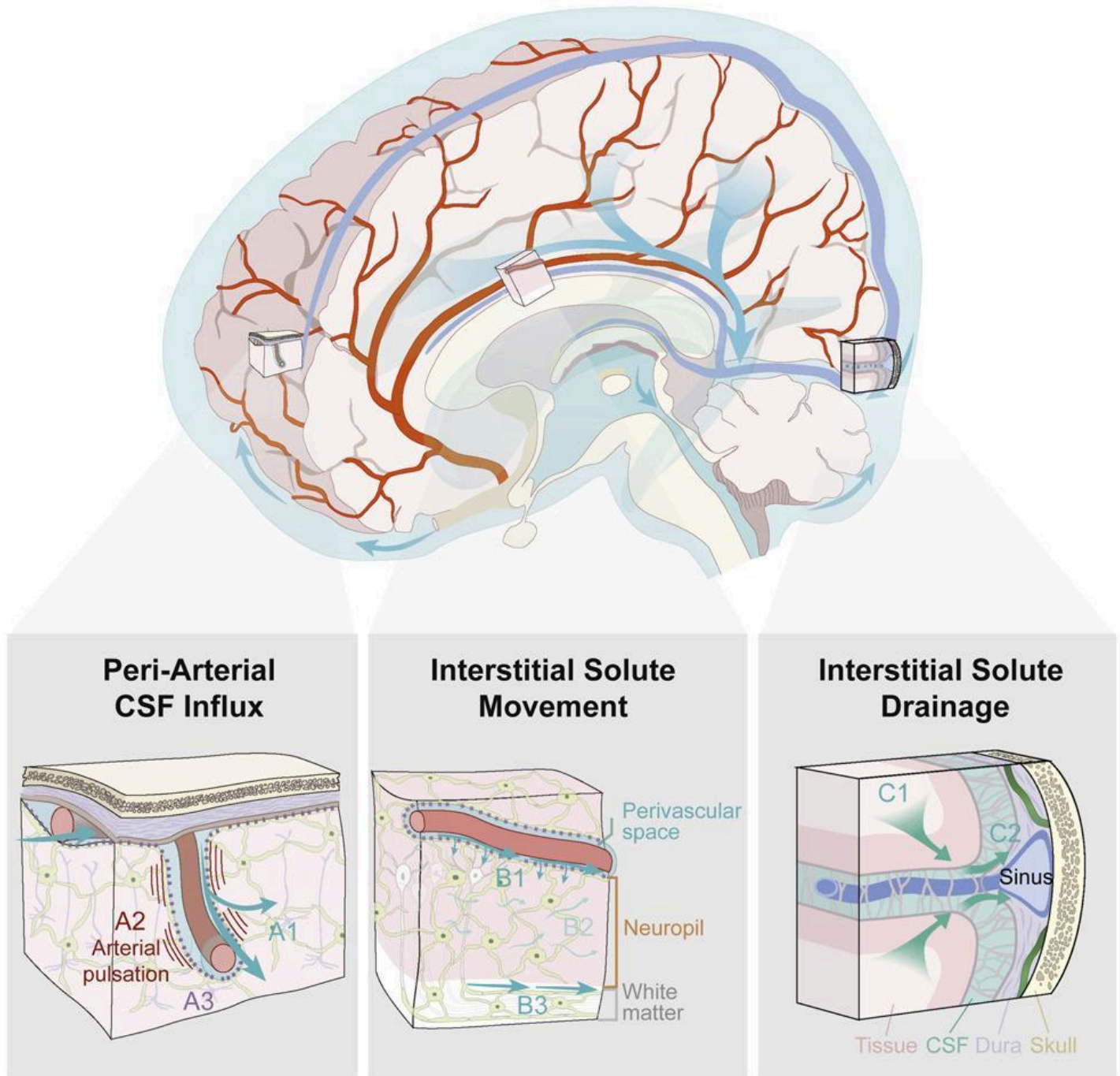


Figure 2. Flow of CSF through the brain. CSF exits the ventricular system and circulates the outer surface of the central nervous system. Then, CSF travels along perivascular spaces (A1) and, because of arterial pulsations (A2), enters the brain parenchyma (A3). Next, CSF influx from perivascular spaces (B1) mixes with interstitial fluid (ISF) and brain solutes in the neuropil (B2) and travels along the white matter (B3). Finally, this CSF-ISF mixture drains out of the parenchyma (C1) along perivenous spaces (C2) into lymphatic vessels in the dural sinuses.¹⁰ Figure acquired from “The glymphatic system: Current understanding and modeling”.⁴

While arterial pulsations from the cardiac cycle are dissipated by compliant vessels in the periphery to achieve nearly continuous blood flow, the rigidity of the skull contributes to a measurably pulsatile flow in the brain.

The hydrostatic pressure this pulse generates and the pressure gradients created by respiration and slow

vasomotion drive the CSF along the periarterial spaces and into the brain parenchyma. When CSF enters the neuropil, it mixes with interstitial fluid and cellular waste. This composite enters perivenous spaces, becoming increasingly concentrated with metabolic by-products as it effluxes to classical lymphatic vessels in the dura mater that recirculate CSF and process the extra fluid and waste. Aquaporin-4 (AQP4) water channels embedded in the astrocytic endfeet surrounding the brain vasculature facilitate this directional flow through the brain parenchyma. Figure 3 below, acquired from *Fluid Transport in the Brain*, illustrates the distinction between peripheral lymphatics and waste clearance in the brain.¹¹

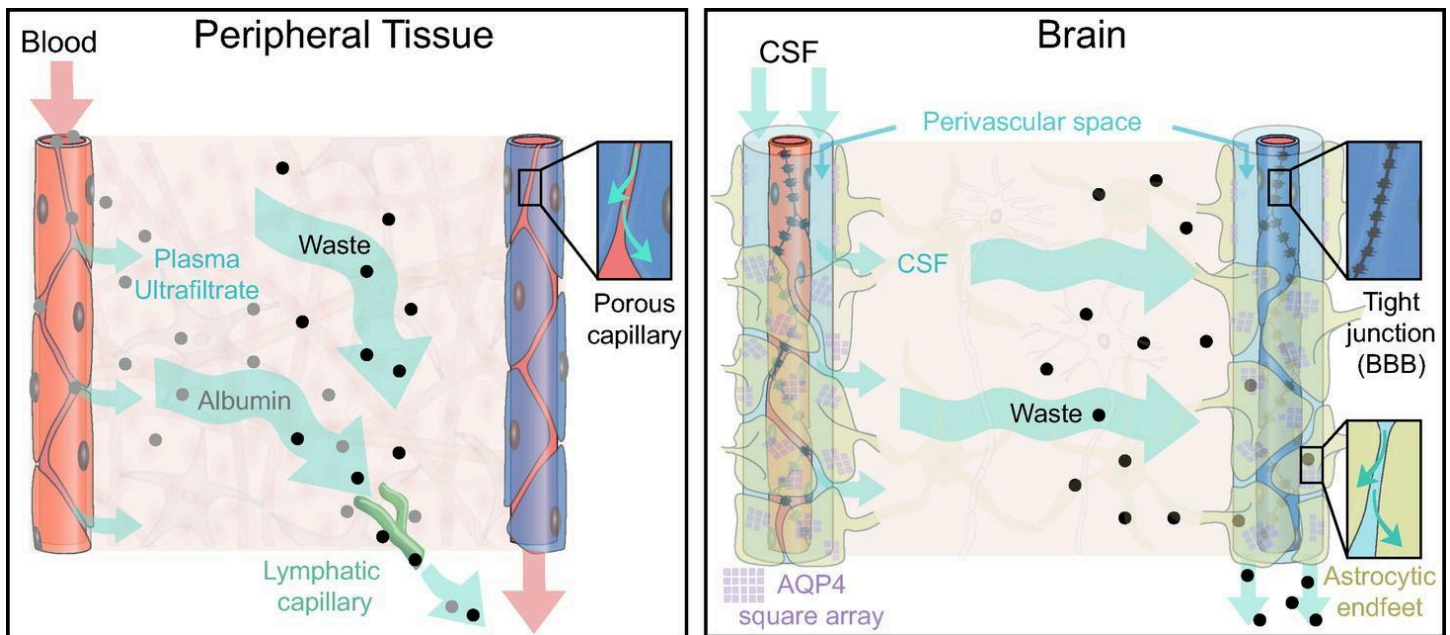


Figure 3. The distinction between classical lymphatic waste clearance in the peripheral tissue versus the brain.

Glymphatic waste clearance is hypothesized to be primarily active during sleep.¹² During this period, the brain behaves fundamentally differently than the awake state. Experimental evidence in various mammalian models, including humans, has shown that sleep increases flow through the perivascular spaces, interstitial space, and brain parenchyma. Thus, the long unanswered question of the biological basis for sleep has enhanced glymphatic waste clearance as a compelling explanation. This idea is supported by the fact that the need for sleep and the existence of glymphatic anatomical structures are both evolutionarily conserved, with continuity between rodents, pigs, non-human primates, and humans. In line with this thinking, it has been demonstrated that dementia is strongly associated with sleep disruption and that essentially all neurodegenerative disorders

arise from the accumulation of cellular waste products in the brain.^{13,14} Altogether, current research strongly supports the idea that sleep facilitates glymphatic clearance, thereby preventing neurodegeneration and maintaining brain homeostasis. Understanding sleep as an important biological regulator of waste clearance can help researchers develop therapeutics that harness similar mechanisms to restore malfunctioning glymphatics.

Focused Ultrasound

FUS is a therapeutic technology with a wide range of applications. By delivering focused acoustic pressure waves to a specific tissue region, FUS can produce mechanical or thermal bioeffects. These include opening the blood-brain barrier, ablating tumors, modulating neuronal activity, promoting macromolecule uptake in cells, enhancing targeted drug or gene delivery, or modifying a tissue's physical characteristics.^{15,16} With the ability to produce such a range of effects, FUS has produced promising results in treating various ailments, such as metastatic disease, cerebral cavernous malformations (CCMs), AD, and essential tremor.^{15,17,18} Some of these effects are shown in Figure 4 below.

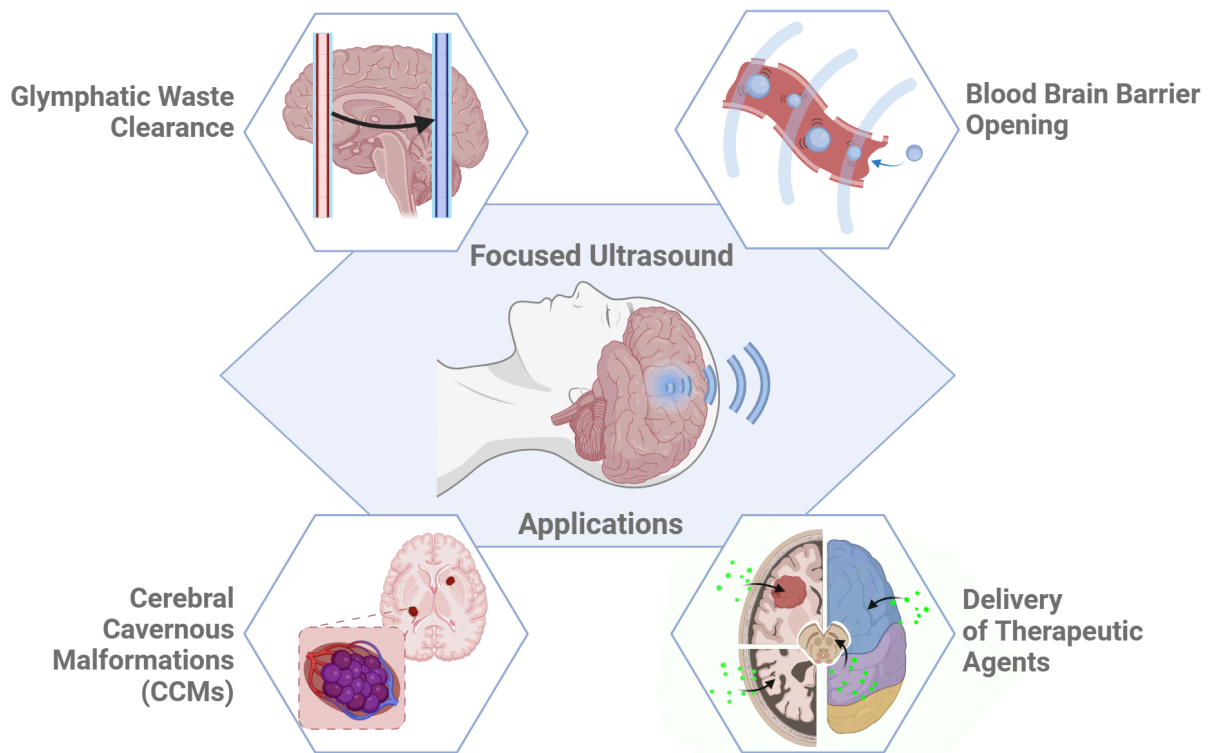


Figure 4. Applications of Focused Ultrasound. Figure adapted from Gorick et al. (2022)¹⁵

Perhaps the most exciting of the effects elicited by FUS is transient blood-brain barrier opening (BBBO). FUS, being a pressure wave, can induce volumetric changes in gases. When FUS is used to sonicate intravenously delivered microbubbles (MBs), the bubbles will cavitate, or undergo cycles of compression and rarefaction, due to the inverse relationship between the pressure of the sinusoidal FUS wave and the MB volume.^{15,19} With proper FUS parameters, the expanding and contracting MBs can exert mechanical stress on surrounding vasculature. At low acoustic pressures, this volume oscillation is consistent and known as stable cavitation. At higher acoustic pressures, the volumetric oscillations increase in magnitude and can lead to MB collapse. This event is known as inertial cavitation and can damage the surrounding environment. In the brain, either form of cavitation can cause BBBO, but inertial cavitation can potentially damage neuronal tissue despite creating a larger opening in brain vessels.^{15,20,21} Still, for some clinical applications, the risk is worth allowing larger therapeutics to enter the brain.

The BBB often hinders attempts at treating serious or fatal neurological issues like glioblastoma or AD by blocking the entry of drug or gene therapies. FUS BBBO has incredible promise as a therapeutic strategy because it can temporarily disrupt the BBB, which tightly controls the bidirectional flow across the brain vasculature. The brain, being the most vascularized organ in the body and the most difficult to deliver therapeutics over ~500 kDa to, would benefit immensely from a technology that could selectively and non-invasively permeabilize its vasculature.²² FUS achieves non-invasive, safe, targeted, and repeatable BBBO in a transient manner that tends to heal within 24 hours. For this reason, there has been a myriad of preclinical and clinical studies investigating FUS BBBO as a lone or combinatorial therapeutic technique.²³⁻³⁰

FUS for Enhanced Glymphatic Clearance

Beyond allowing larger molecules to bypass the BBB, FUS BBBO produces a variety of changes in the brain, ranging from increasing the proportion of neuroprotective disease-associated microglia (DAMs) in the brain's resident macrophage population to improving nanoparticle transfection.^{31,32} A more recently explored effect is

the enhancement of glymphatic waste clearance.^{32,33} Researchers have demonstrated that FUS BBBO augments glymphatic waste clearance, including for pathological proteins such as amyloid- β in AD.^{34,35} These studies are the pioneering evidence that FUS could be used as a treatment for mammalian glymphatic malfunction.

Curley et al. (2020)³² investigated how treatment delivery to brain tumors could be enhanced with focused ultrasound. The group utilized magnetic resonance (MR)-guided FUS BBBO in conjunction with nonviral gene therapy brain-penetrating nanoparticles (BPNs) in glioma-bearing mice. Due to abnormal vasculature development, pressure gradients and convective mass transport are significantly disrupted in the tumor environment. The researchers aimed to overcome this challenge by increasing particle penetration with FUS BBBO. They observed that FUS BBBO enabled the delivery of therapeutics across both the BBB and the blood-tumor barrier (BTB). BPN transgene expression was significantly enhanced in the brain tumors treated with FUS compared to untreated controls. Interstitial fluid flow in the brain and tumor was also affected, with the median flow velocity approximately doubling and the Péclet number, the proportion of convective to diffusive flux, more than tripling. These findings strongly suggest that FUS improves nutrient distribution and waste clearance in the brain by increasing the advection rate.

Ye et al. (2023)³³ sought to understand if MB pumping effects caused by FUS-induced compression and rarefaction of circulating MBs could enhance glymphatic transport by replicating the base driver of glymphatics, cardiac pulsatility. They tested this by administering albumin-MBs intranasally, followed by FUS sonication at the thalamus in mouse brains. They compared their results to mice that received intracisterna magna tracer injections, the standard method of measuring glymphatics in mammalian brains. Using confocal microscopy, this study confirmed a FUS BBBO-dependent increase in MB albumin in the perivascular spaces and into the interstitial space of the targeted brain regions. This study supported the notion that FUS enhances glymphatic transport.

Lee et al. (2020) demonstrated that FUS improved beta-amyloid clearance in AD mouse models. The researchers found that FUS BBBO enhanced soluble beta-amyloid clearance out of the brain and into CSF, but this effect was not shown for plaques. Additionally, FUS BBBO increased the cognitive score of the mice compared to the control. To ensure the FUS's effect was due to glymphatic enhancement, the researchers performed a lymphatic ligation that led to increased beta-amyloid accumulation and decreased cognitive score and observed that FUS BBBO rescued both deleterious effects. These observations indicate that FUS can prevent and ameliorate neurodegeneration by promoting waste clearance before pathogenic compounds like amyloid plaques form.

FUS BBBO was the first technology to characterize glymphatic dynamics in the human brain.³⁶ Despite advances in augmenting and characterizing waste clearance in the brain, the exact mechanisms by which FUS BBBO improves the glymphatic system are still poorly understood. FUS BBBO represents an extremely hopeful avenue for addressing the pathological accumulation of neurotoxic solutes, and would greatly benefit from investigations into its therapeutic potential for the glymphatic system.

Modeling the Glymphatic System

Computational modeling is a powerful tool to overcome technological challenges in directly measuring some biological phenomena. Consequently, many researchers have designed computational models for the glymphatic system or brain vasculature. Nedergaard et al., *The Glymphatic System: Current Understanding and Modeling*, reviewed many recently developed glymphatics models.⁴ Models have simulated many potential glymphatic mechanisms, including perivascular pumping, the interface between perivascular spaces and the parenchyma, waste efflux routes, neuronal activity and vasomotion, and mass transport through the brain parenchyma. One model notably modeled interstitial fluid flow in mammalian brain parenchymas by estimating how idealized brain vasculature arrangements and orientations affect hydraulic resistance.³⁷ Others have evaluated the possibility of advective mass transport as a waste clearance mechanism for glymphatics.^{38, 49,52} Another explored

how elevations in intracranial pressure change CSF dynamics in the brain.⁵⁰ Still more have attempted to statistically predict the topology of brain vasculature, or have tried to understand the role of glymphatics in the pathogenesis of neurodegenerative diseases like AD.^{42,43}

Finite element modeling (FEM), a computational method of solving partial differential equations related to physical processes like heat and mass transfer, fluid movement, and structural deformations, is an increasingly popular way of circumnavigating laborious or challenging data collection. Many biomedical engineering projects have used FEM to generate novel biological insights, such as ones related to breast tissue, bone, skin, and more.³⁹⁻⁴¹ Thus, this study aims to leverage FEM as a novel mode of investigation for FUS BBBO-enhanced glymphatic waste clearance.

Methods

The model design was completed in COMSOL Multiphysics using the microfluidics package. All values were collected from a literature review. FUS BBBO was modeled as changes in permeability, porosity, flow, and perivascular space geometries. It should be noted that FUS BBBO is not modeled as a delivery mechanism for any of the species. Instead, FUS is treated simply as a system perturbation that affects the clearance of pre-existing solutes in the brain parenchyma. FUS was modeled after the pre-clinical RK50 device developed by FUS Instruments Inc. (center frequency 1.66 MHz, element diameter 43 mm, focal length 35 mm). Solute distributions were modeled based on measured diffusion coefficients in the mammalian brain parenchyma. The effects FUS BBBO has on glymphatic waste clearance at different spatial targets, for different solutes, and for different solute distributions, were explored. A comprehensive list of parameter values is included in Tables 1 and 2.

Assumptions

Constant temperature and pressure are assumed. It is also assumed that no chemical reactions are occurring and that the physical deformation of vessels caused by cardiac pulsations is negligible. FUS BBBO is assumed to occur downstream of the model vessels, which are so large that it is feasible to assume that FUS BBBO might not occur therein. Because of this, blood flow and influx of any species from the plasma can be ignored. Finally, all tissue heterogeneity stemming from microglia, astrocytes, neurons, or other brain tissue is considered captured by tissue parameters like porosity and permeability.

Table 1. Glymphatics model parameters

Parameter	Value	Unit	Reference
Base model geometry			
Length	100	um	[38], [42]
Arteriole Diameter	20	um	[6], [44], [45], [46], [47]
Venule Diameter	30	um	[6]
Perivascular Space Width	10	um	[6], [44], [48]
Glia Limitans Width	1	um	[6], [49], [50]
Mean distance from arteriole to venule	280	um	[51], [52]
Parenchyma Porosity	20	%	[53], [54], [55]
Parenchyma Permeability	10^{-12}	m^2	[56]
Parenchyma Tortuosity	1.7	dimensionless	[57]
Glia Limitans Porosity	0.3	%	[56], [58]
Glia Limitans Permeability	$5 * 10^{-14}$	m^2	[52], [56]
Pressure Gradient Across Vessels	3	mmHg/m	[59], [60]
Periarterial CSF Velocity	18.7	um/s	[11], [48]
Perivenous CSF Velocity	3	um/s	[61]
CSF Viscosity	1	mPa/s	[62]
CSF Density	1	g/mL	[63]

Table 2. Parameters for modeling FUS and various solutes

Parameter	Value	Unit	Reference
FUS Parameters			
Focal Volume Cross-Sectional Diameter	0.9	mm	[64]
Perivascular Space Size Increase	175	%	[65]
Parenchyma Porosity Increase	167	%	[66]
Parenchyma Permeability Increase	300	%	[67]
FUS Fluid Inlet	0.8	um/s	[32]
Solute Diffusion Coefficients			
Solube Tracer	10^{-9}	$\frac{m^2}{s}$	[68]
amyloid- β	1.8×10^{-10}	$\frac{m^2}{s}$	[57]
α -synuclein	7.8×10^{-10}	$\frac{m^2}{s}$	[69]

Results

Base Design

Figure 5 shows the base model's design. The broad outer cylinder represents the brain parenchyma, while the inner concentric cylinders represent the glia limitans, perivascular spaces, and vasculature, respectively. The single arteriole-venule (AV) unit was modeled to characterize CSF ingress and egress dynamics in the glymphatic system.

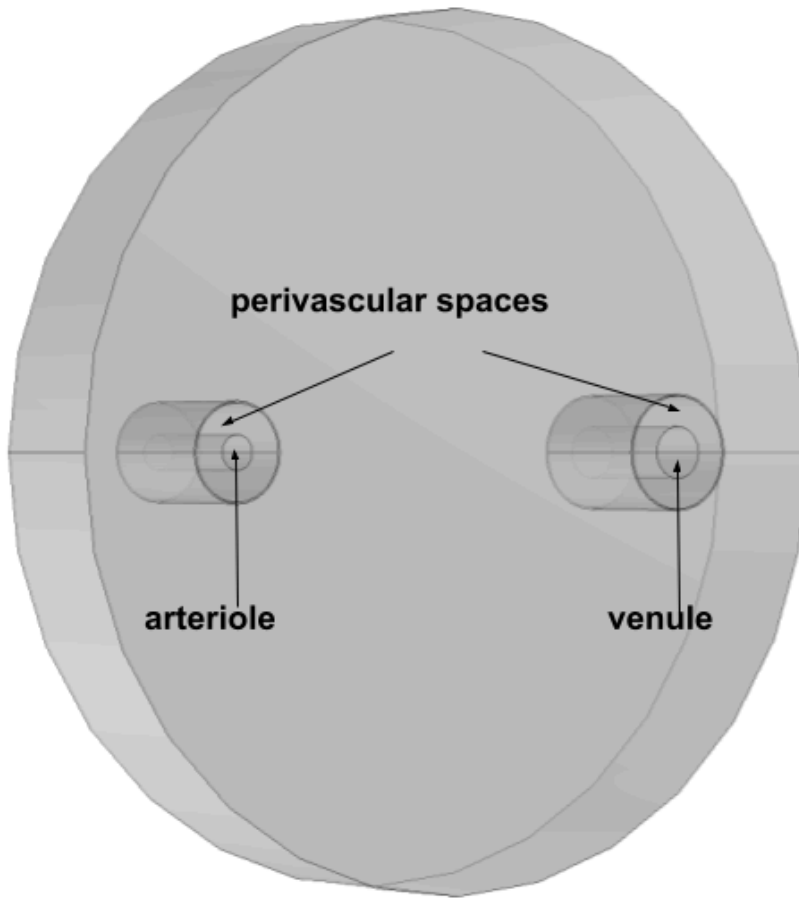


Figure 5. General Model geometry

All models were simulated until 95% of the initial mass was cleared, at which point the simulation terminated. Temporal and spatial data related to solute flux, pressure, and flow were collected.

Clearance of Centralized Soluble Tracer (NO FUS)

The model's first iteration simulated the clearance of a cylindrical bolus of tracer centralized between the vessels, shown in the following figures. Figure 6 shows the steady-state flow profile, and Figure 7 illustrates the pressure gradient which drives that flow. Tracer in this bolus formation was simulated first to visualize the glymphatic profile. This tracer was simulated with a diffusion coefficient of $10^{-9} \frac{m^2}{s}$, which is on the order of magnitude of a macromolecule tracer.⁶⁸ The bolus shape was chosen because it is visually simple.

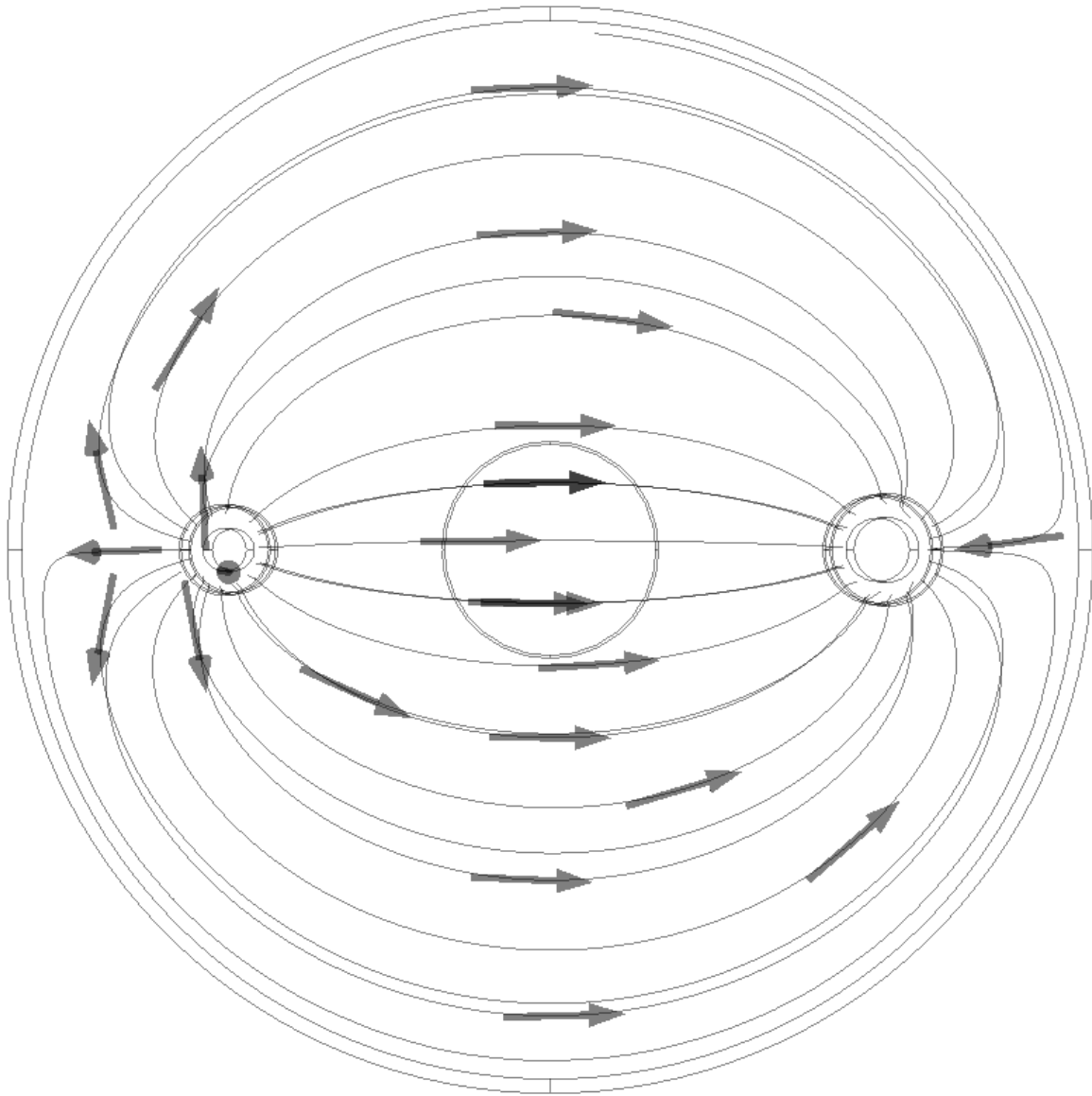


Figure 6. *Steady-state flow profile of base model*

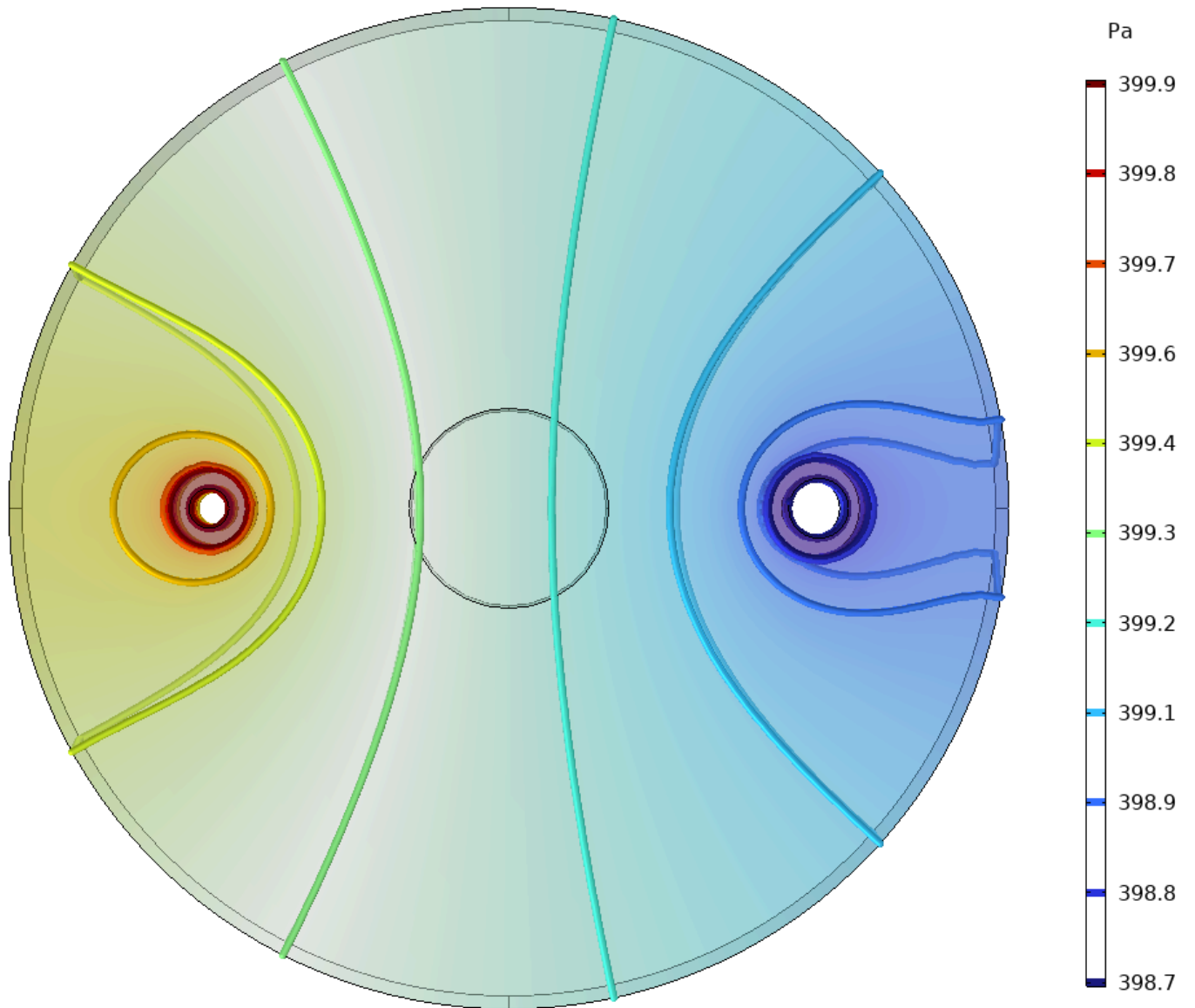


Figure 7. Pressure profile of base model

Figures 8, 9, and 10 show the concentration flux at $t = 1$, 10, and 30 respectively. The color scale represents the spatial solute concentration while the arrows point in the direction of flux. These three timepoints were selected to illustrate the evolution of solute clearance over time. Note that the color scale is relative to each time point.

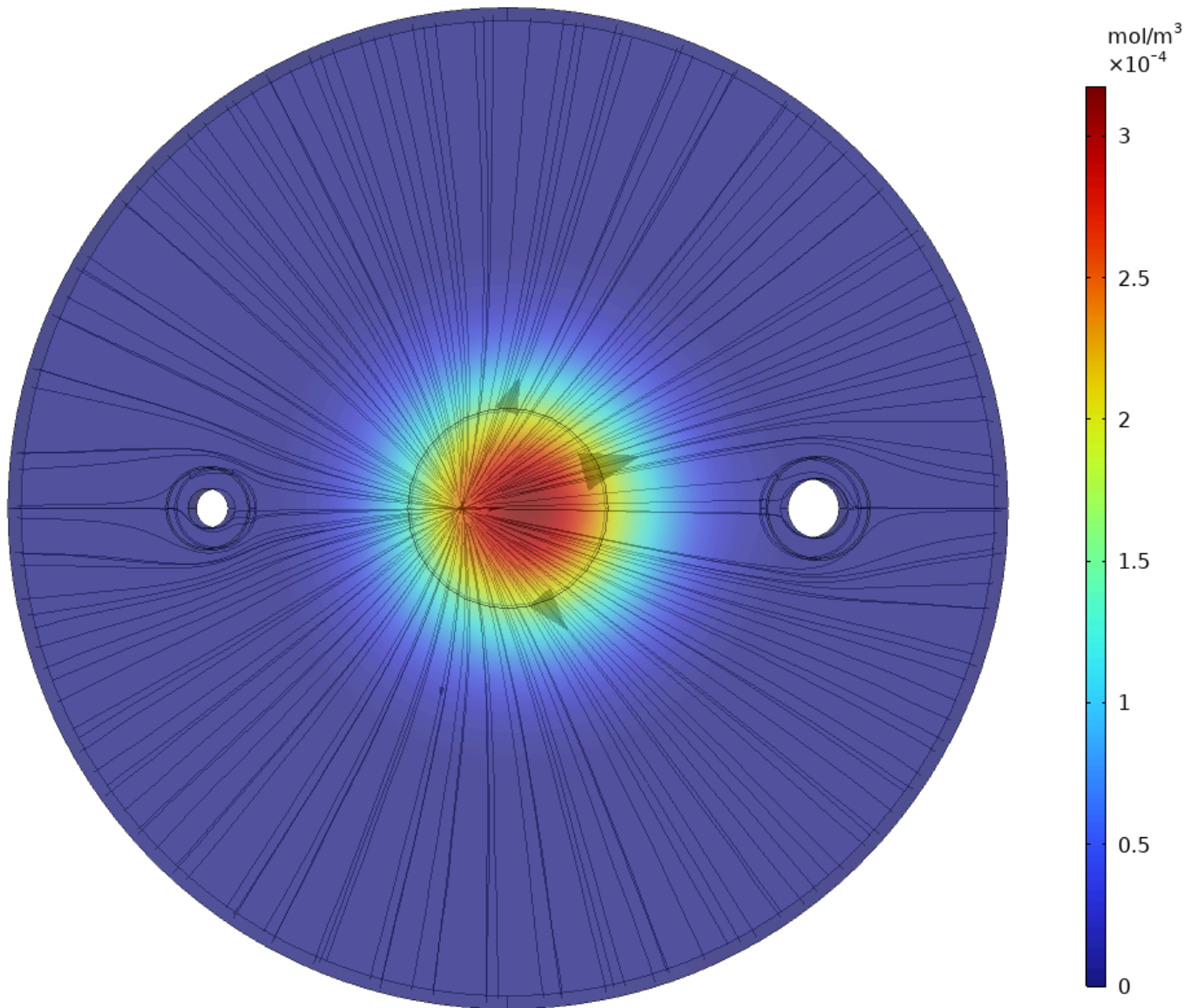


Figure 8. Concentration flux of centralized tracer at $t = 1$ s for base model

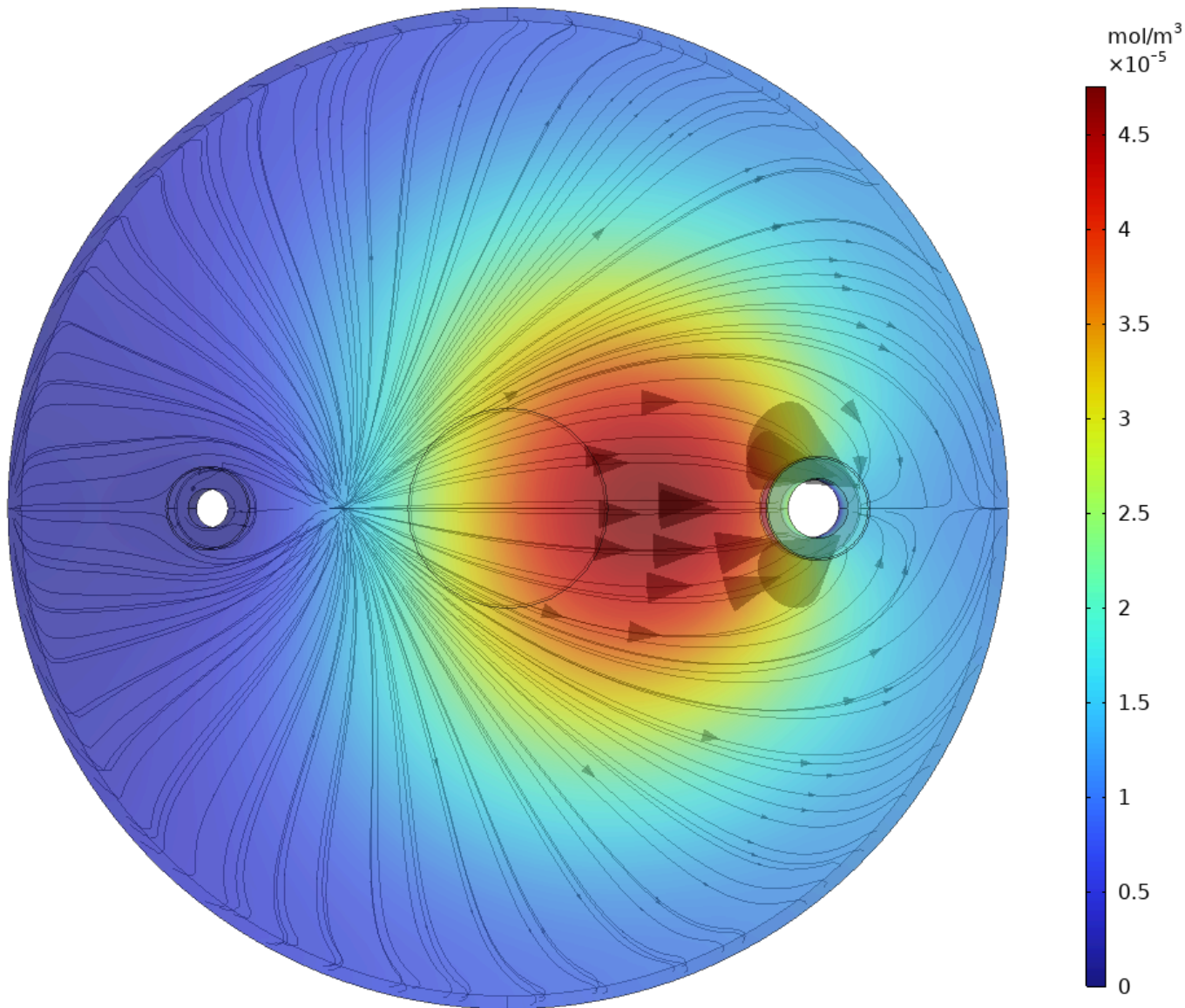


Figure 9. Concentration flux of centralized tracer at $t = 10$ s for base model

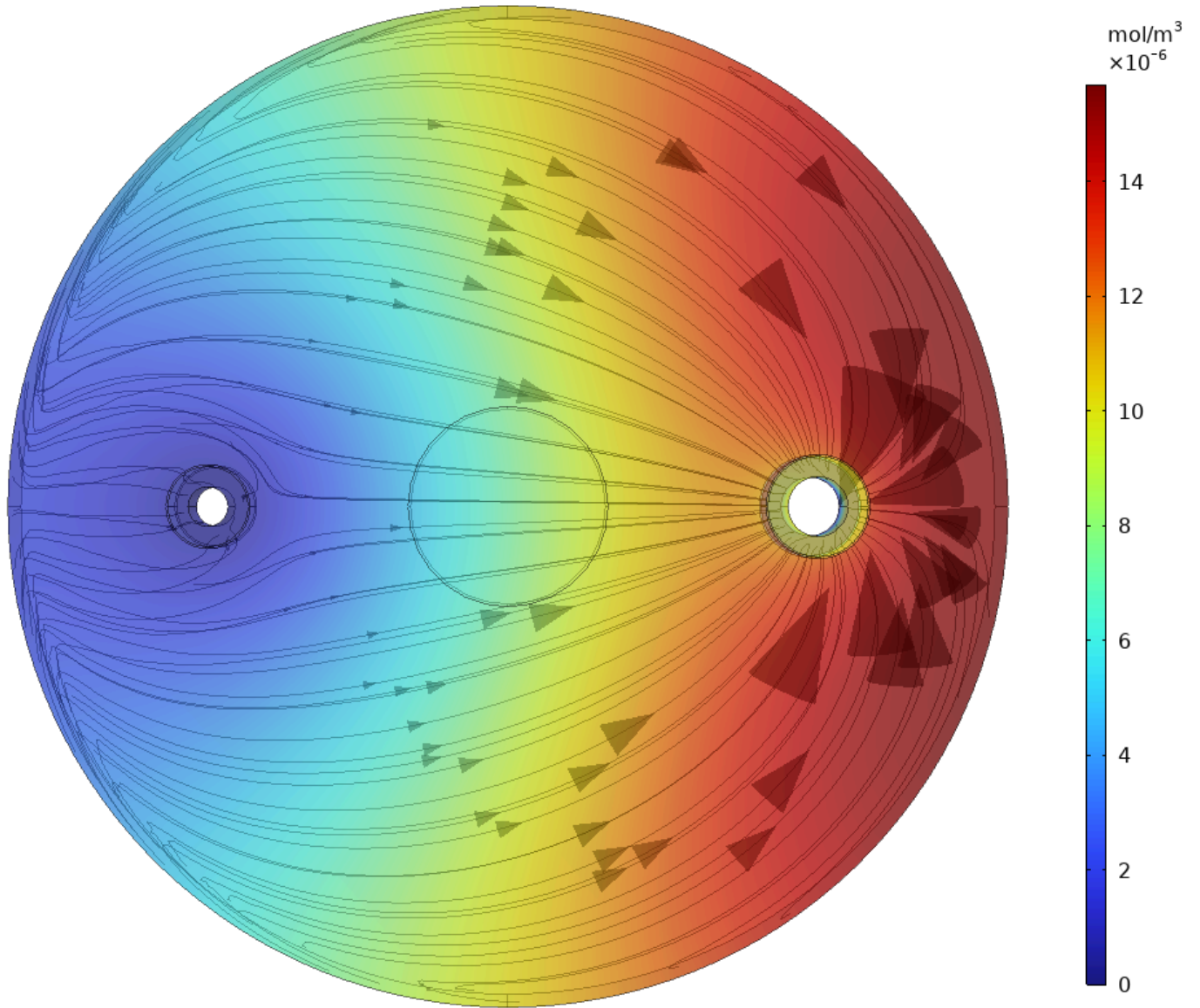


Figure 10. Concentration flux of centralized tracer at $t = 30$ s for base model

Finally, Figure 11 shows the relative contributions of convective and diffusive flux and the resulting Péclet number.

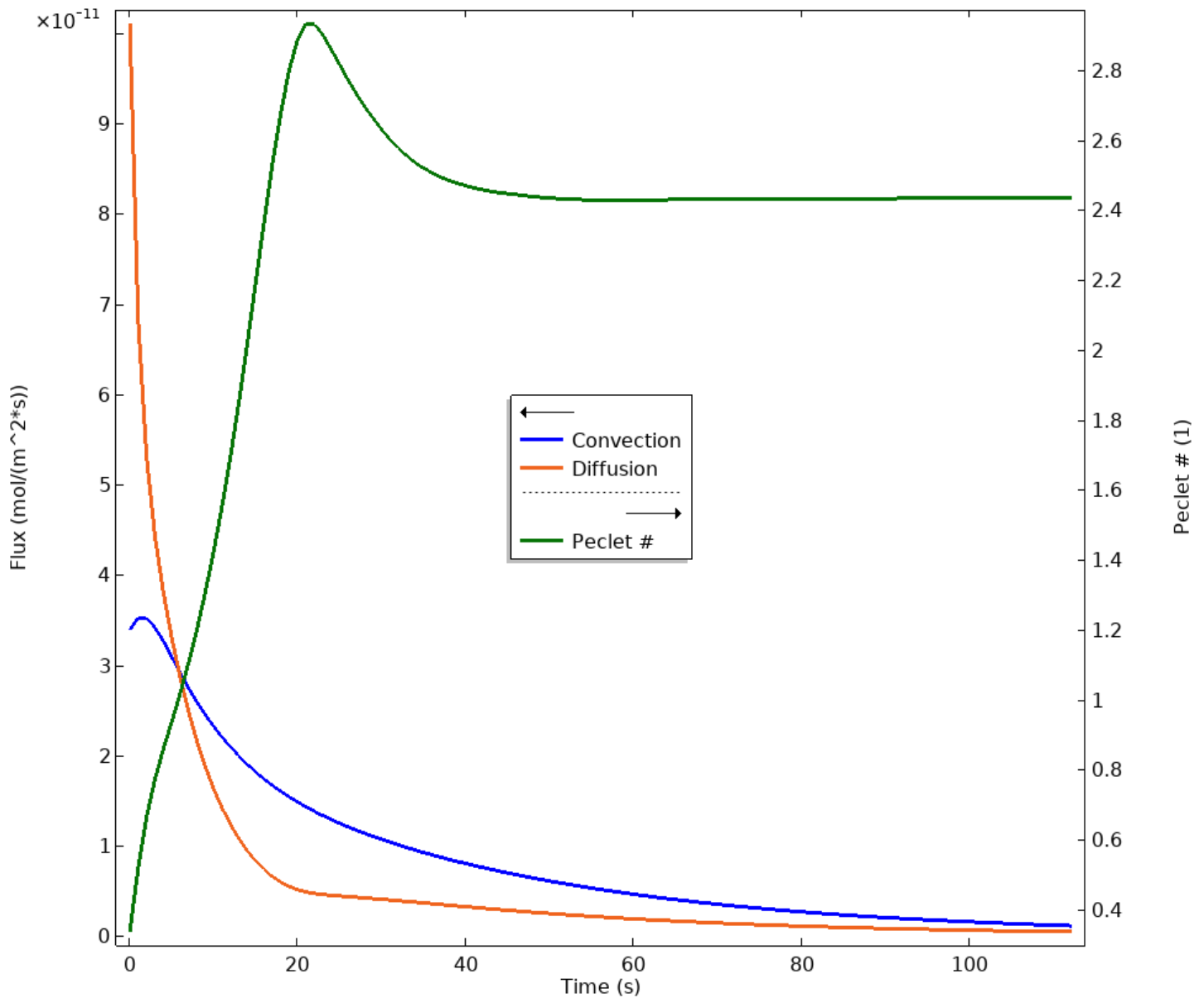


Figure 11. Contributions to flux and Péclet number for base model

This figure was generated to evaluate the modes of clearance over time and provide an intuitive visualization for the Péclet number.

Clearance of Centralized Tracer with FUS BBBO Applied on the Arterial Side (PAS FUS)

Changes in dynamics were modeled in the presence of FUS BBBO only on the arterial side. Figures 12 and 13 show the flow and pressure profiles, respectively, while figures 14, 15, and 16 again show the tracer

concentration over time. Figure 17 shows the flux analysis. This model was created to generate insight into the spatial effects of FUS BBBO on the arteriole, which is the source of CSF for glymphatic flow.

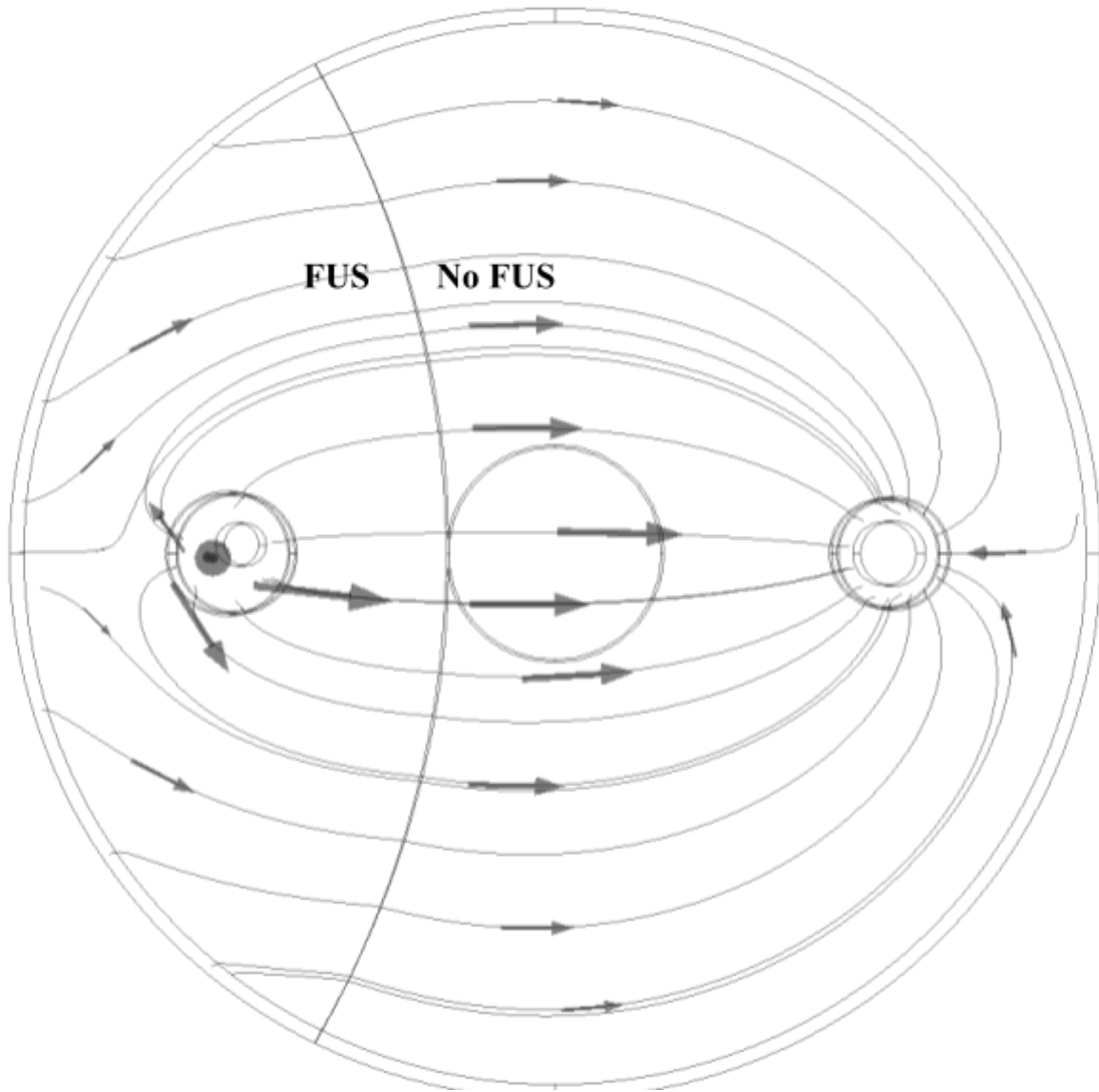


Figure 12. *Steady-state flow profile of arterial FUS BBBO model*

As one can see, the model is affected by an additional fluid inlet on the arterial side and by increased PAS volume.

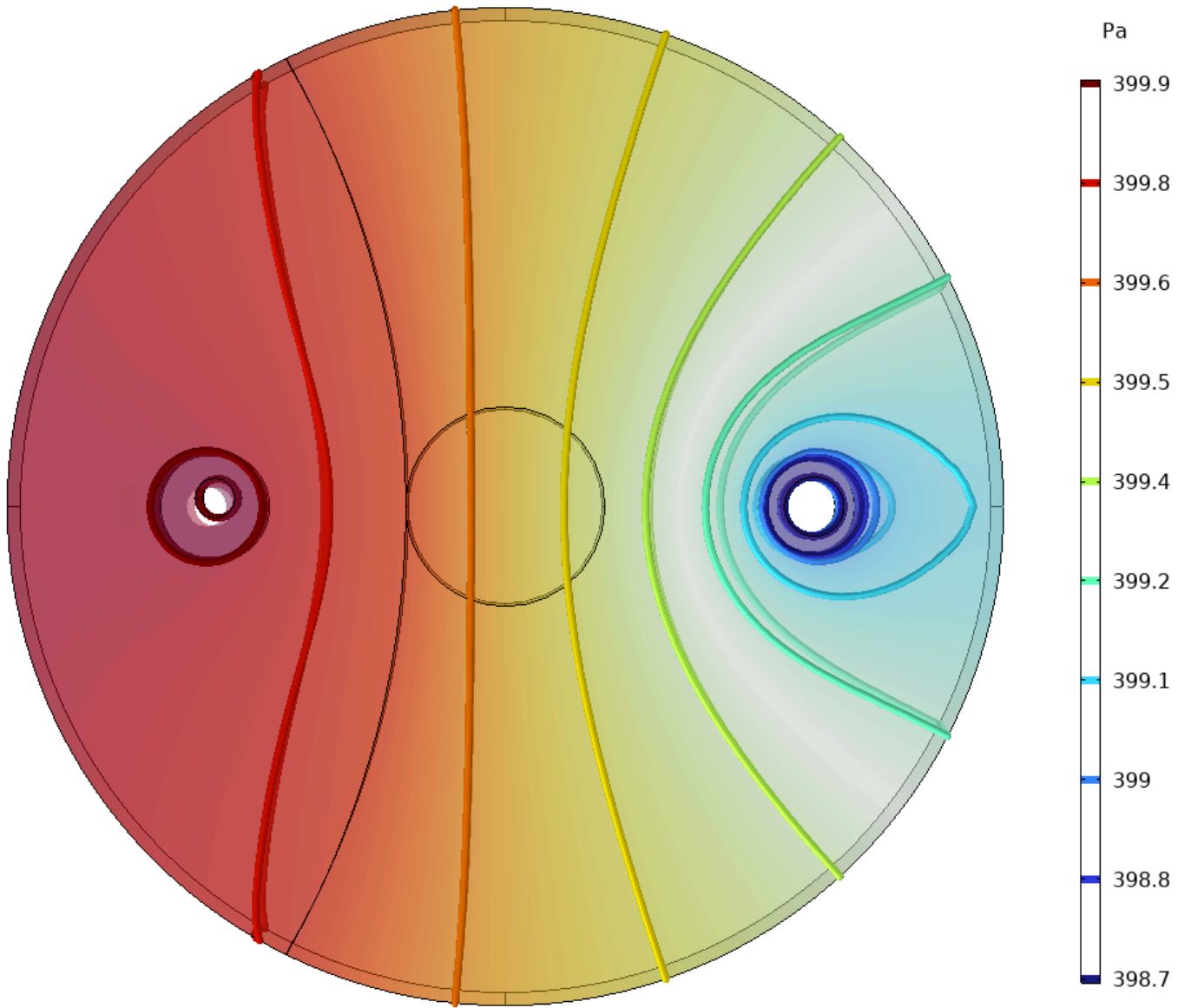


Figure 13. Pressure profile of arterial FUS BBBO model

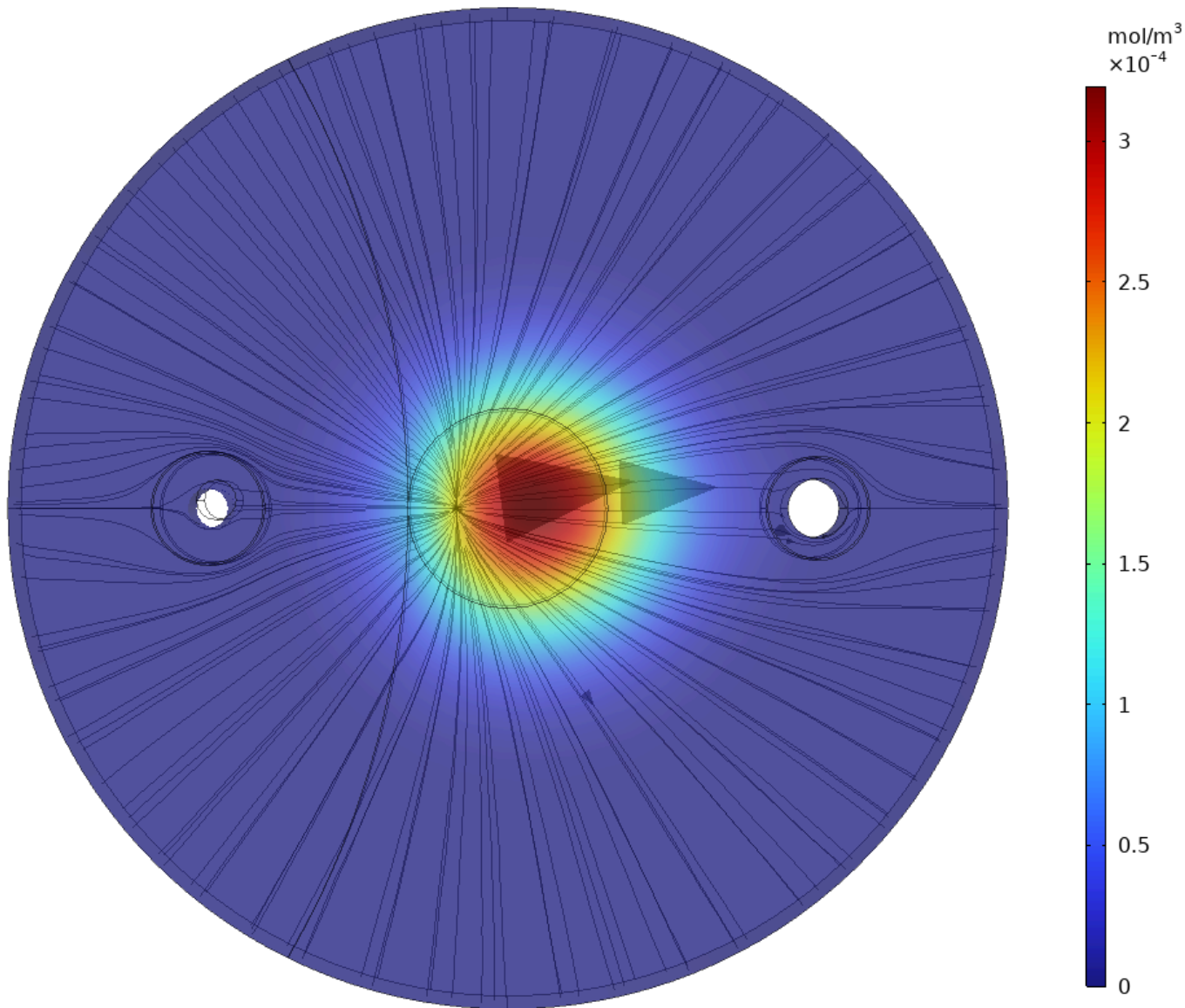


Figure 14. Concentration flux of centralized tracer at $t = 1$ s for arterial FUS BBBO model

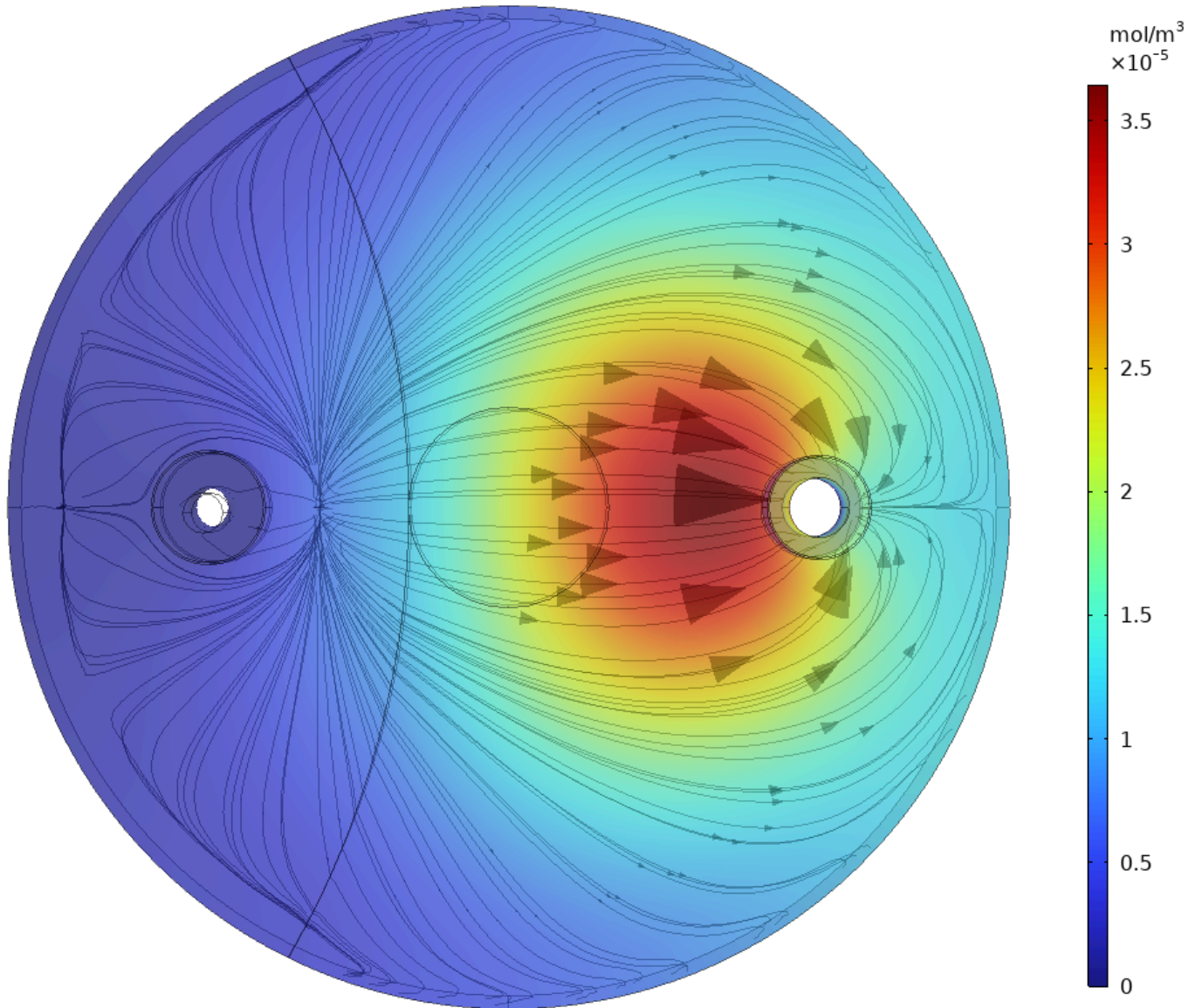


Figure 15. Concentration flux of centralized tracer at $t = 10$ s for arterial FUS BBBO model

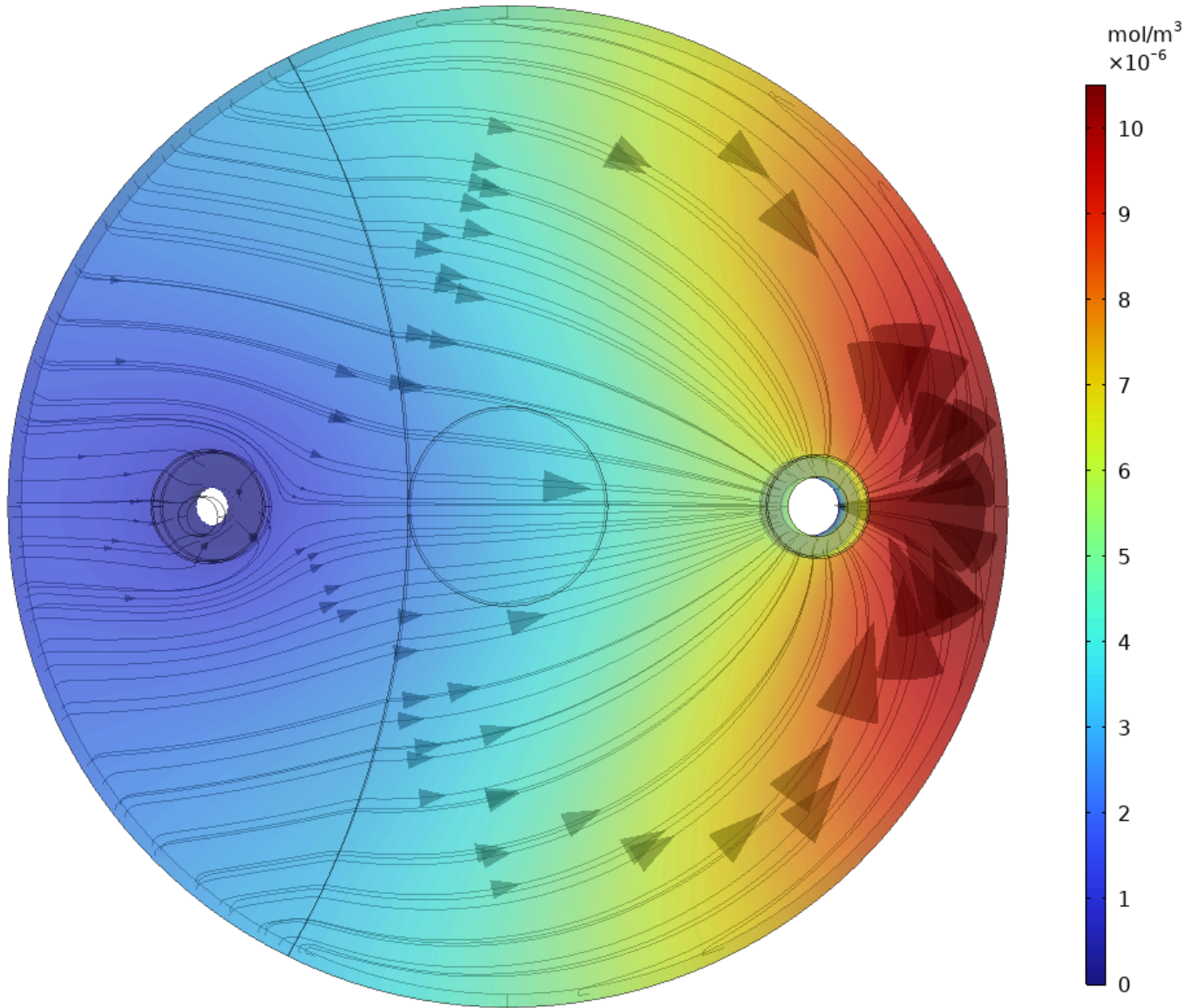


Figure 16. Concentration flux of centralized tracer at $t = 30$ s for arterial FUS BBBO model

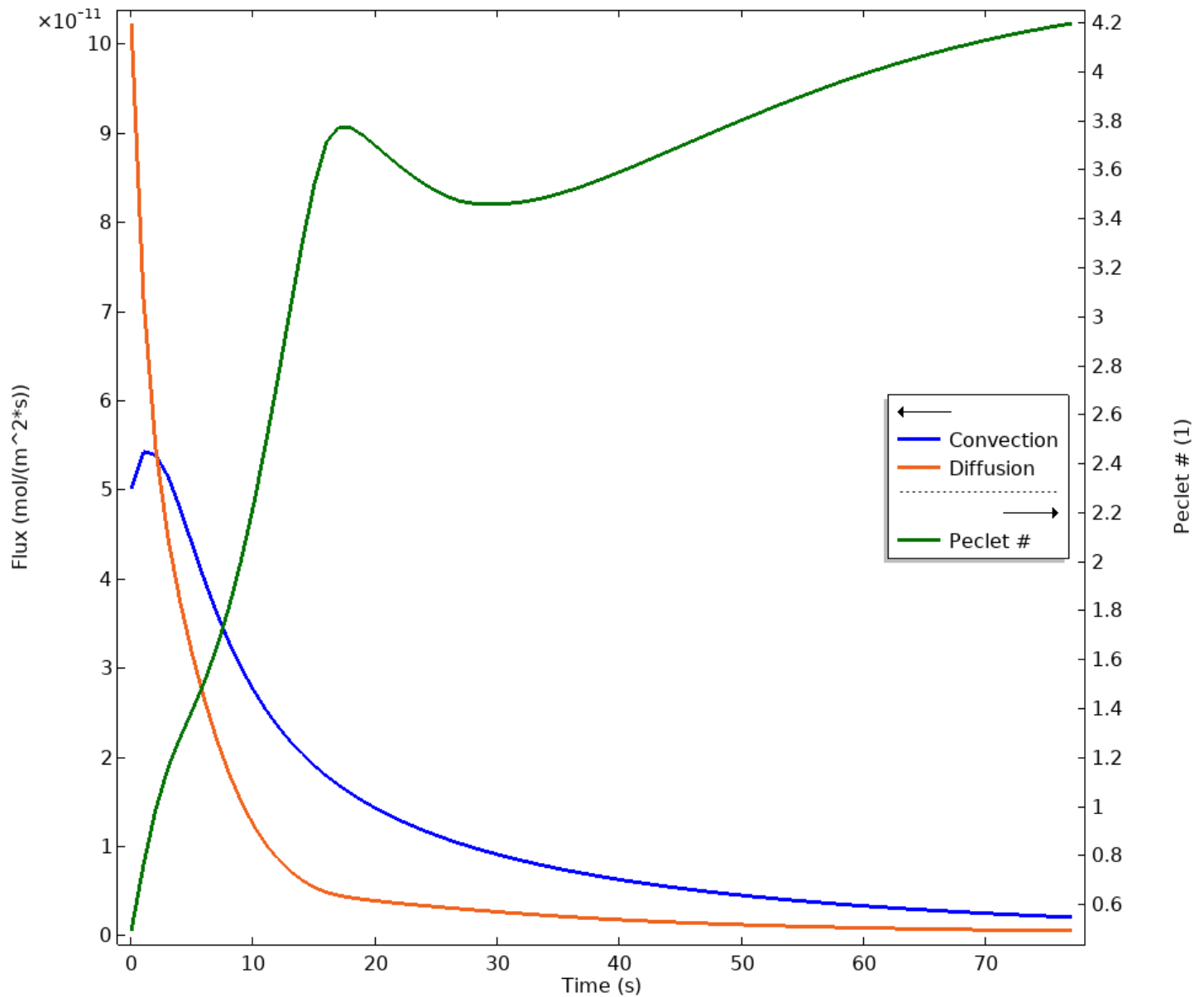


Figure 17. Relative contribution to flux and Péclet number for arterial FUS BBBO model

Clearance of Centralized Tracer with FUS BBBO Applied on the Venous Side (PVS FUS)

The same data were generated by a model with FUS BBBO occurring around the venule region, and are shown in figures 18, 19, 20, 21, 22, and 23 below. This model was created to complement the previous model by applying FUS at the venule region.

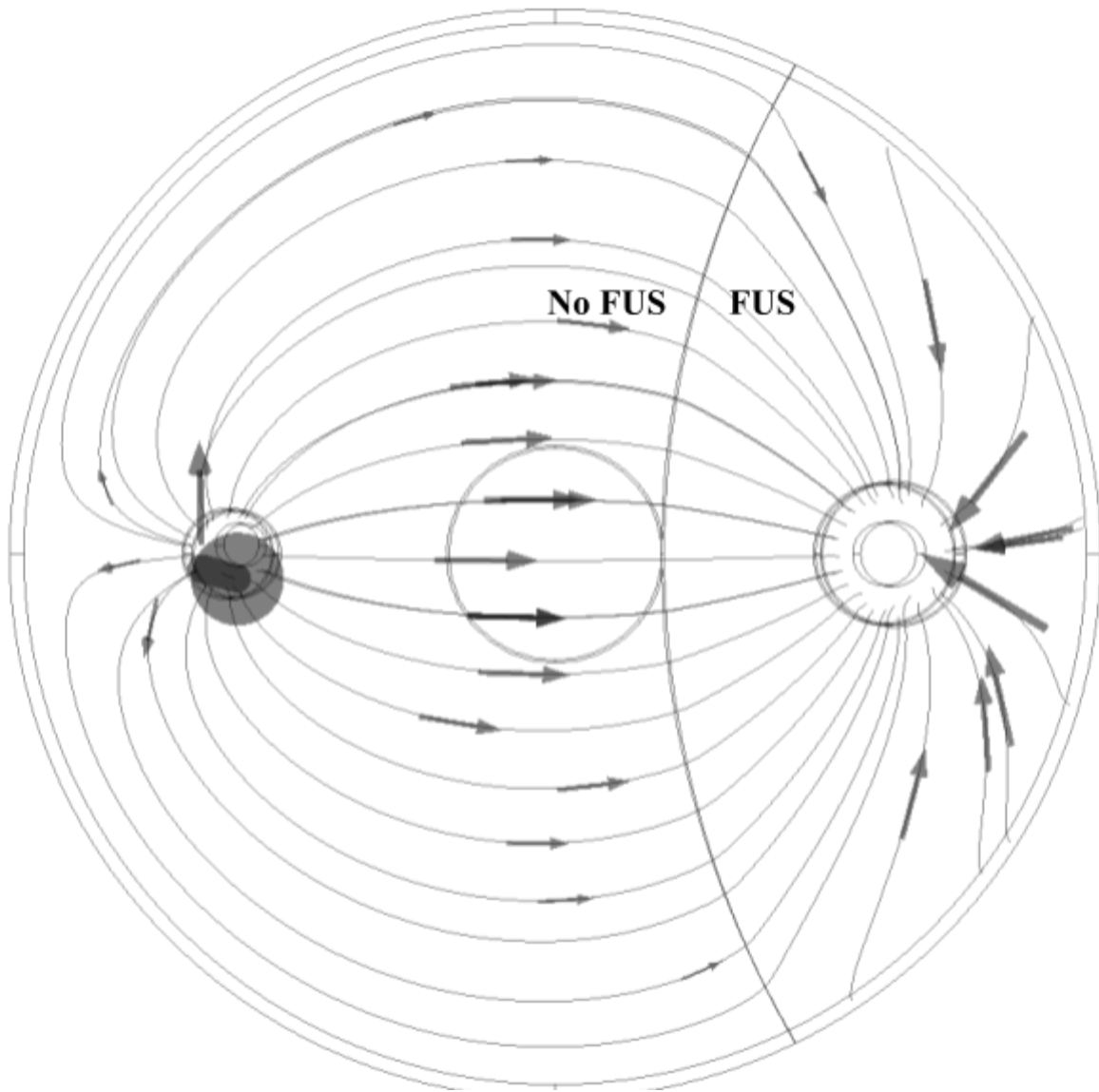


Figure 18. *Steady-state flow profile of venule FUS BBBO model*

Similar to the FUS PAS model, one can observe additional fluid inlets on the venule side, along with expanded PVS volume.

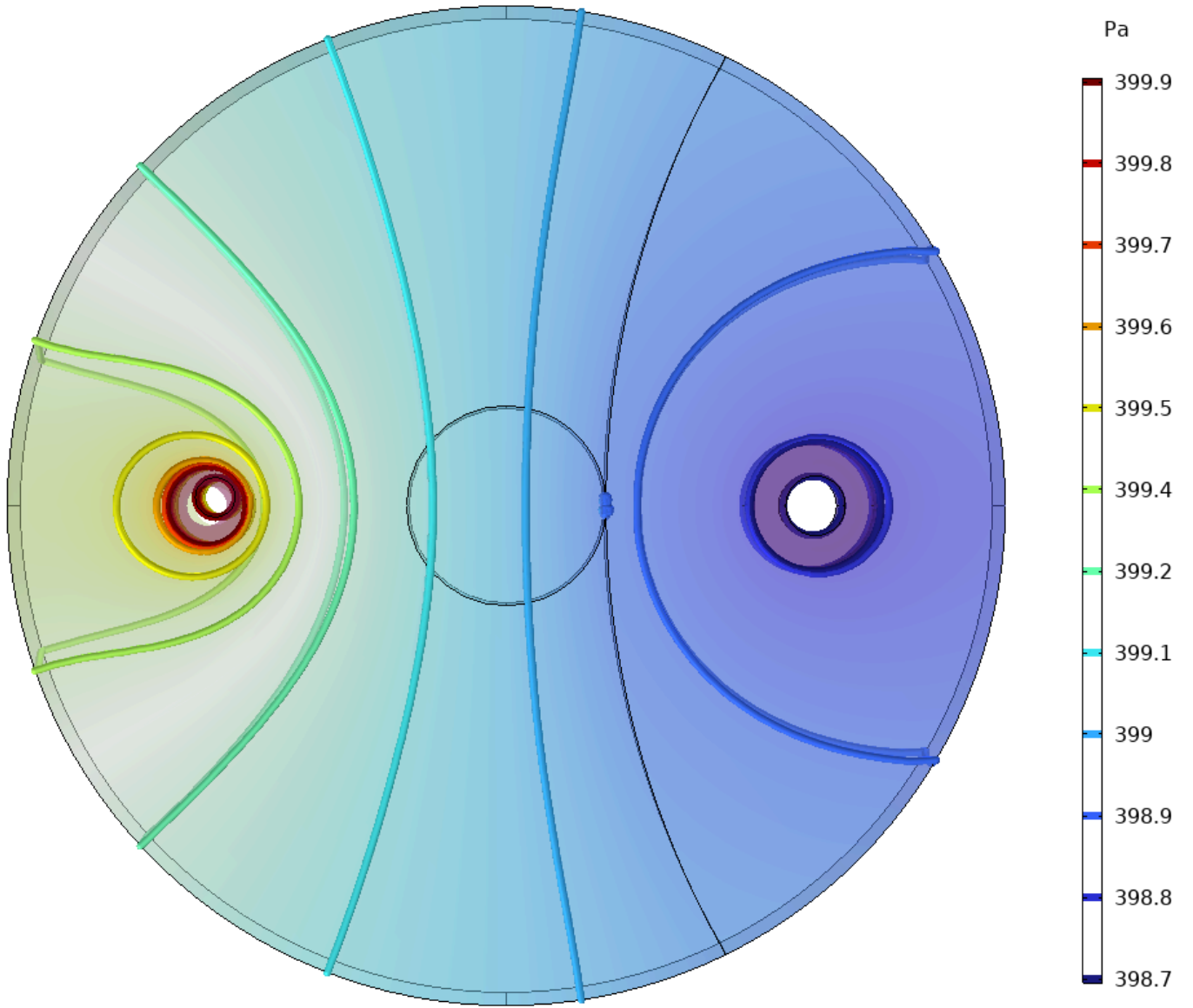


Figure 19. Pressure profile of venule FUS BBBO model

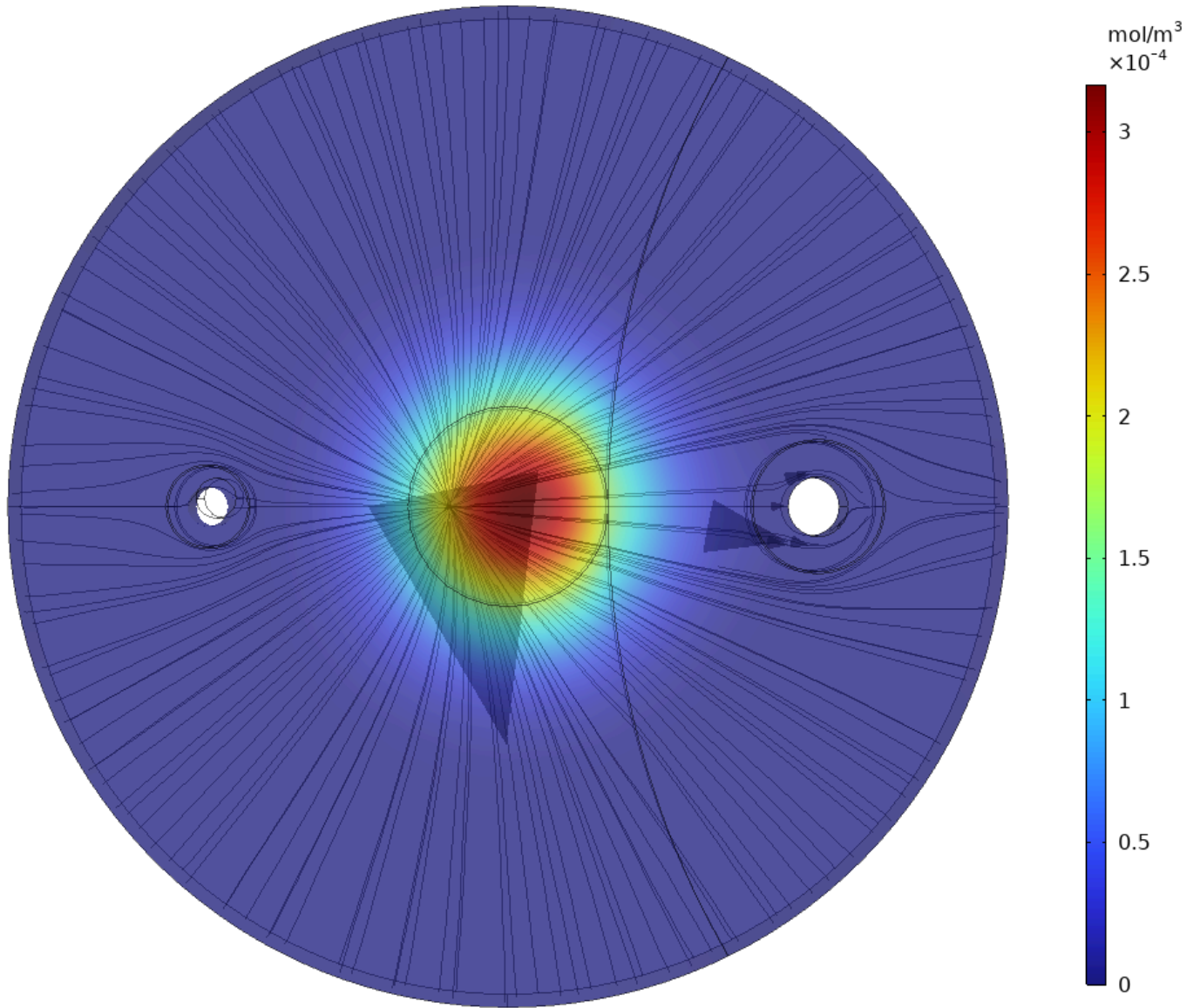


Figure 20. Concentration flux of centralized tracer at $t = 1$ s for venule FUS BBBO model

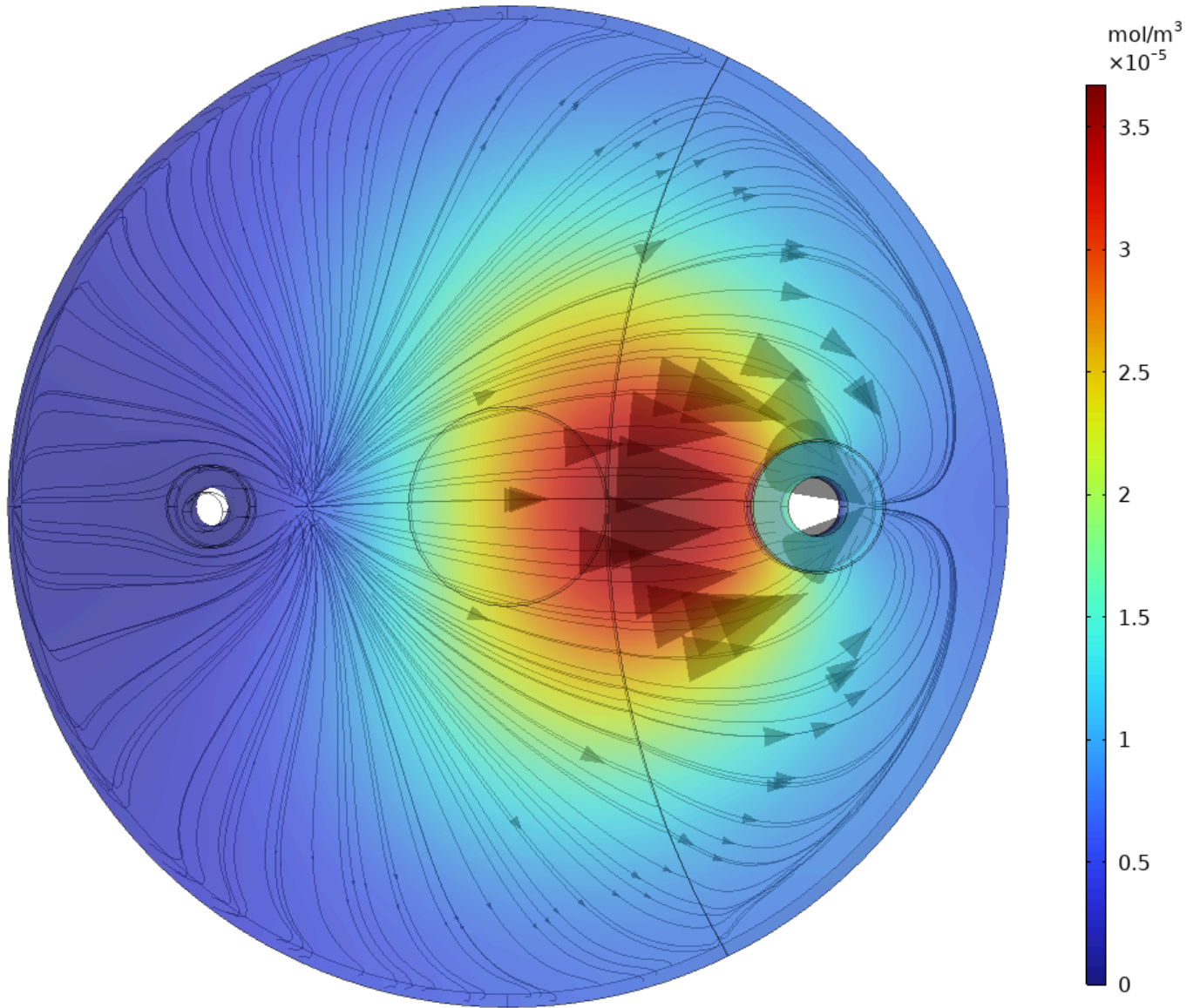


Figure 21. Concentration flux of centralized tracer at $t = 10$ s for venule FUS BBBO model

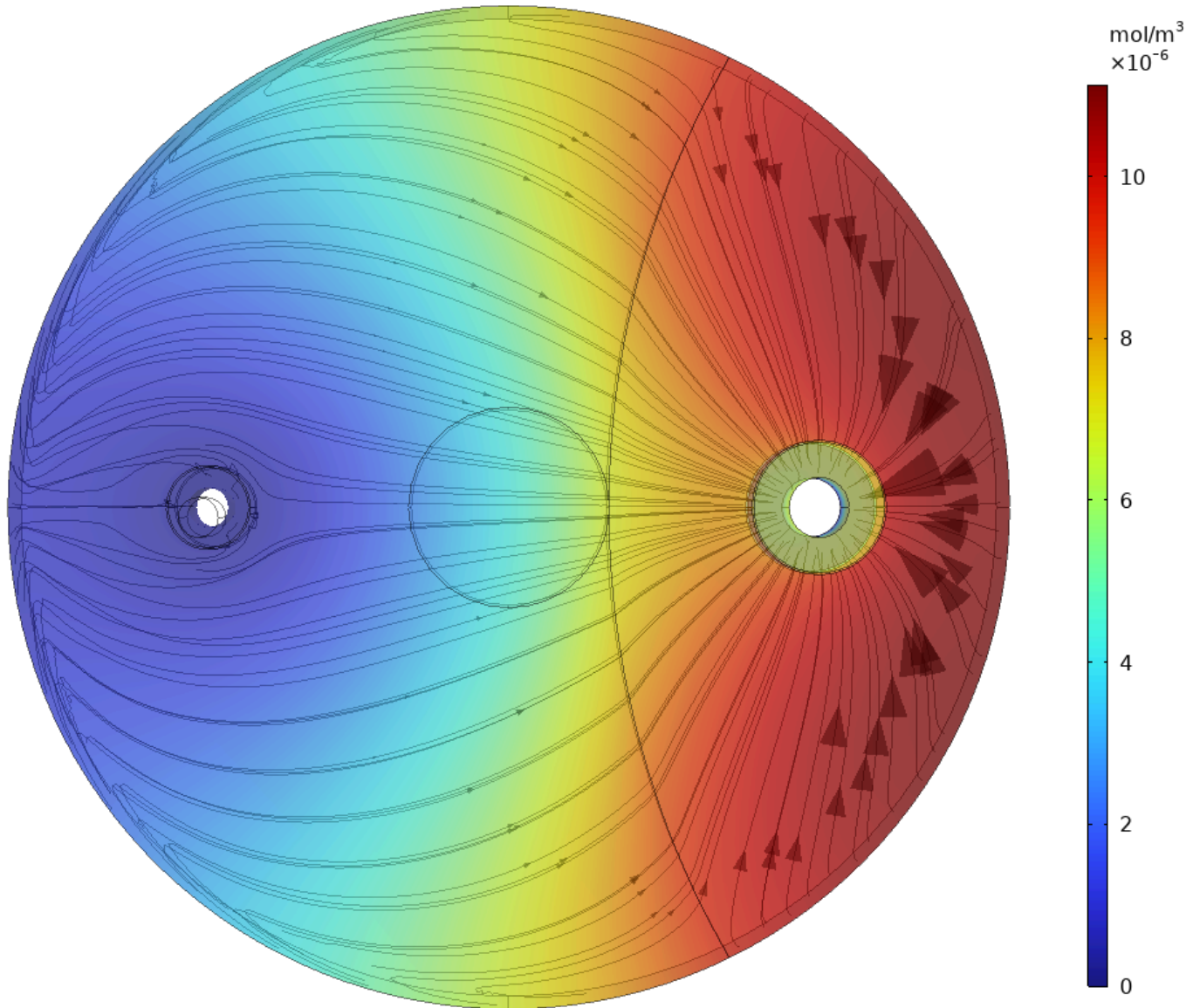


Figure 22. Concentration flux of centralized tracer at $t = 30$ s for venule FUS BBBO model

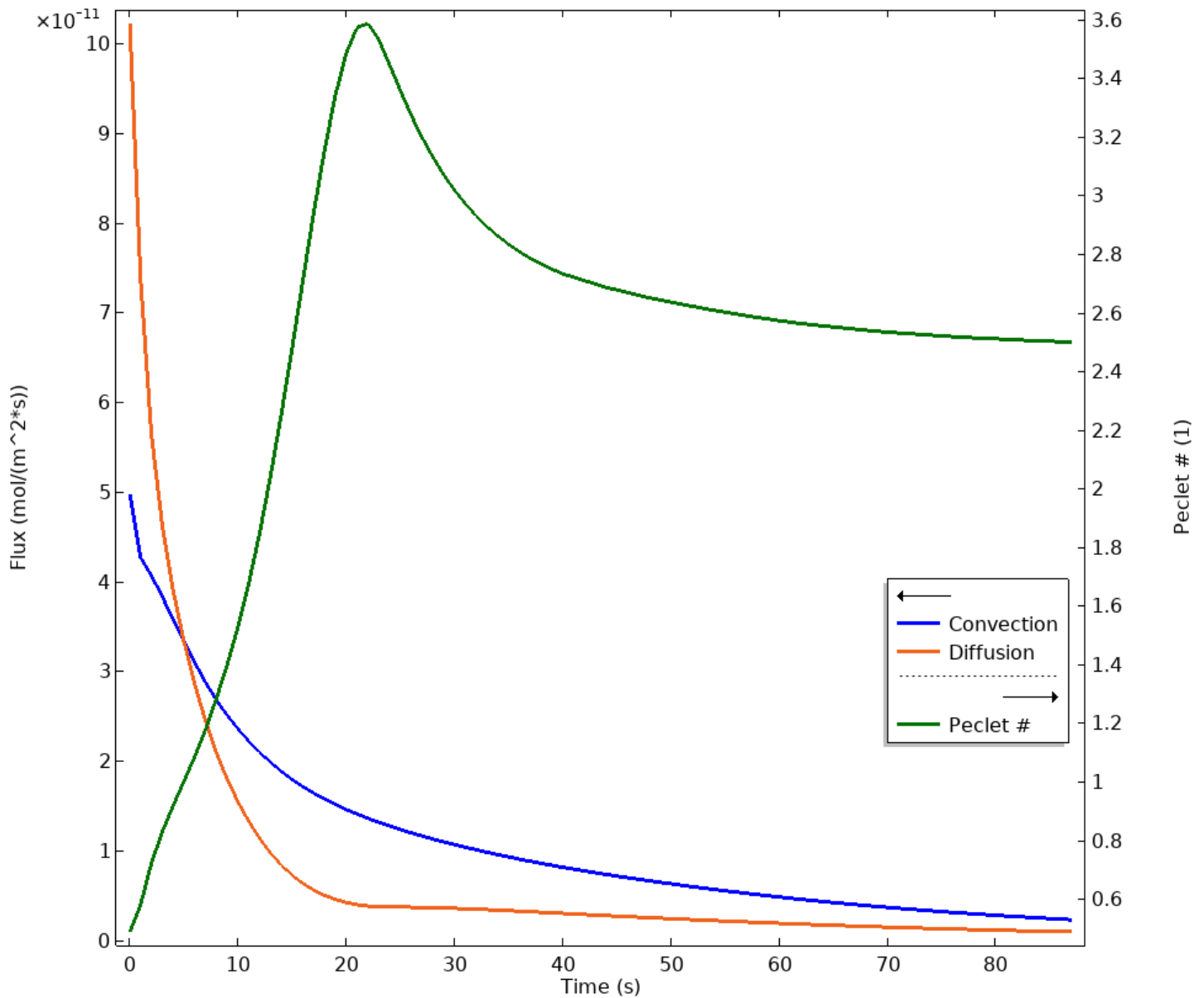


Figure 23. Relative contribution to flux and Péclet number for venule FUS BBBO model

Clearance of Centralized Tracer with FUS BBBO Applied on the Whole Model (Whole FUS)

The same simulations were repeated with FUS BBBO covering the entire model, and are shown in figures 24, 25, 26, 27, 28, and 29. This model aimed to evaluate the overall increase in glymphatic clearance for an entire AV unit because the RK50 focal volume greatly exceeds the AV unit size.

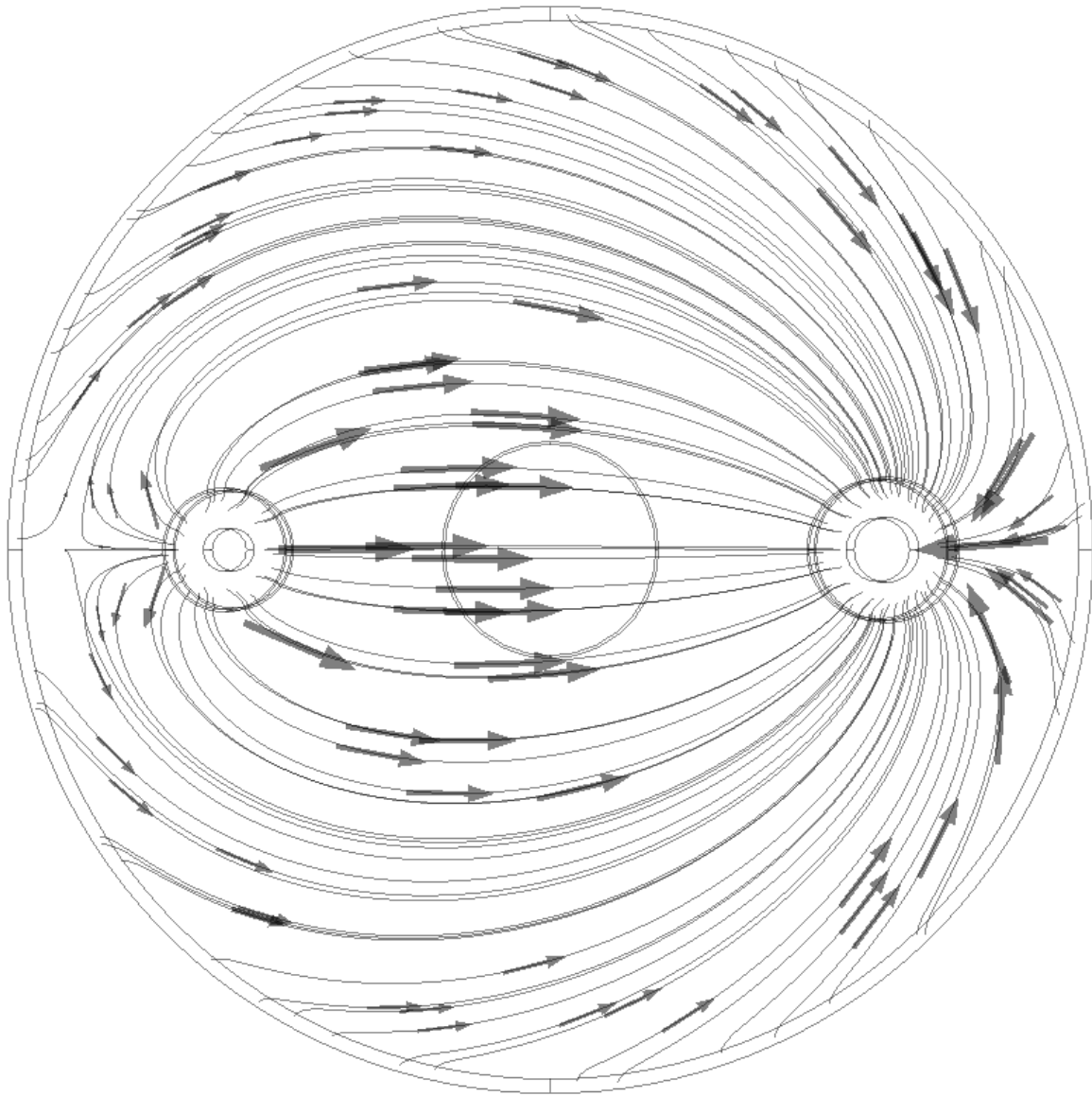


Figure 24. *Steady-state flow profile of whole FUS BBBO model*

Both the perivascular spaces are expanded, and the entire model experiences additional fluid inlets along its circumference.

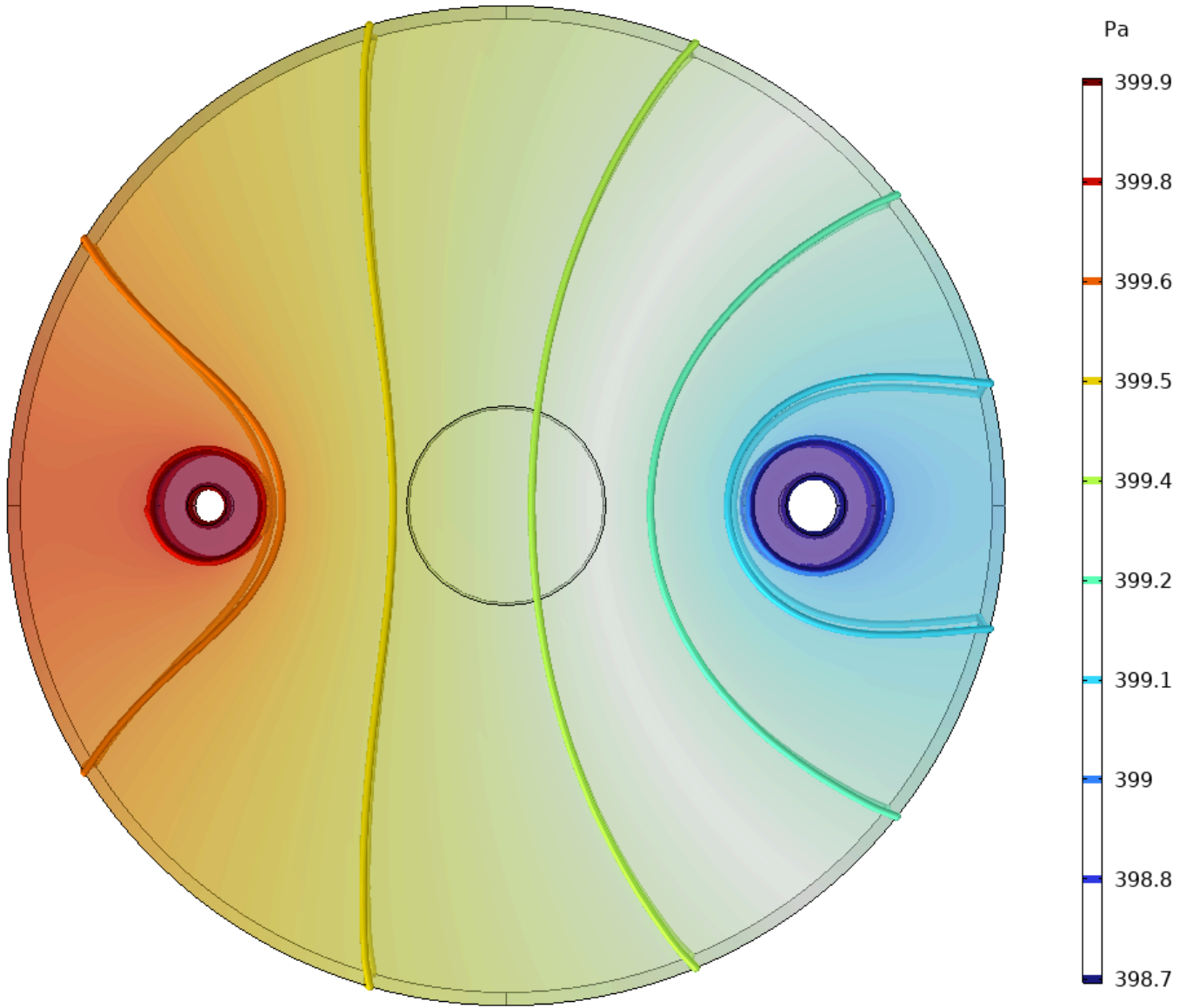


Figure 25. Pressure profile of whole FUS BBBO model

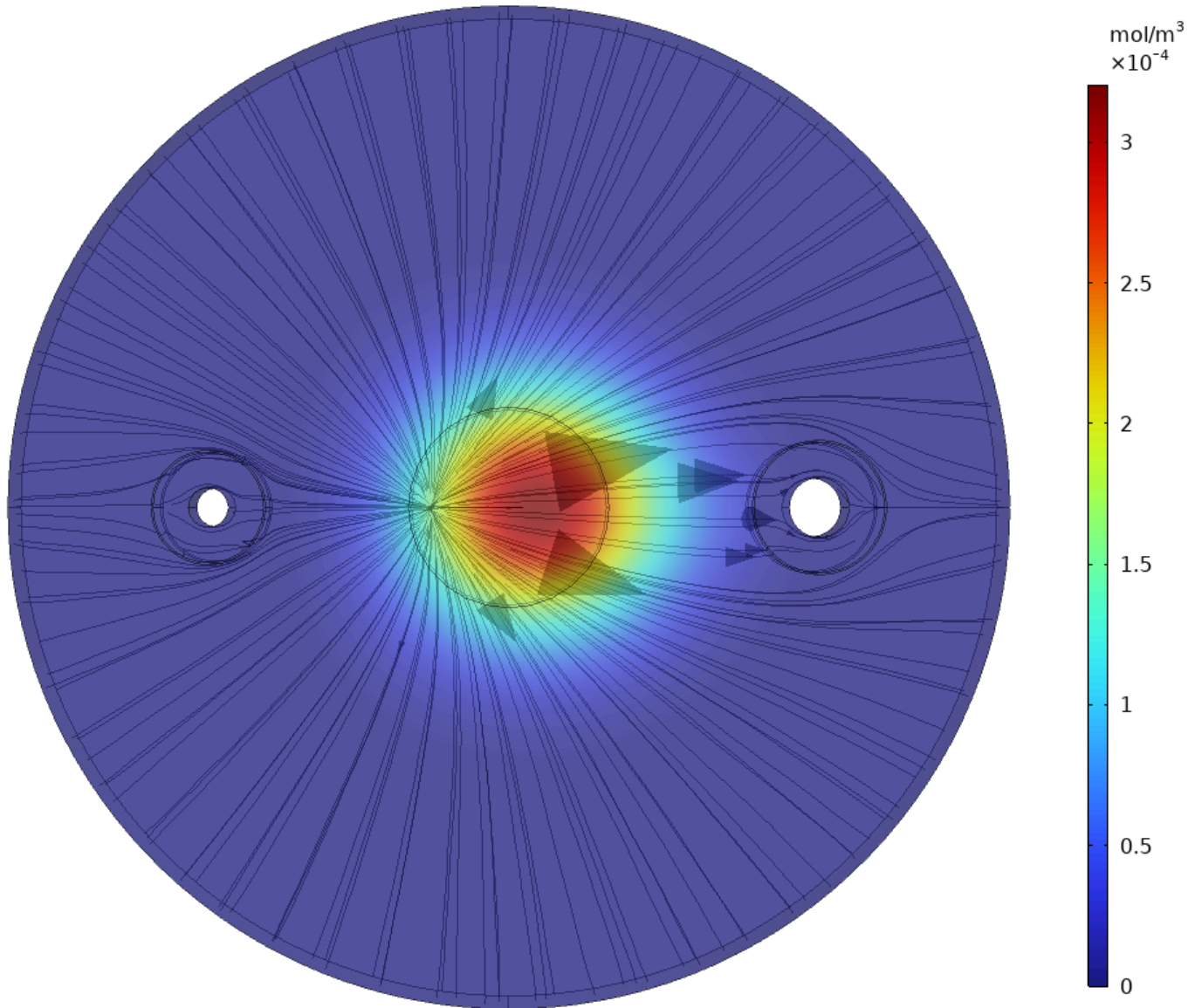


Figure 26. Concentration flux of centralized tracer at $t = 1$ s for whole FUS BBBO model

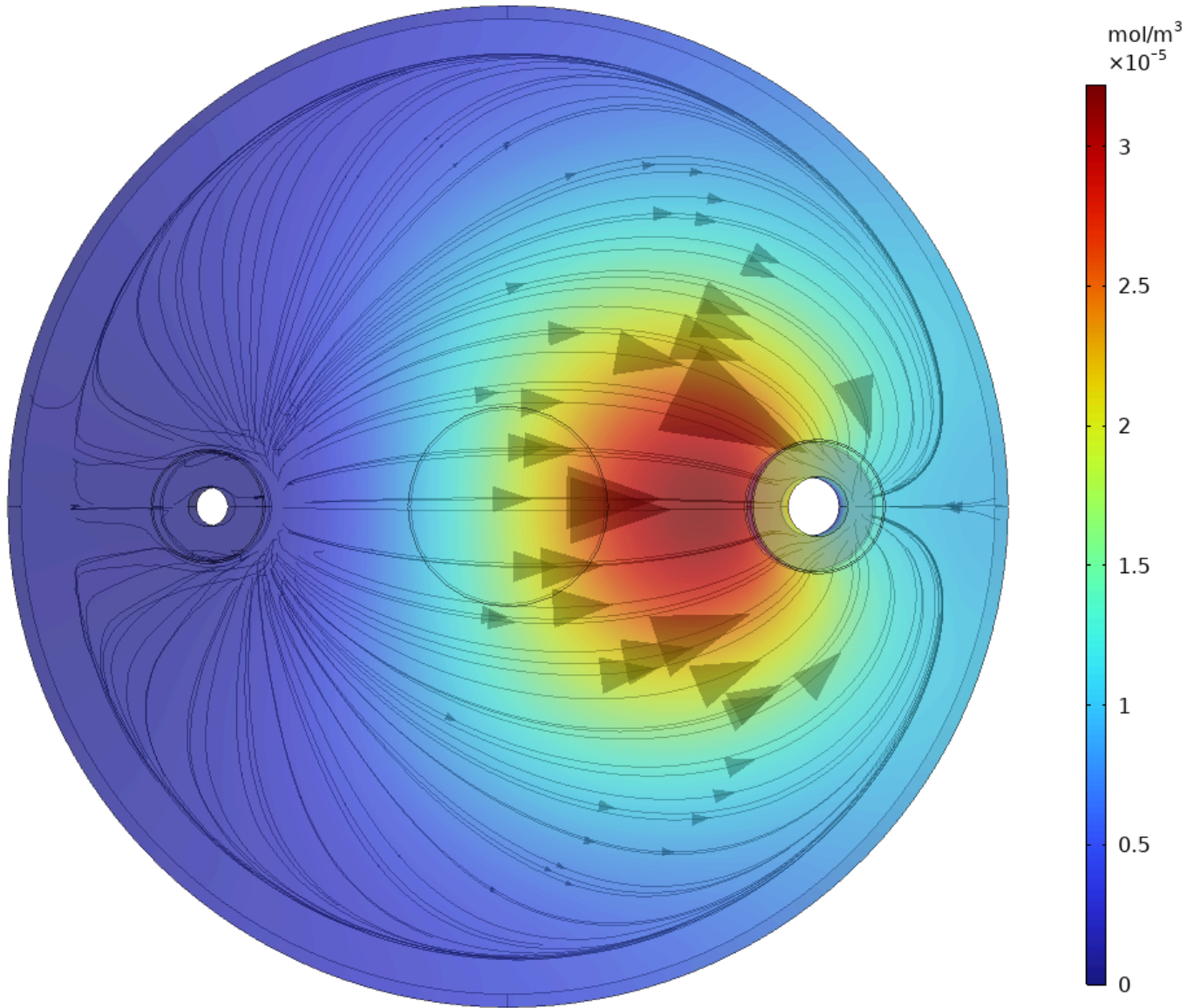


Figure 27. Concentration flux of centralized tracer at $t = 10$ s for whole FUS BBBO model

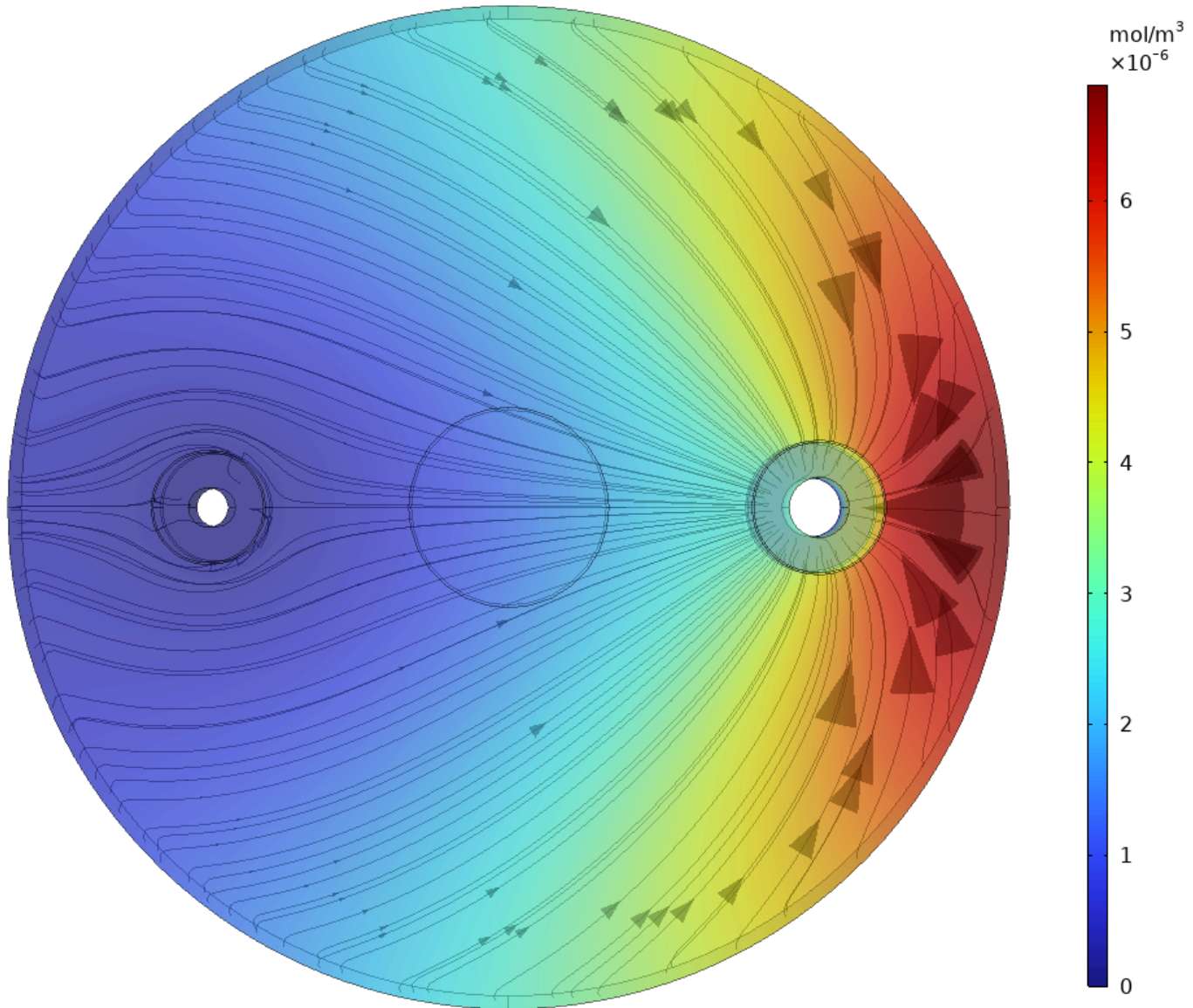


Figure 28. Concentration flux of centralized tracer at $t = 30$ s for whole FUS BBBO model

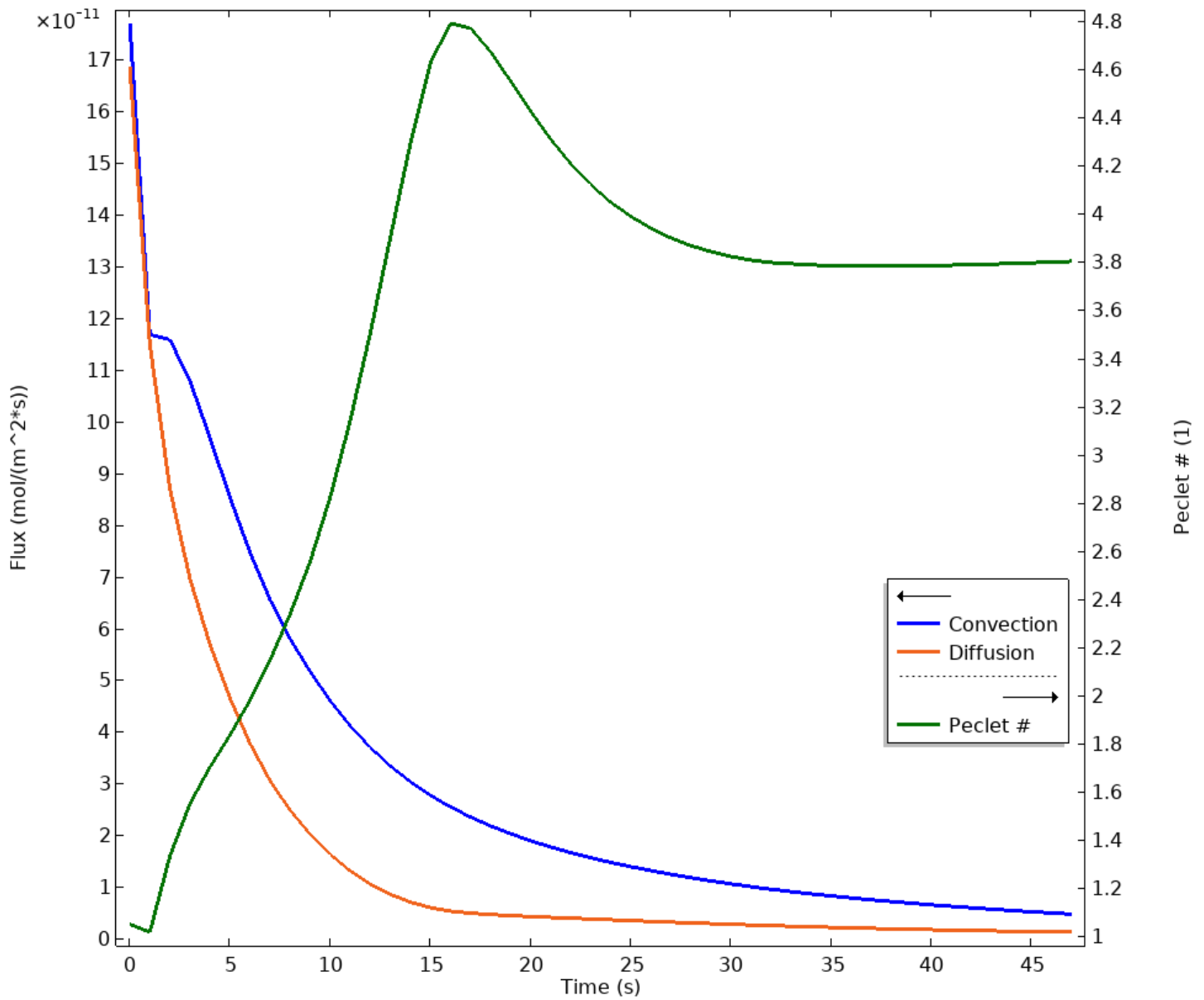


Figure 29. Relative contribution to flux and Péclet number for whole FUS BBBO model

Centralized Tracer Model Comparisons

Figures 30 and 31 show comparisons between the first four model permutations for the rate of waste clearance and the Péclet number, respectively.

Tracer Clearance

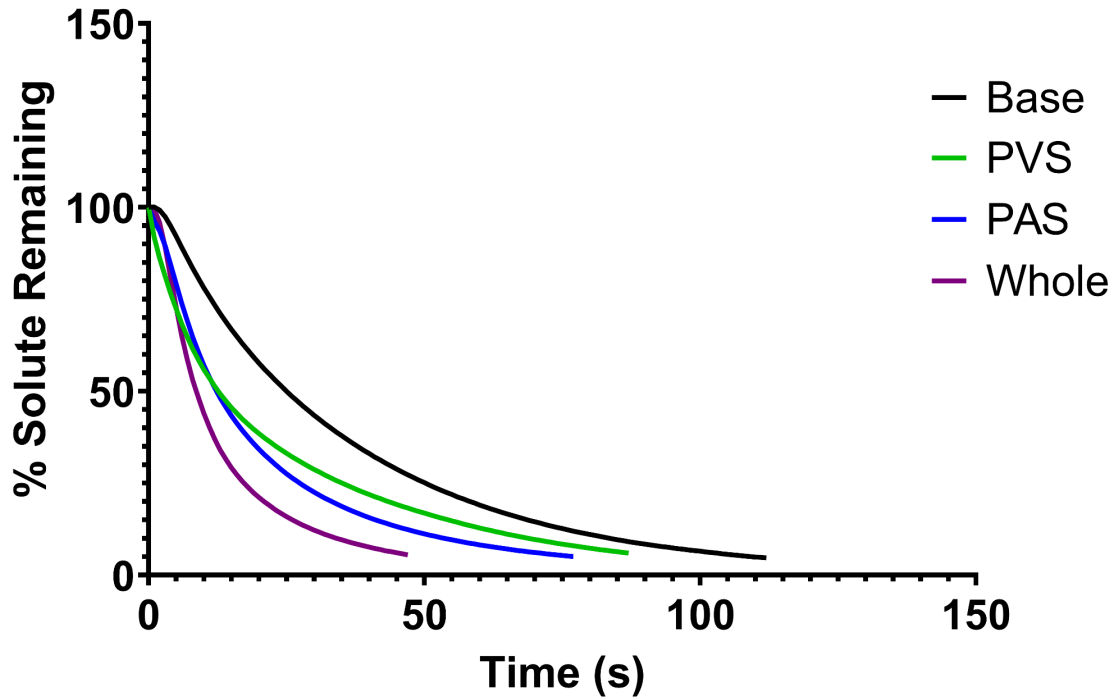


Figure 30. Tracer clearance over time for the various centralized tracer models

Contribution of Convection

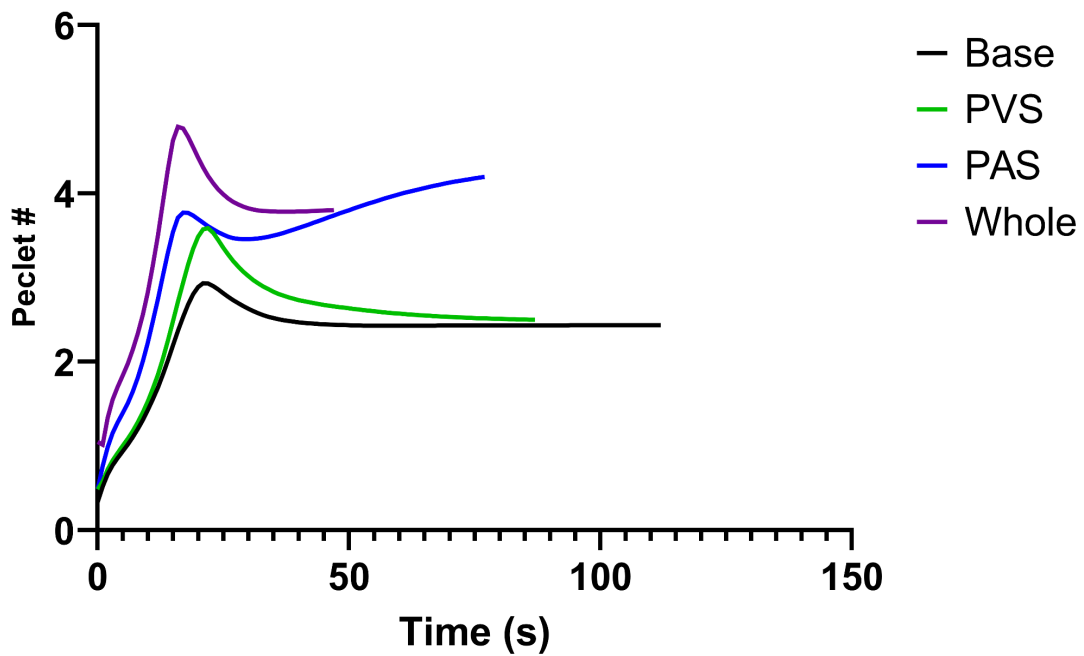


Figure 31. Péclet number for each of the centralized tracer models

Distributed Tracer Model

Figures 32-35 show the outcome of a FUS-negative model where the tracer is equally distributed among the brain parenchyma. Because the flow profile and pressure gradient will be unaffected by the solute distribution, only the concentration flux and its components are shown. The purpose of this model is to simulate a realistic alternative solute distribution in the brain with a familiar solute, to not introduce unnecessary variability.

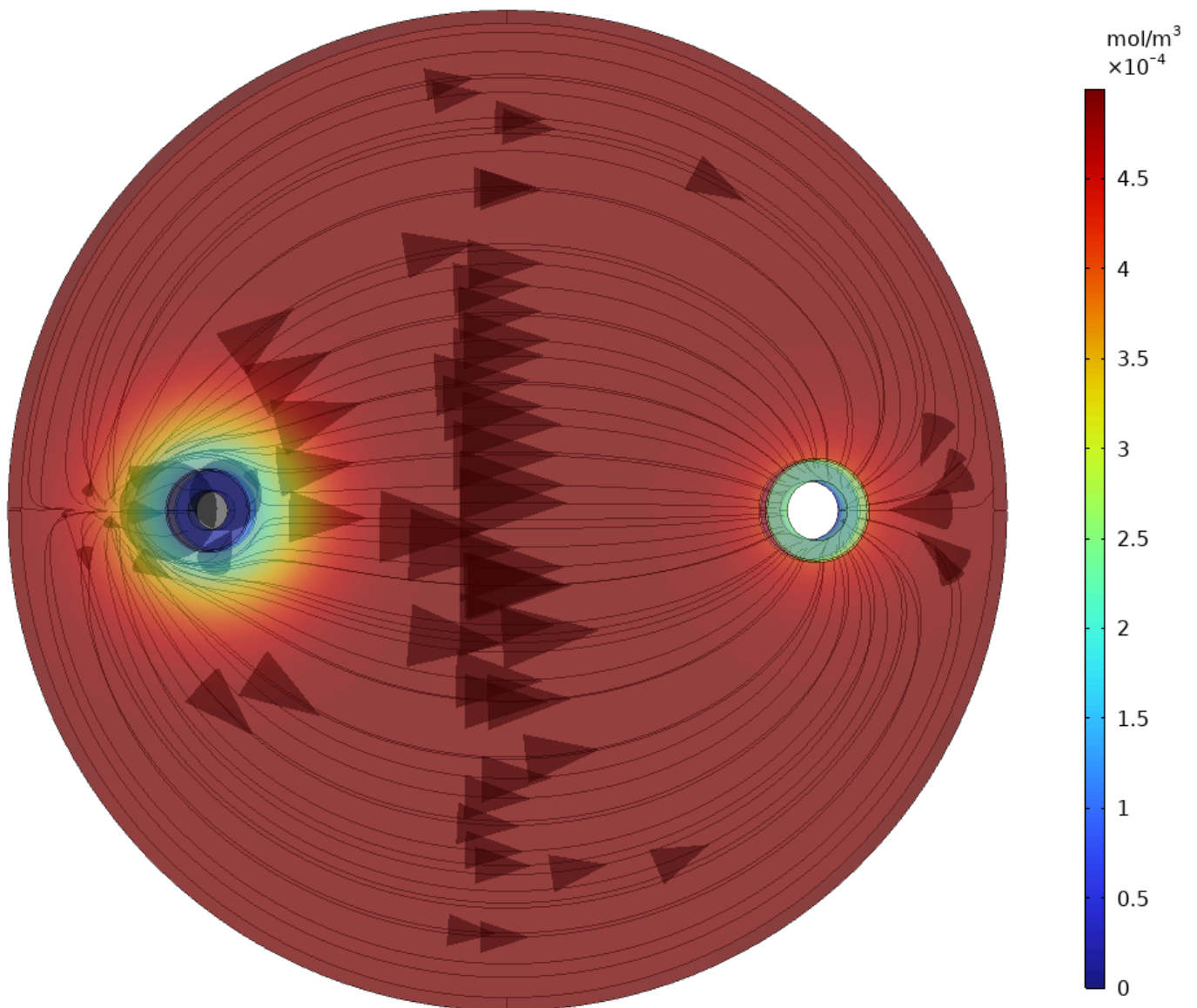


Figure 32. Concentration flux of distributed tracer at $t = 1$ s for base model

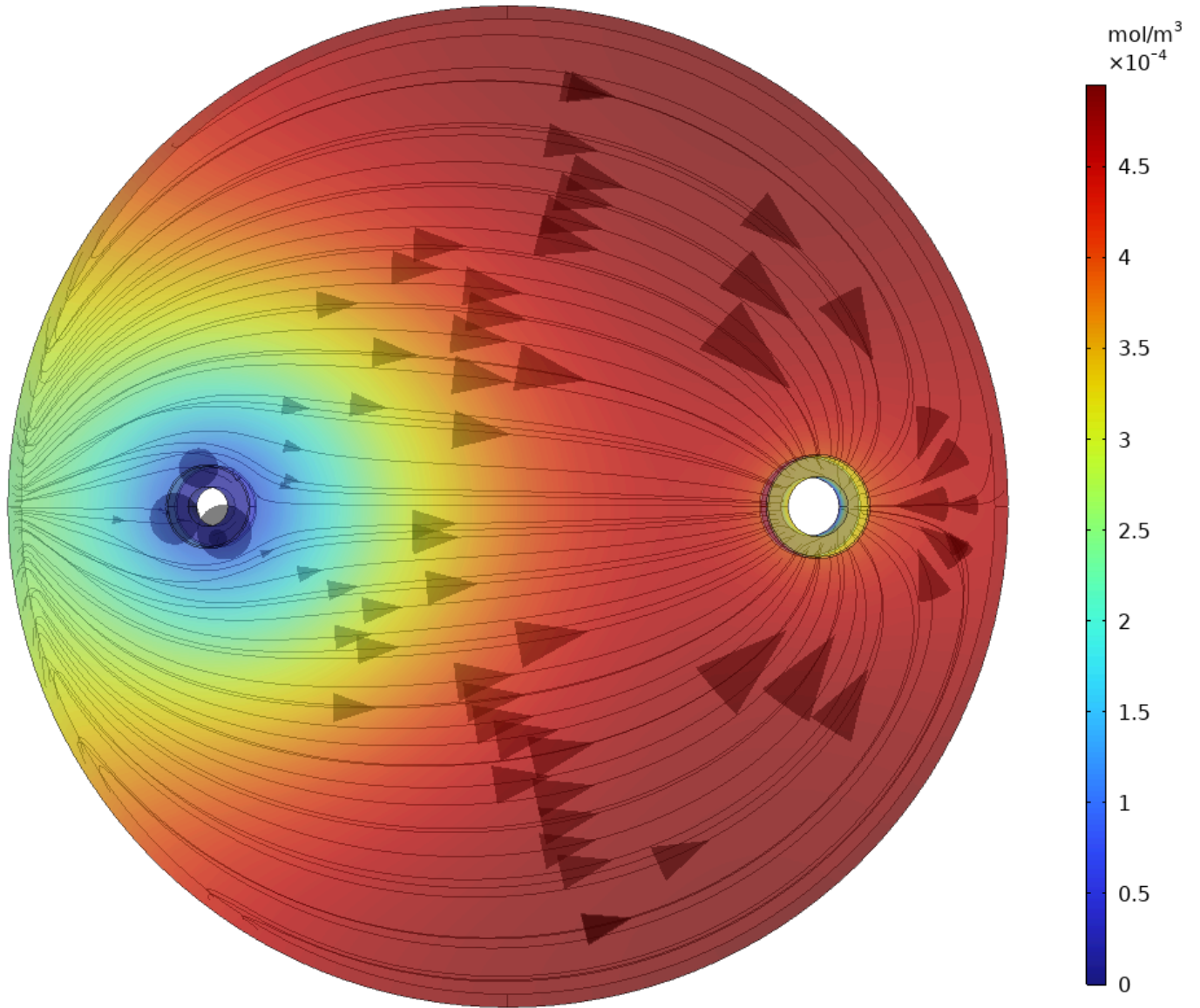


Figure 33. Concentration flux of distributed tracer at $t = 10$ s for base model

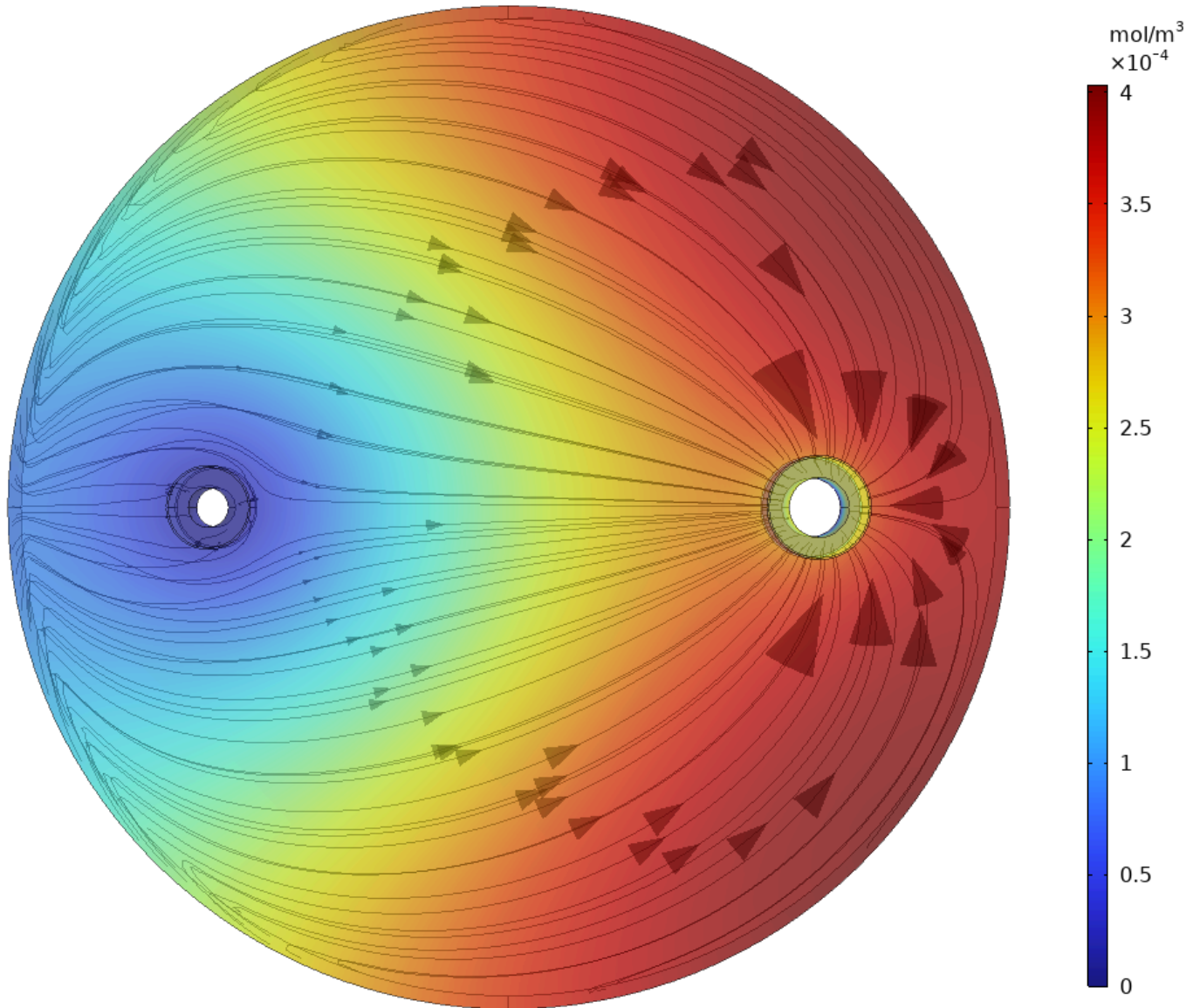


Figure 34. Concentration flux of distributed tracer at $t = 30$ s for base model

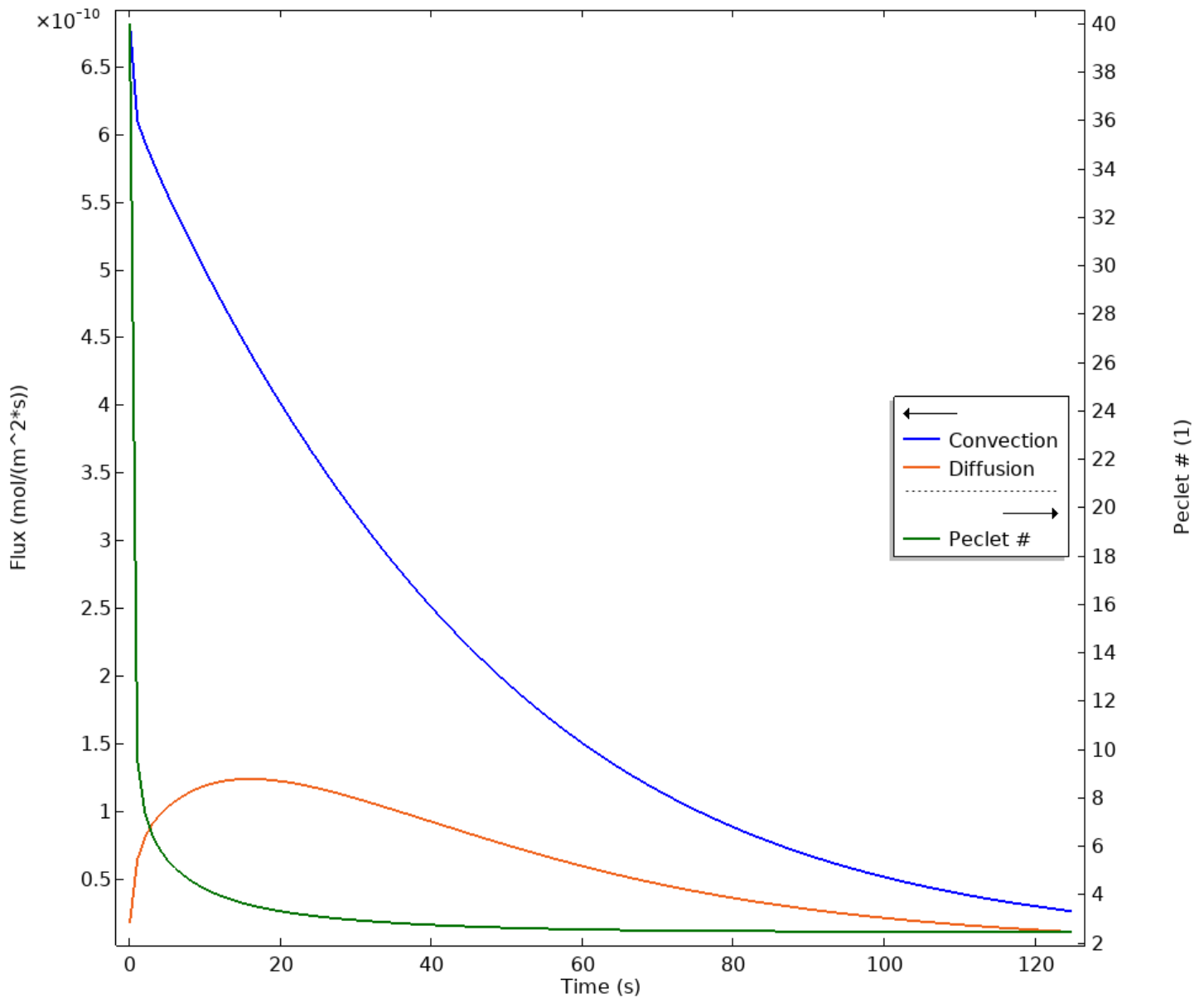


Figure 35. Relative contribution to flux and Péclet number for base distributed tracer model

Distributed Amyloid-β Model

The same experiments were tested for soluble amyloid-β, which was modeled using a diffusion coefficient of $1.8 \times 10^{-10} \frac{m^2}{s}$. This model simulates the baseline glymphatic clearance of amyloid-β, a hallmark lipoprotein that accumulates in the pathogenesis of AD. The results are shown in Figures 36-39.

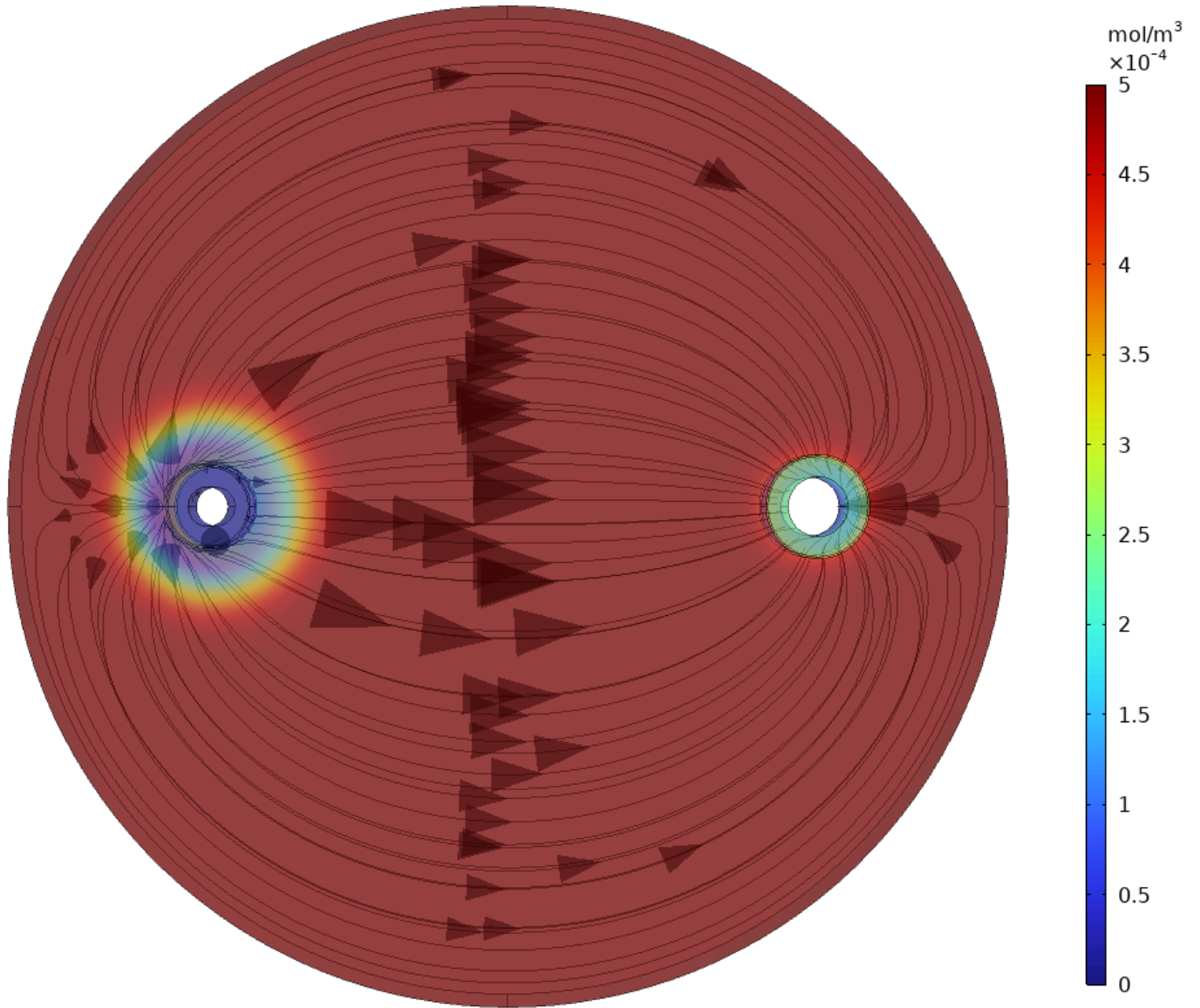


Figure 36. Concentration flux of distributed amyloid- β at $t = 1$ s for base model

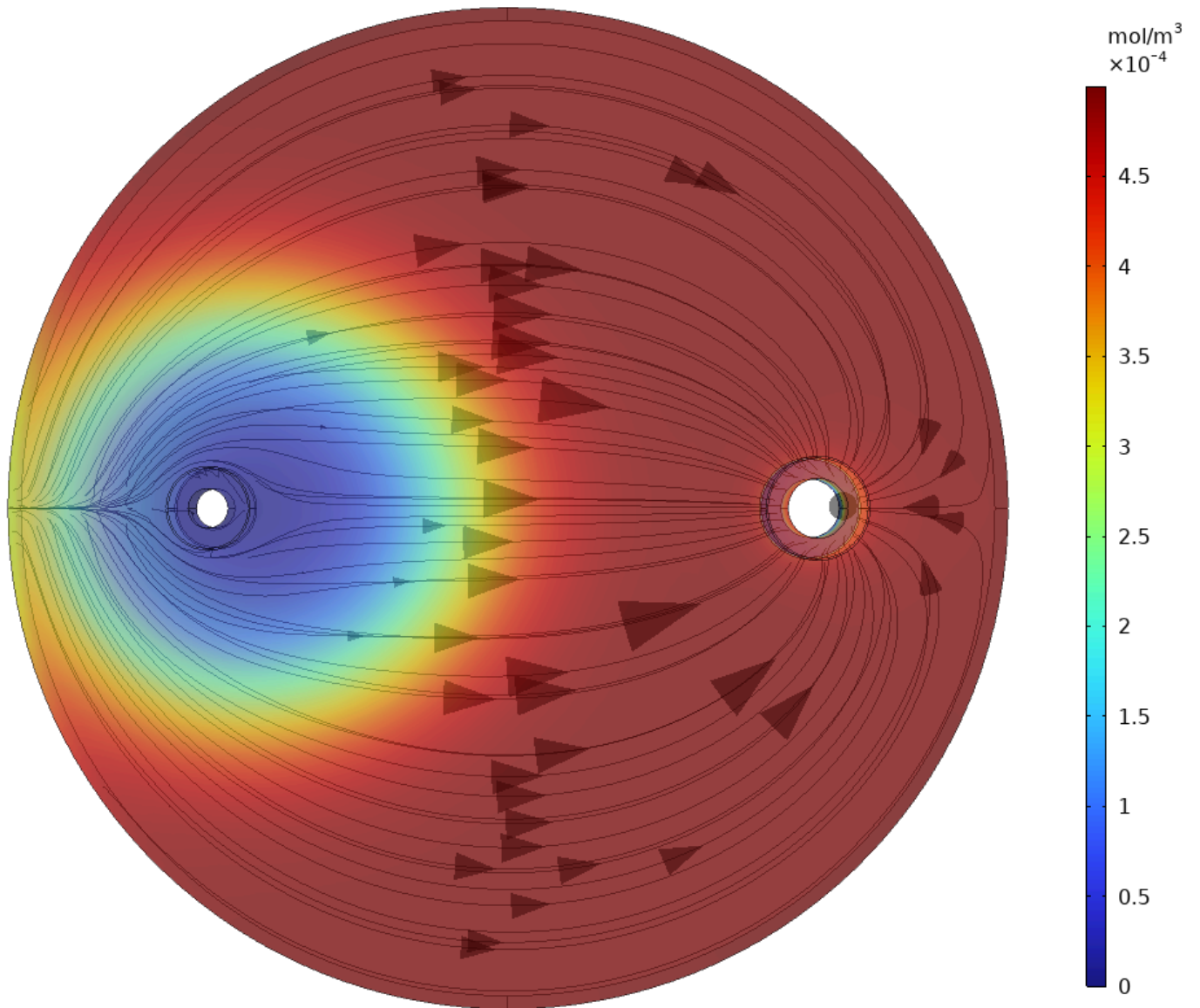


Figure 37. Concentration flux of distributed amyloid- β at $t = 10$ s for base model

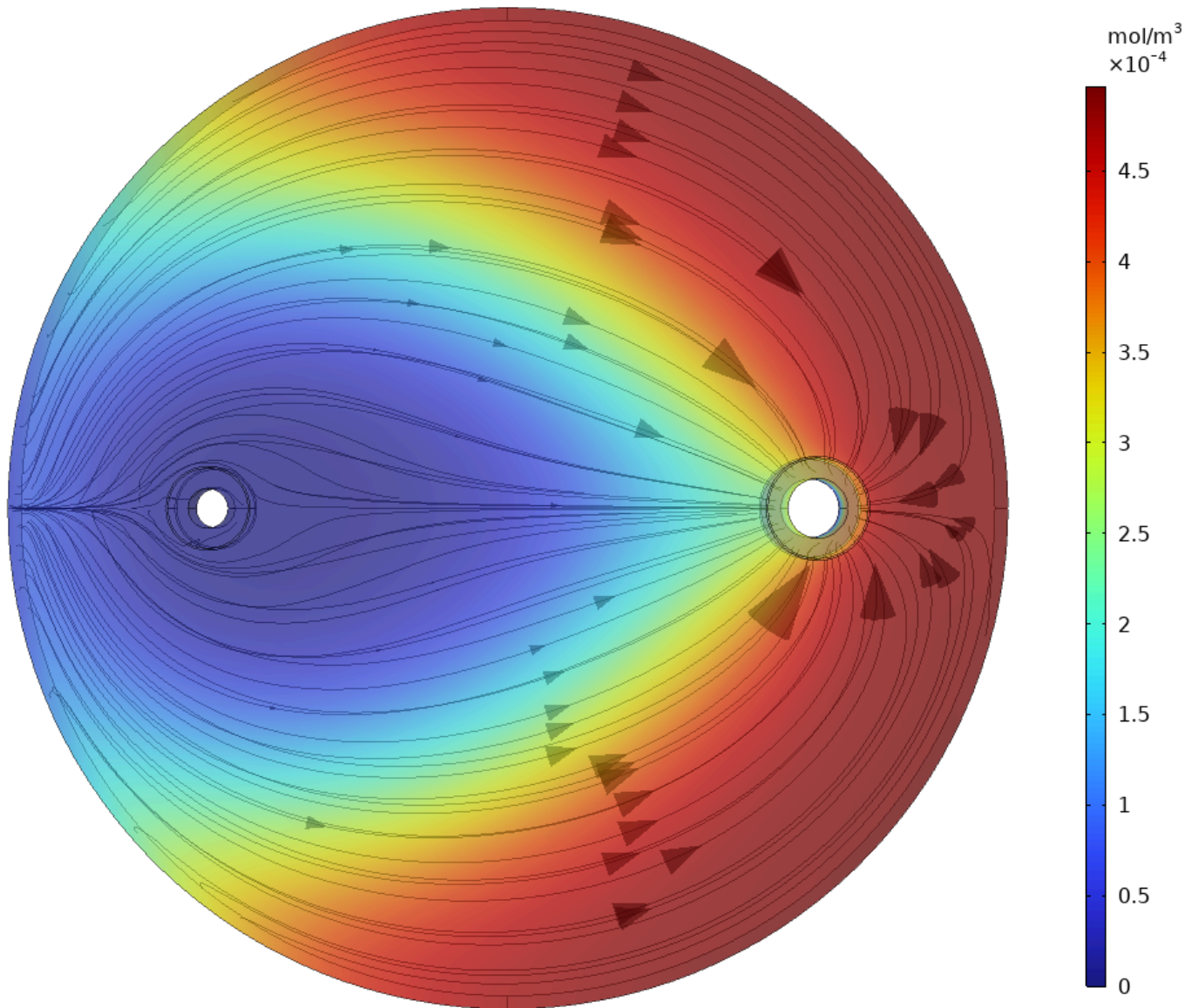


Figure 38. Concentration flux of distributed amyloid- β at $t = 30$ s for base model

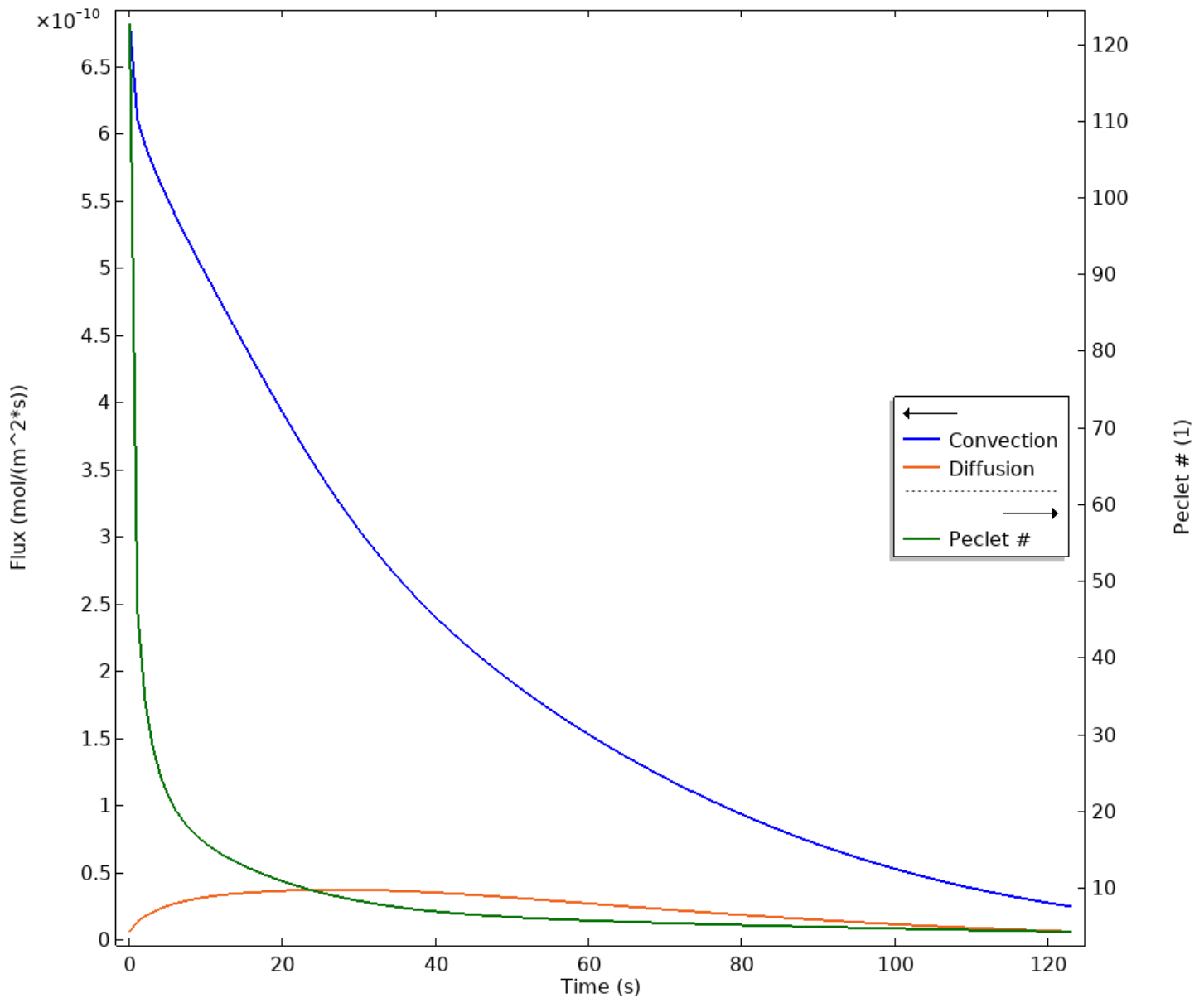


Figure 39. Relative contribution to flux and Péclet number for base distributed Amyloid-β model

Distributed α-Synuclein Model

The same experiments were tested for α-synuclein, a hallmark protein in PD with a DC of $7.8 \times 10^{-10} \frac{m^2}{s}$. The results are shown in Figures 40-43. This model aims to establish baseline glymphatic clearance of a different pathological solute which is common in neurodegenerative diseases.

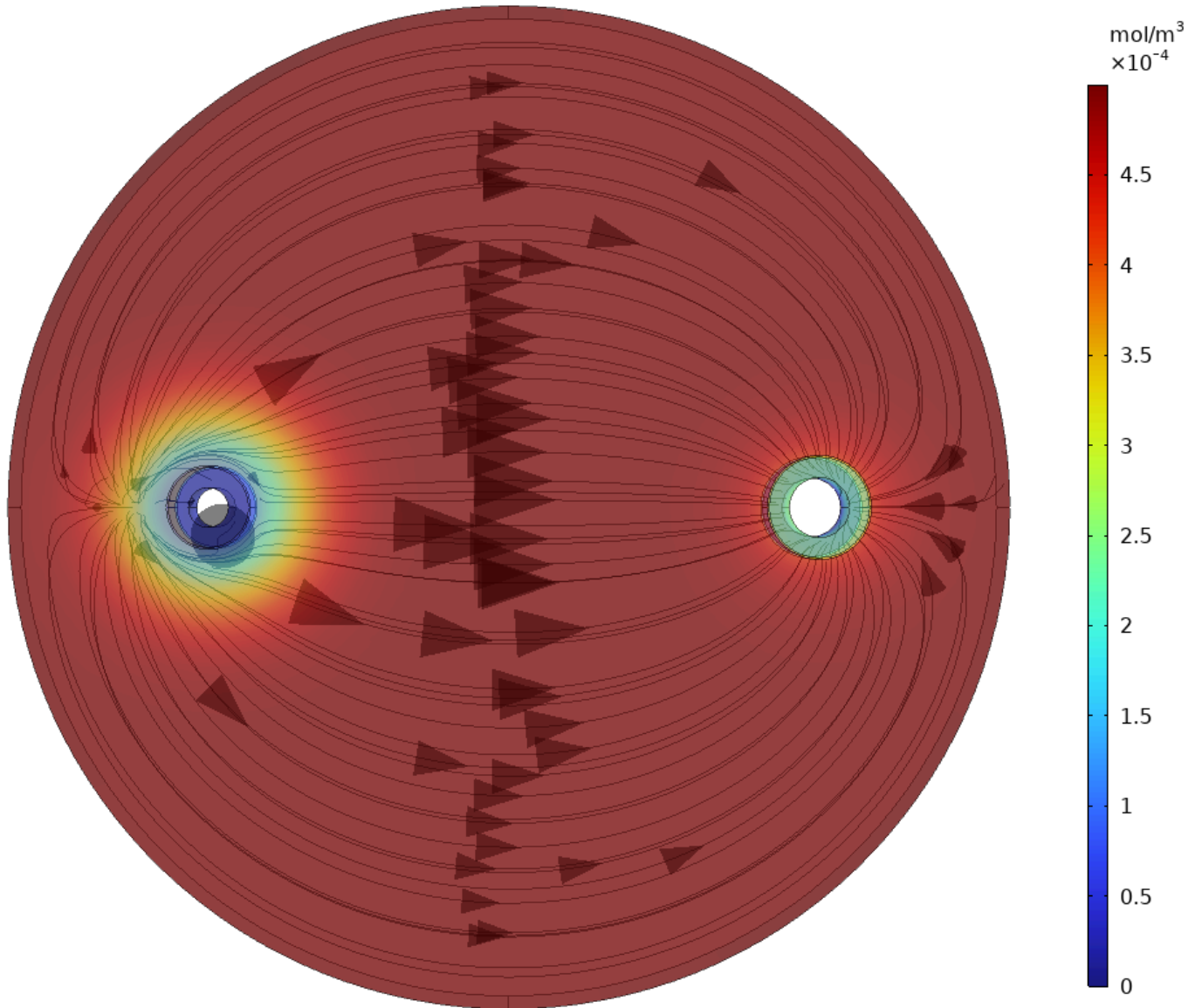


Figure 40. Concentration flux of distributed α -synuclein at $t = 1$ s for base model

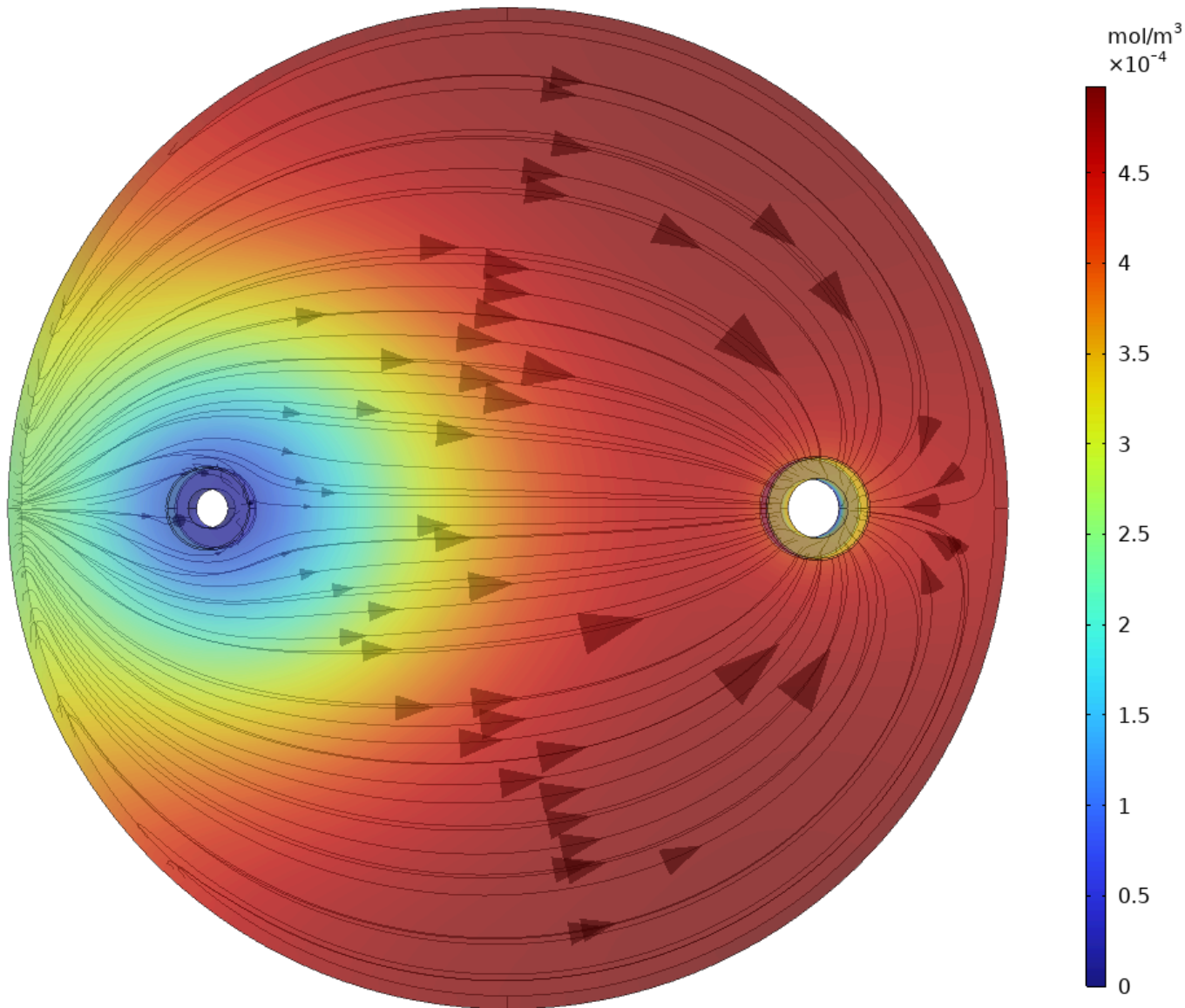


Figure 41. Concentration flux of distributed α -synuclein at $t = 10$ s for base model

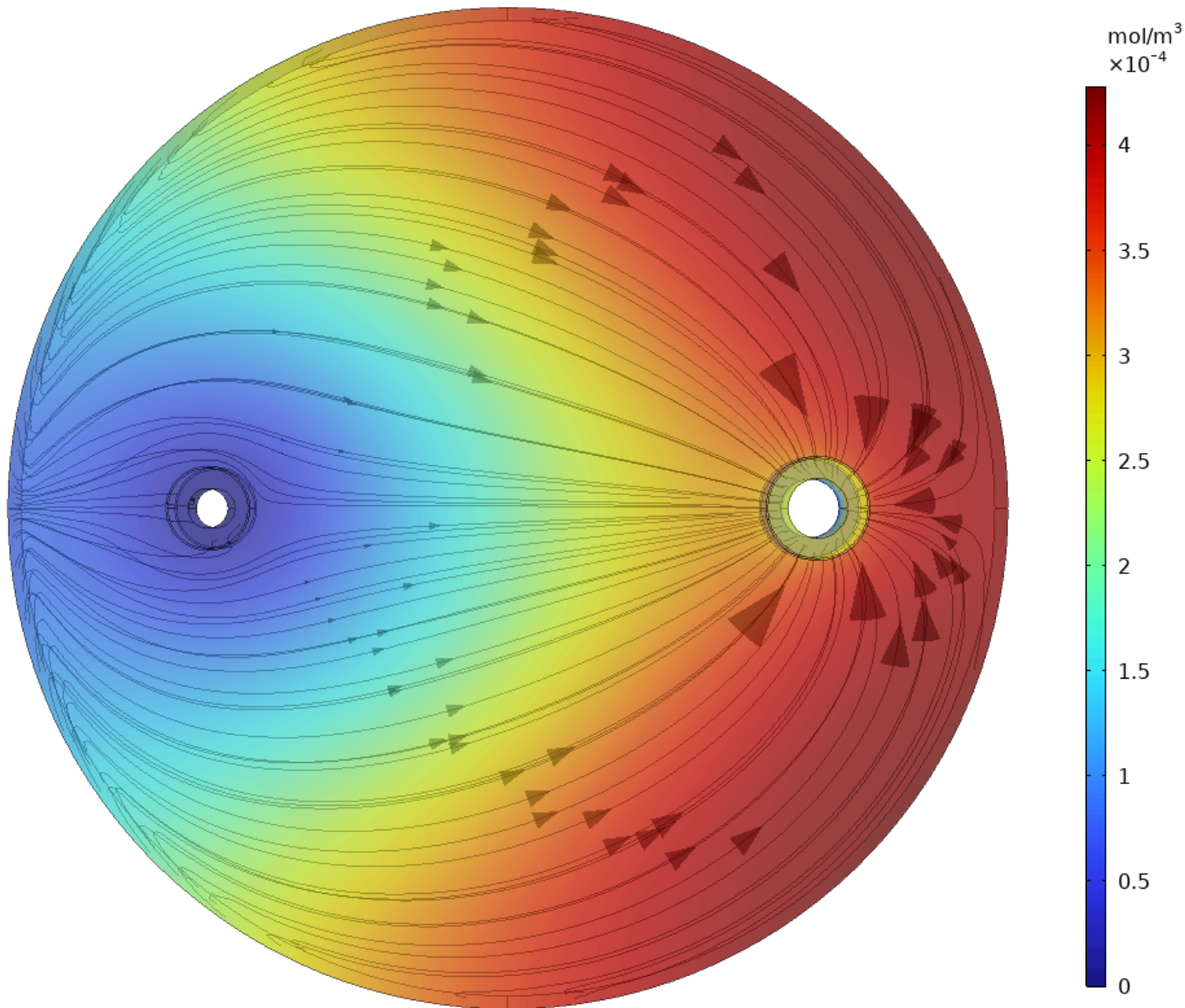


Figure 42. Concentration flux of distributed α -synuclein at $t = 30$ s for base model

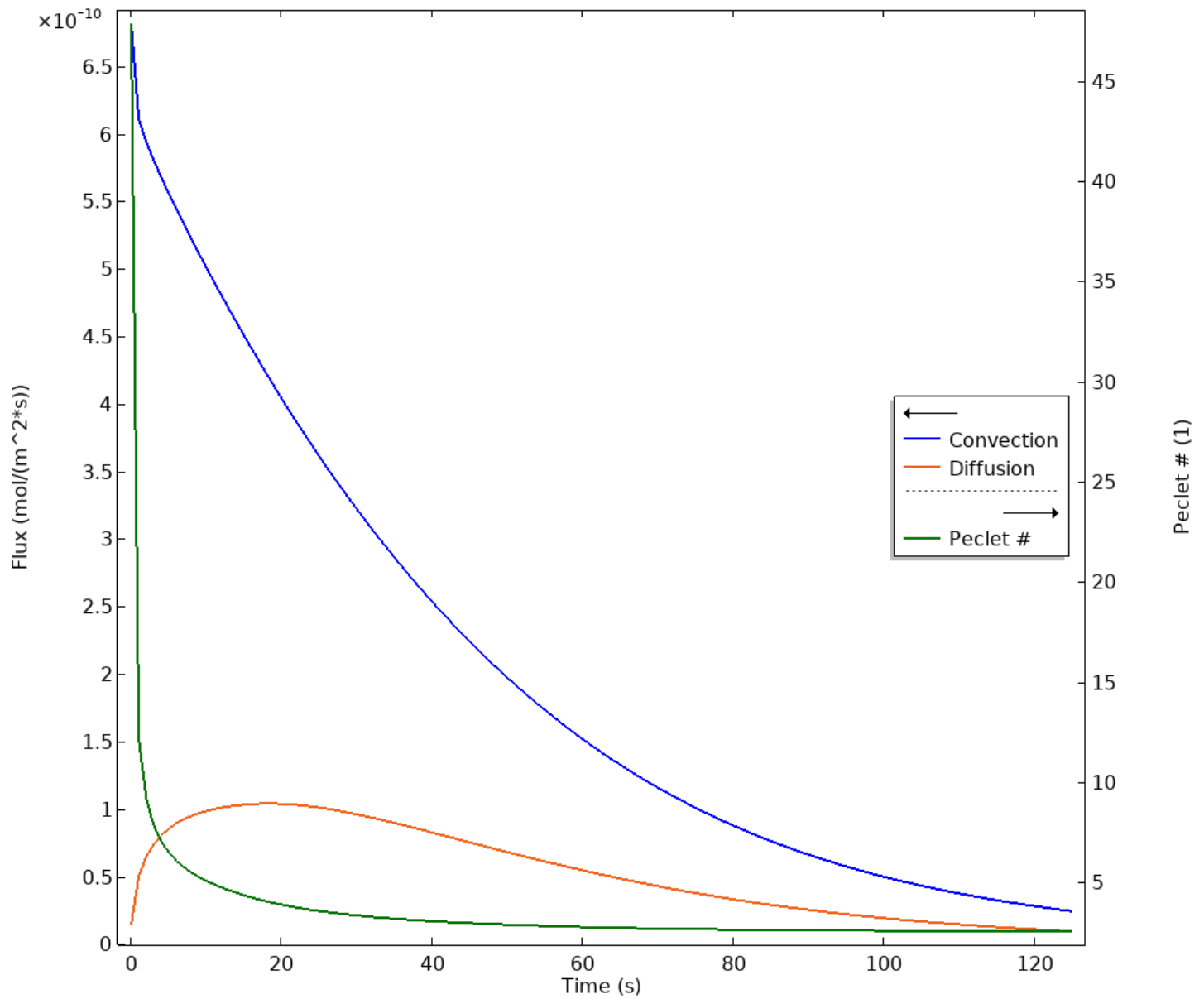


Figure 43. Relative contribution to flux and Péclet number for base distributed α -Synuclein model

Distributed Tracer FUS Model

Figures 44-47 show the simulations of a distributed FUS BBBO model. This model illustrates how FUS BBBO affects the clearance of tracer when it is evenly distributed throughout the brain parenchyma.

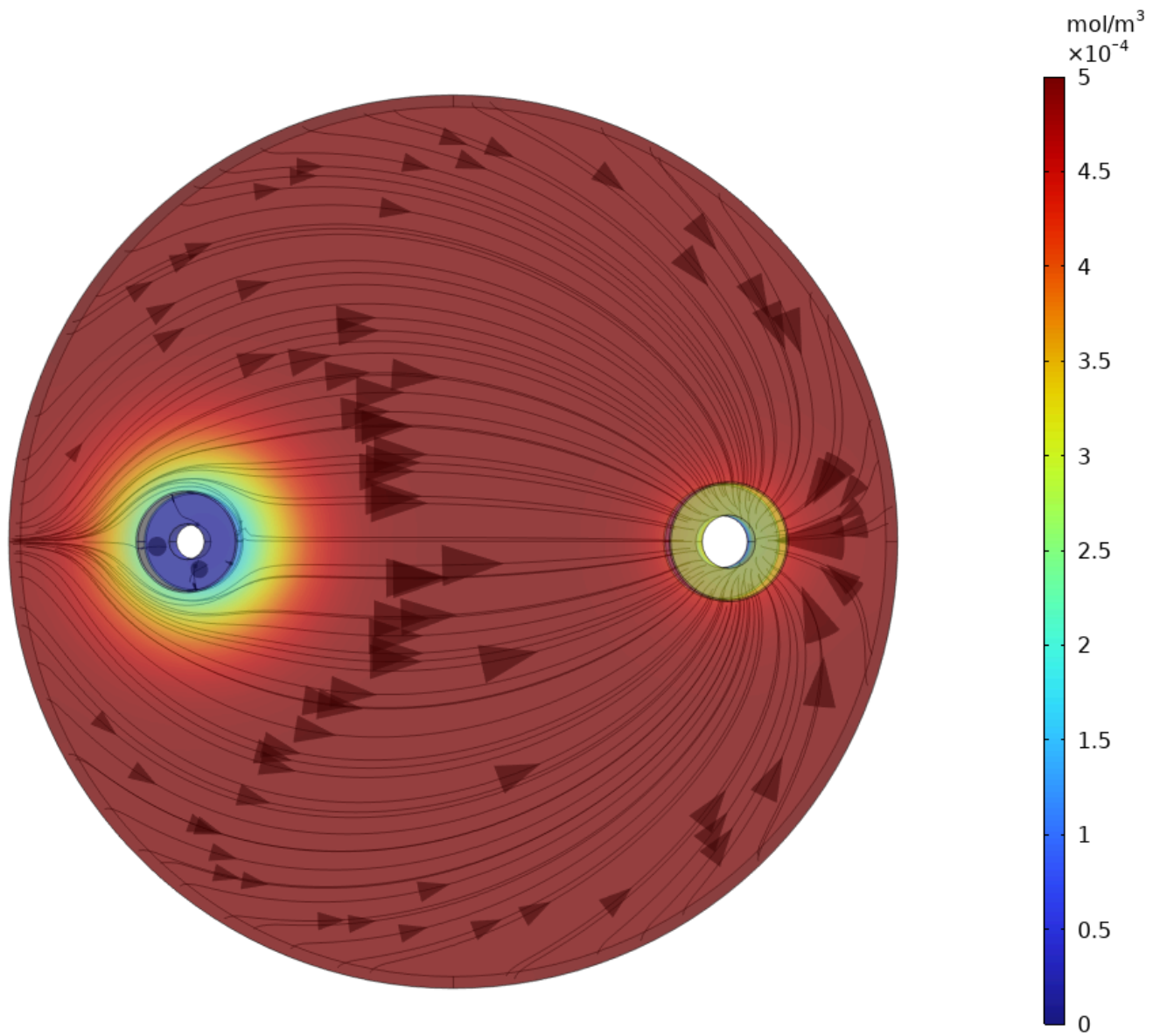


Figure 44. Concentration flux of distributed tracer at $t = 1$ s for FUS BBBO model

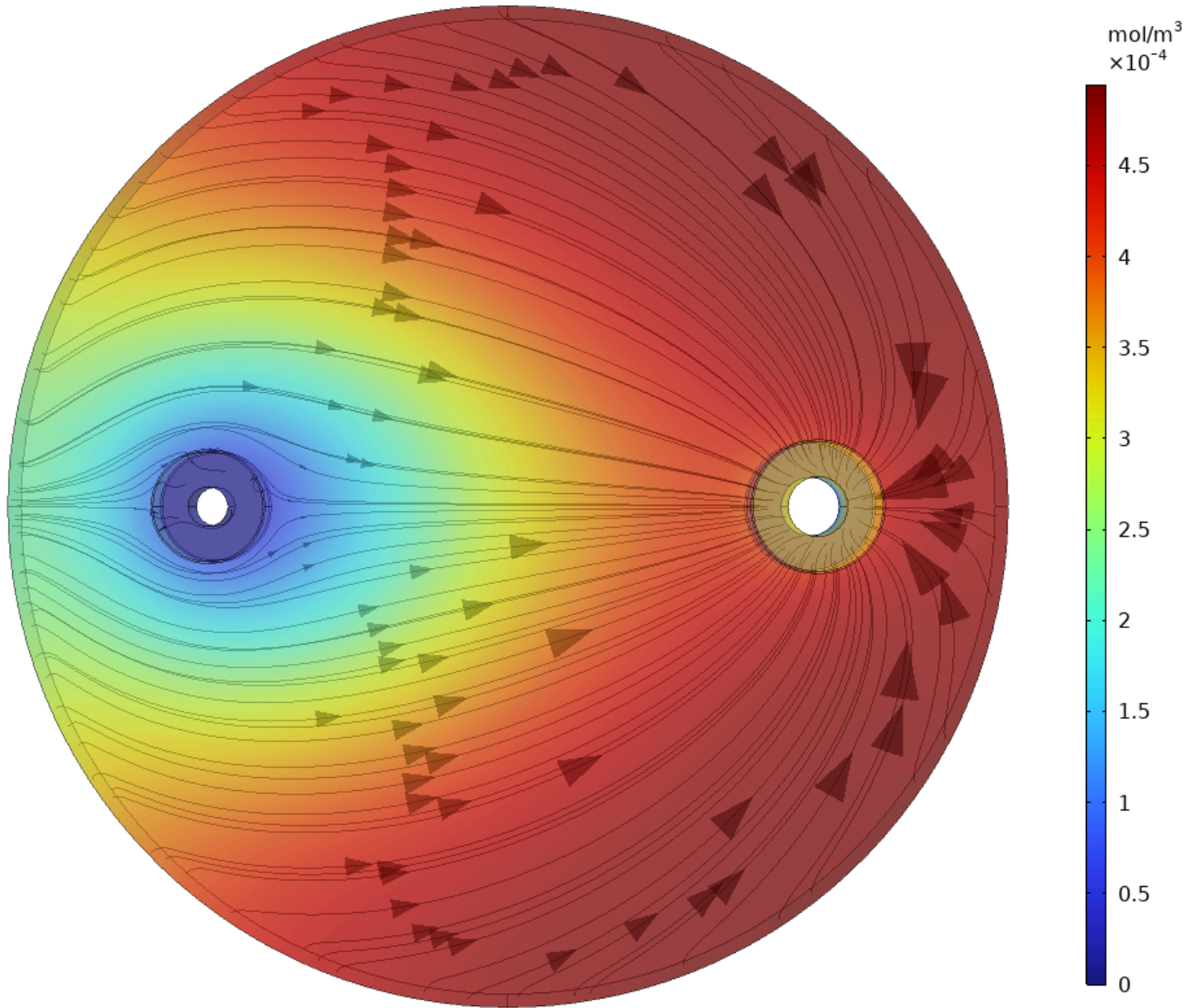


Figure 45. Concentration flux of distributed tracer at $t = 10$ s for FUS BBBO model

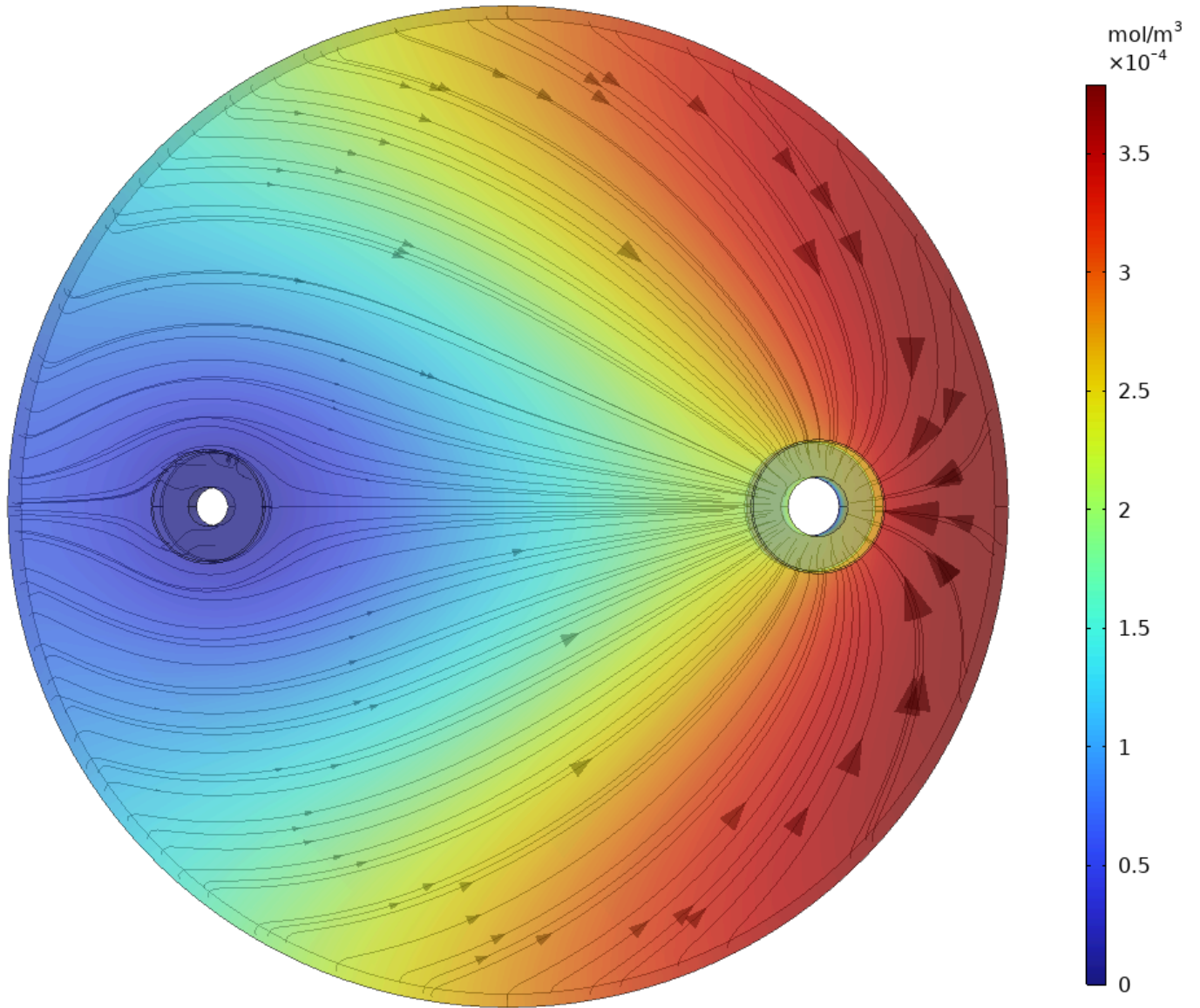


Figure 46. Concentration flux of distributed tracer at $t = 30$ s for FUS BBBO model

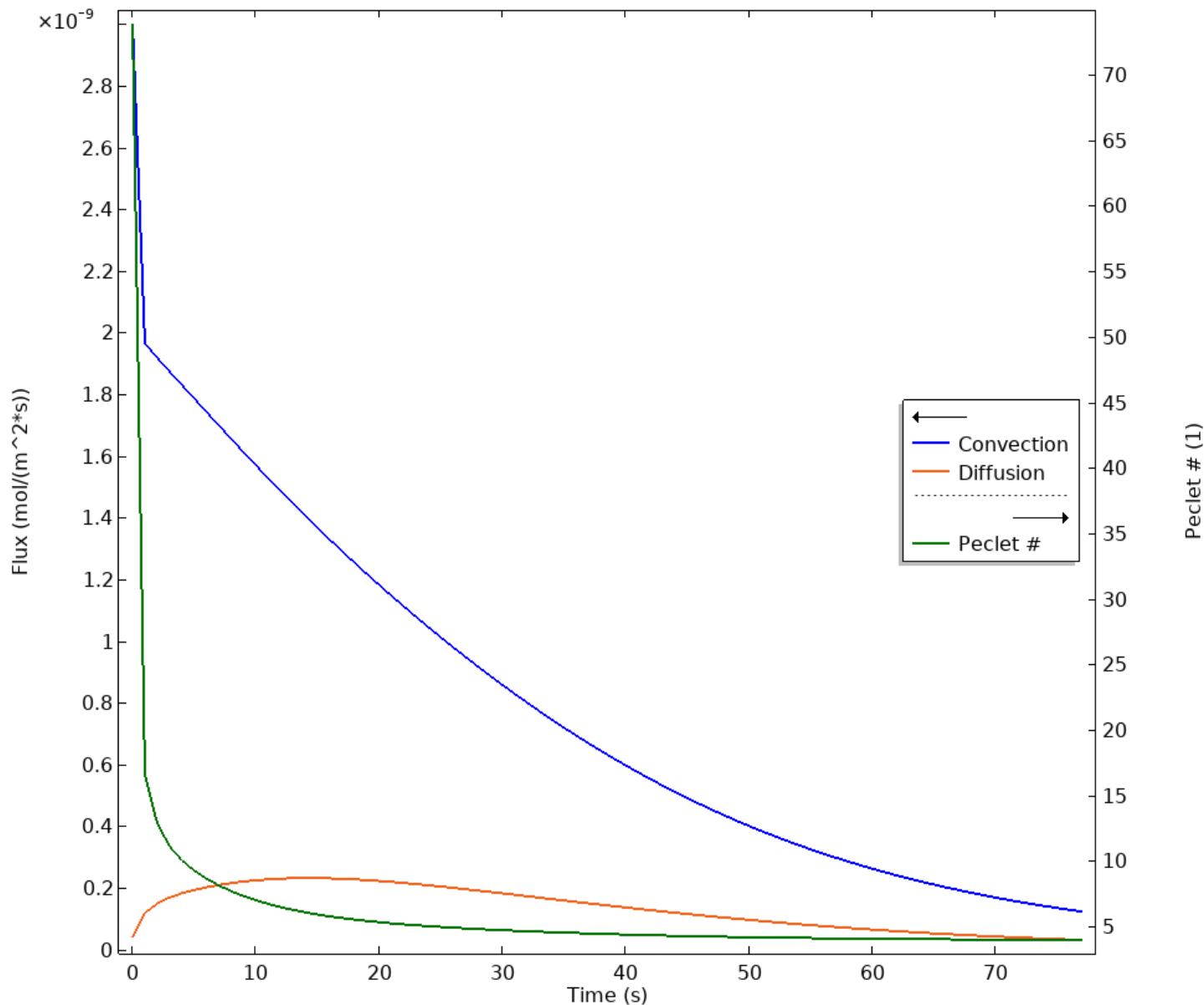


Figure 47. Relative contribution to flux and Péclet number for FUS BBBO distributed tracer model

Distributed Amyloid- β FUS Model

Figures 48-51 show the outcomes of simulations of a distributed Amyloid- β FUS BBBO model. This model aims to evaluate the therapeutic mechanism that FUS has demonstrated for clearing soluble amyloid- β .

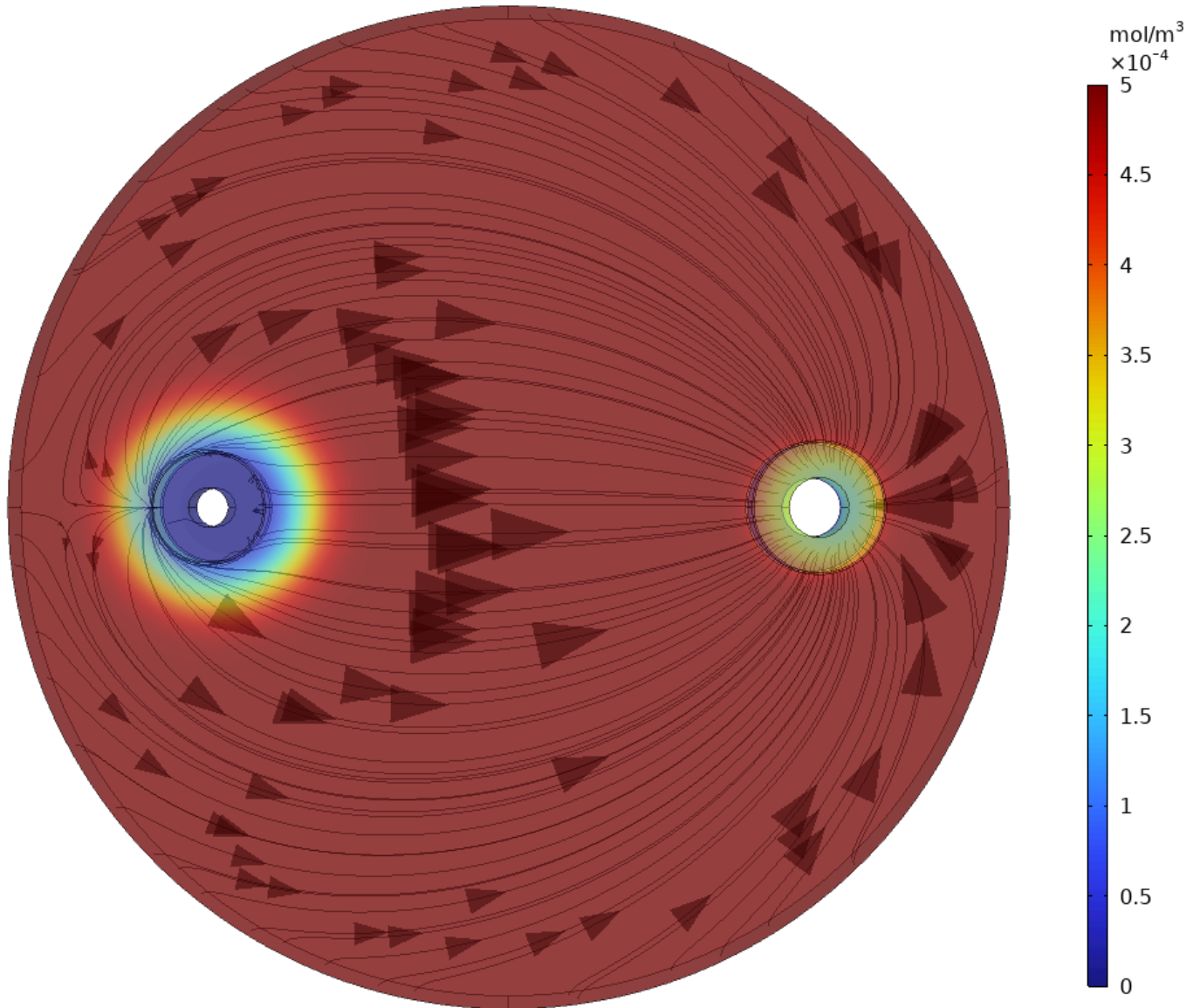


Figure 48. Concentration flux of distributed Amyloid- β at $t = 1$ s for FUS BBBO model

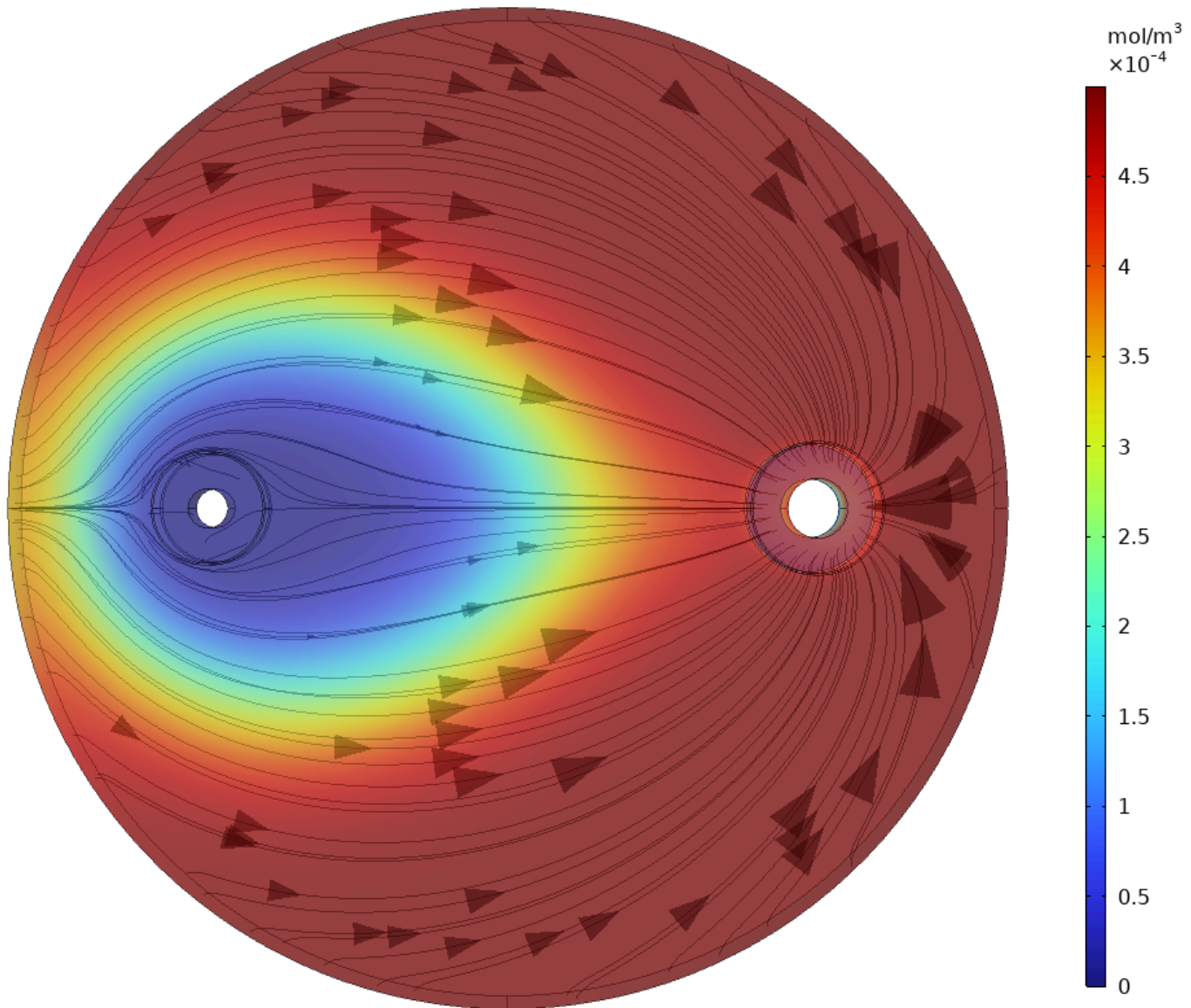


Figure 49. Concentration flux of distributed Amyloid- β at $t = 10$ s for FUS BBBO model

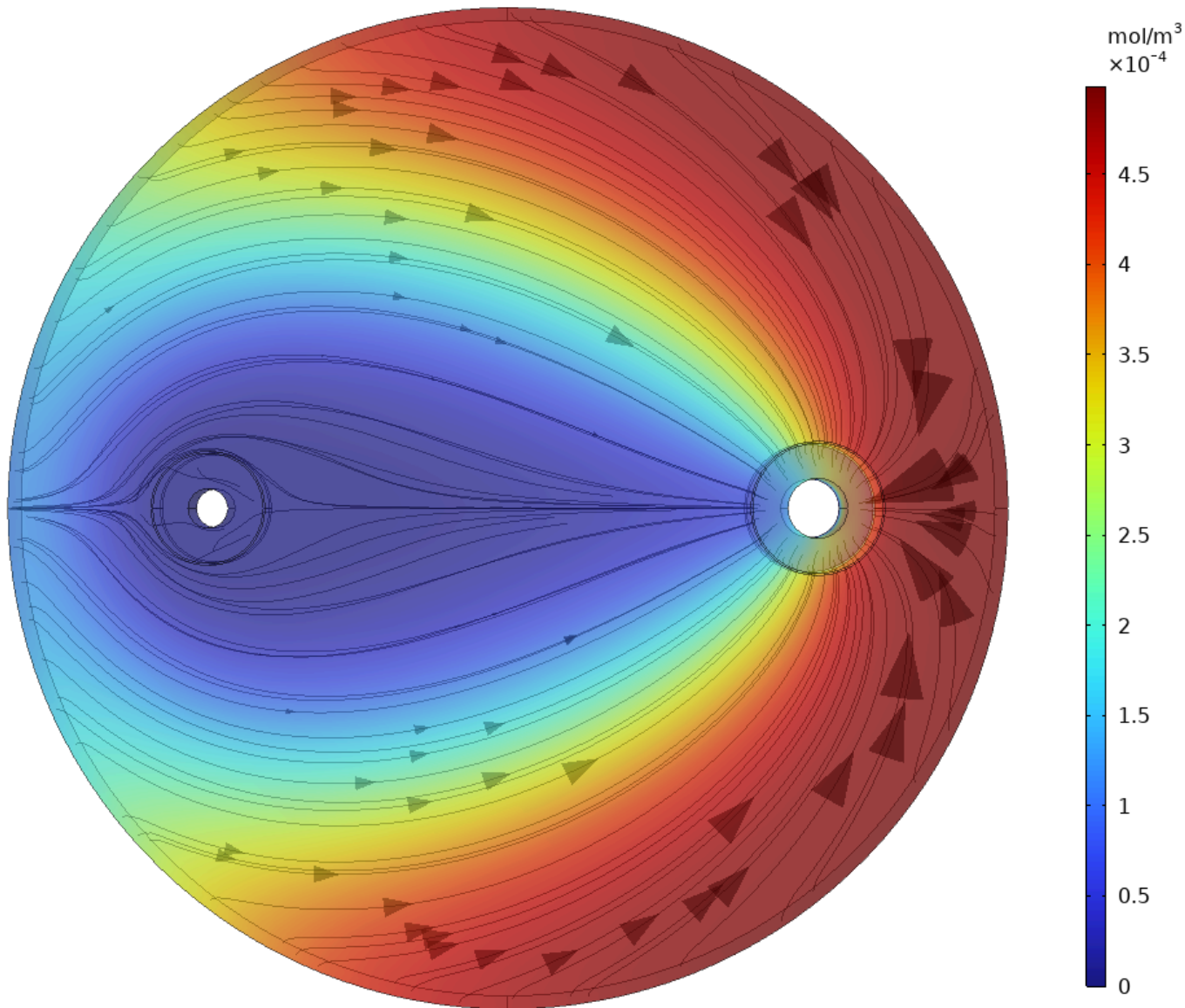


Figure 50. Concentration flux of distributed Amyloid- β at $t = 30$ s for FUS BBBO model

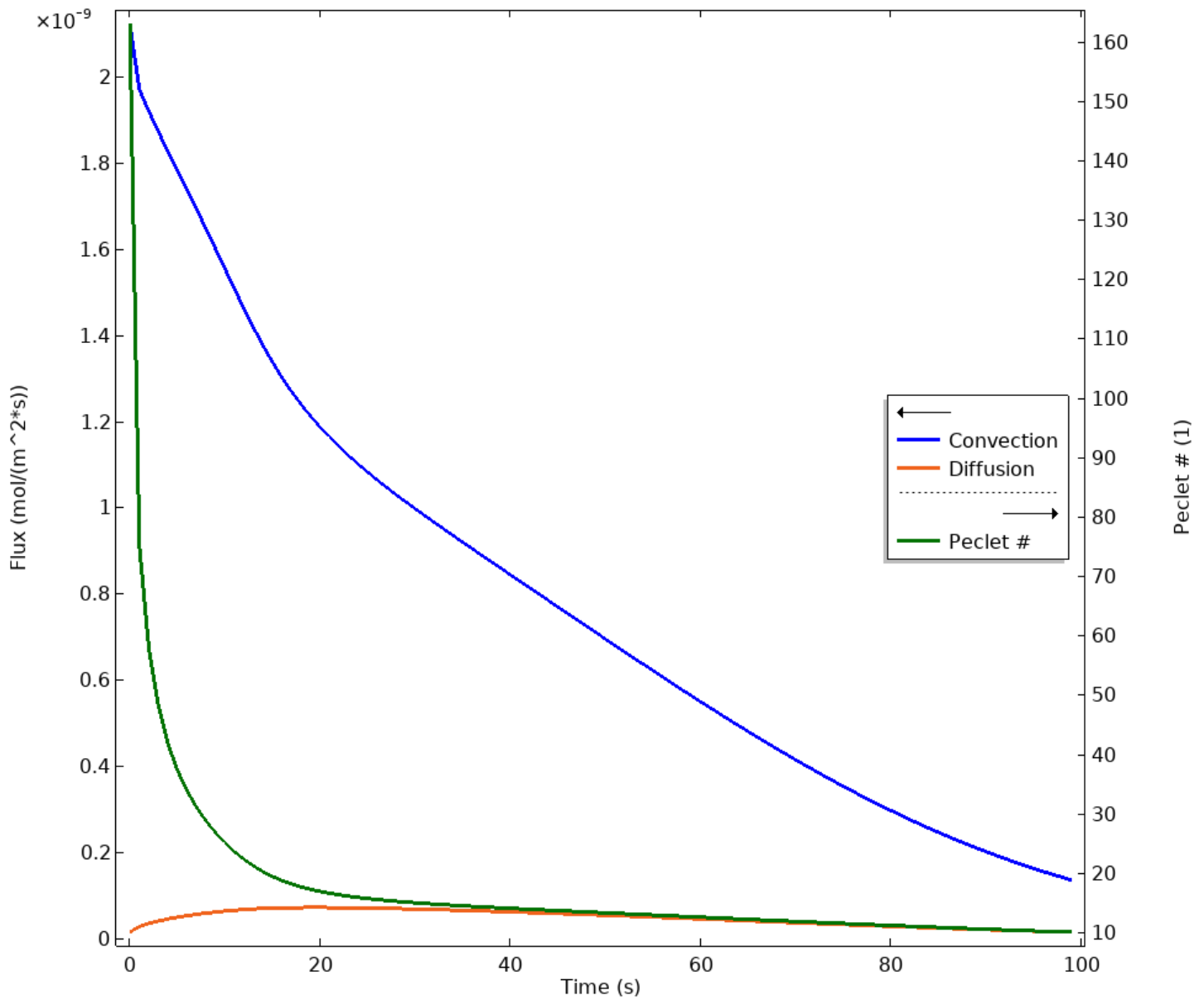


Figure 51. Relative contribution to flux and Péclet number for FUS BBBO distributed amyloid- β model

Distributed α -Synuclein FUS Model

Figures 52-55 show the outcomes of simulations of a distributed α -Synuclein FUS BBBO model. The purpose of this model is to evaluate the solute-specific effects of FUS BBBO, while also exploring its therapeutic potential on different diseases.

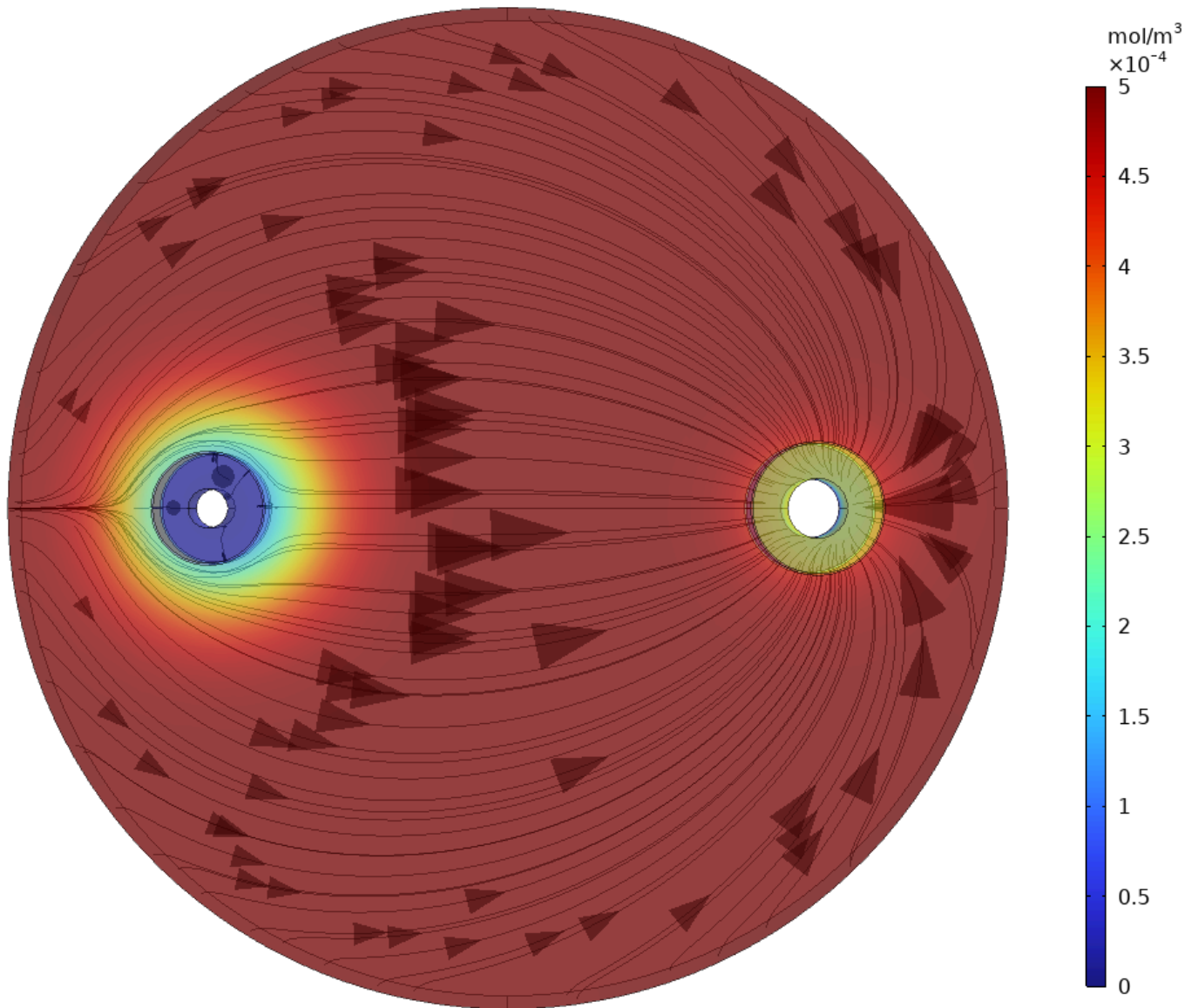


Figure 52. Concentration flux of distributed α -Synuclein at $t = 1$ s for FUS BBBO model

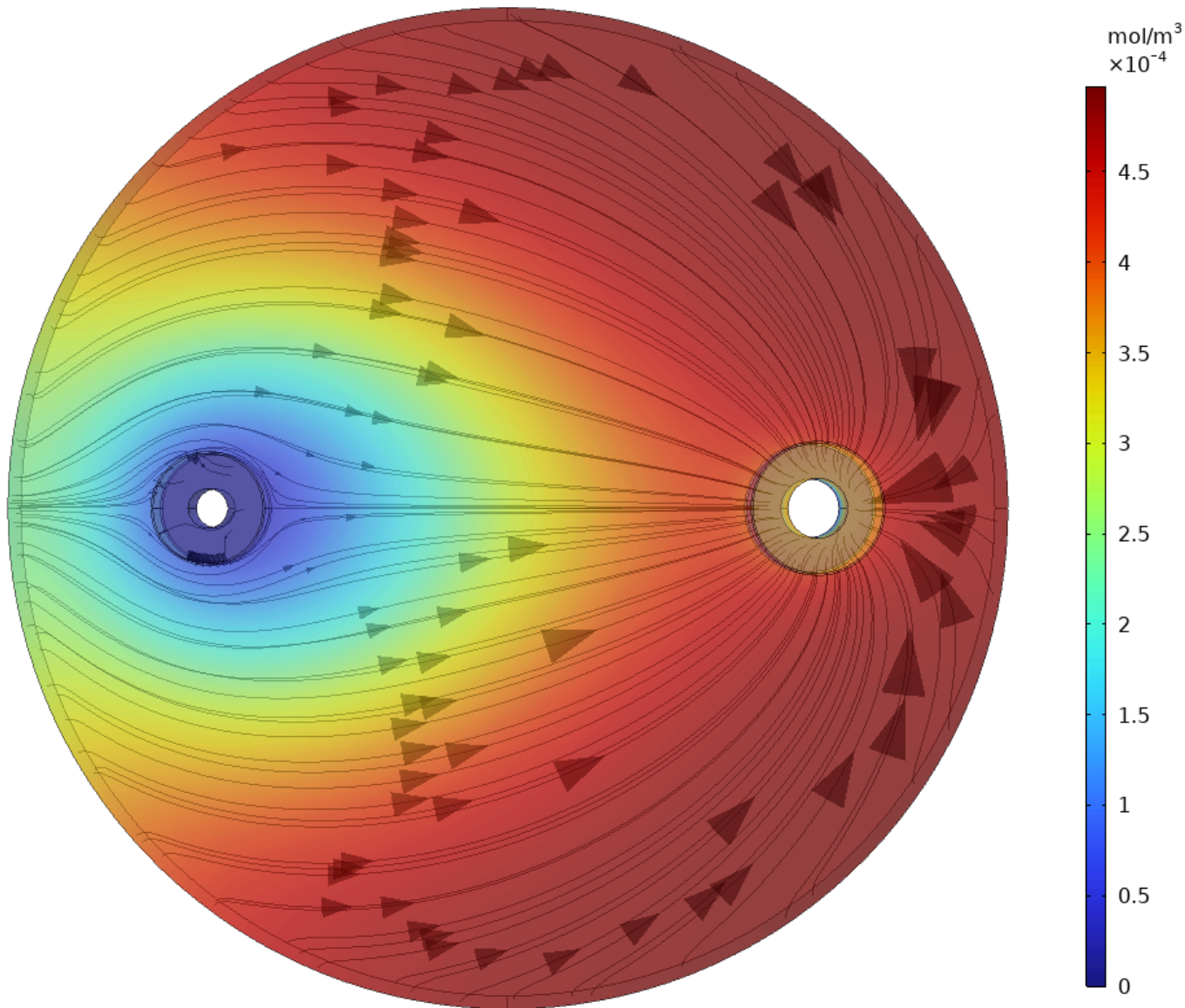


Figure 53. Concentration flux of distributed α -Synuclein at $t = 10$ s for FUS BBBO model

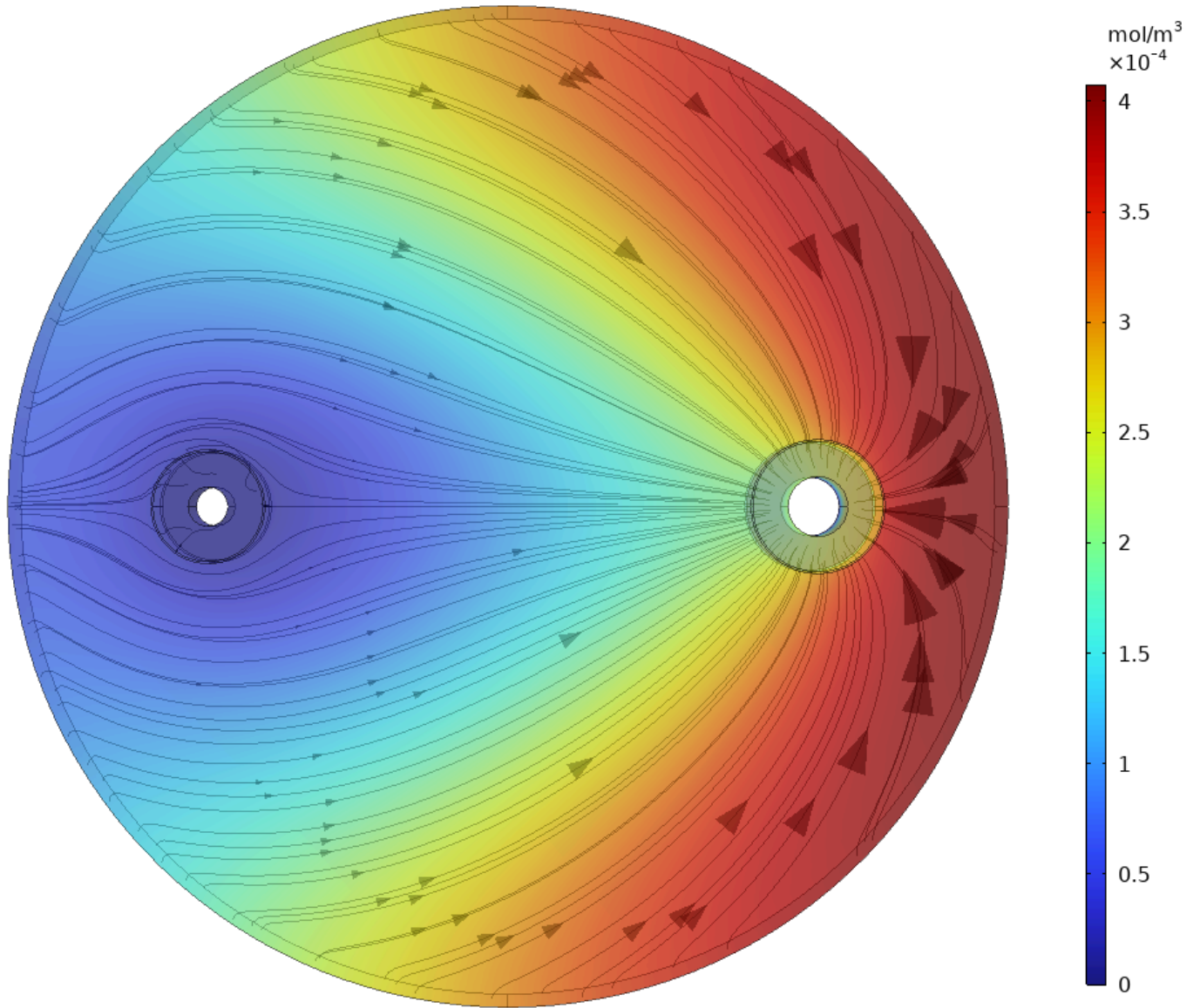


Figure 54. Concentration flux of distributed α -Synuclein at $t = 30$ s for FUS BBBO model

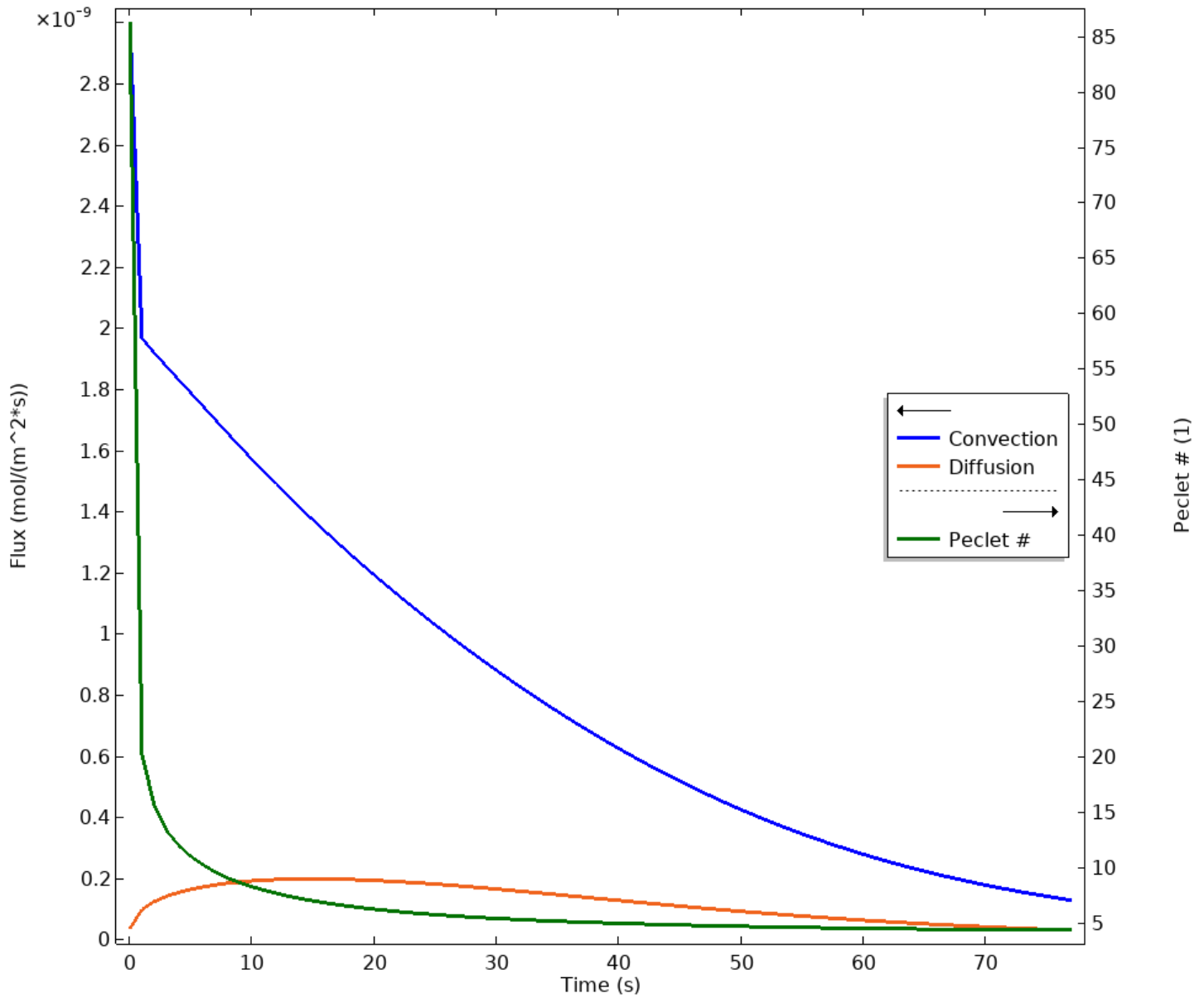


Figure 55. Relative contribution to flux and Péclet number for FUS BBBO Distributed a-Synuclein model

Distributed Solute Model Comparisons

The following figures demonstrate how FUS BBBO affects glymphatic waste clearance for the three modeled solutes. These graphs demonstrate the rate of solute clearance.

Distributed Solute Model Rate of Clearance Comparisons

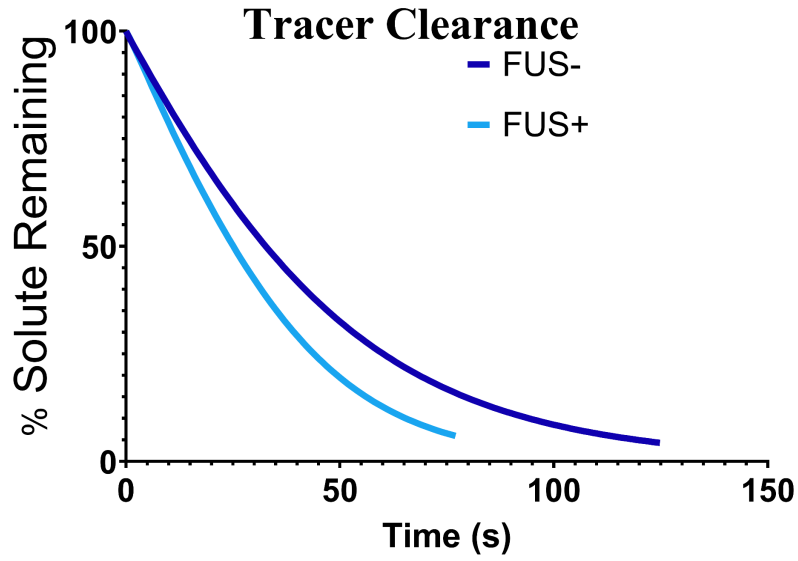


Figure 56. Rate of tracer clearance with and without FUS

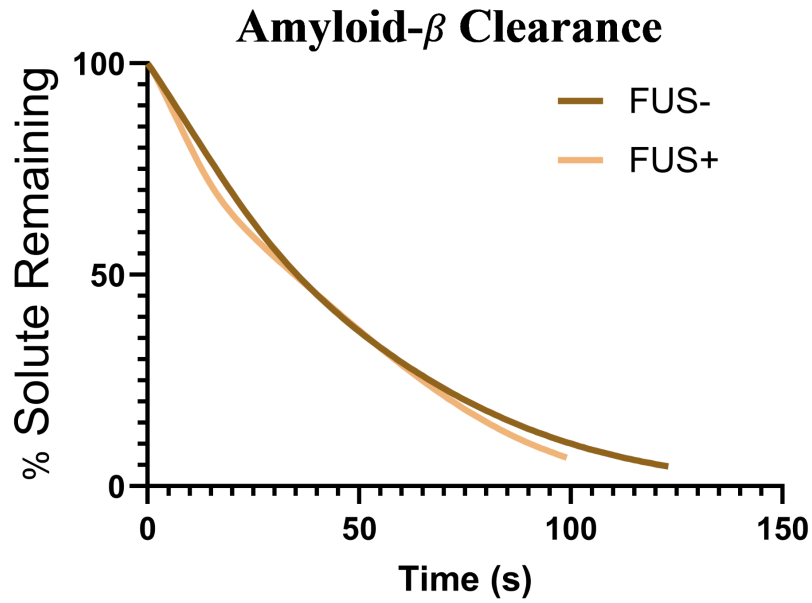


Figure 57. Rate of amyloid- β clearance with and without FUS

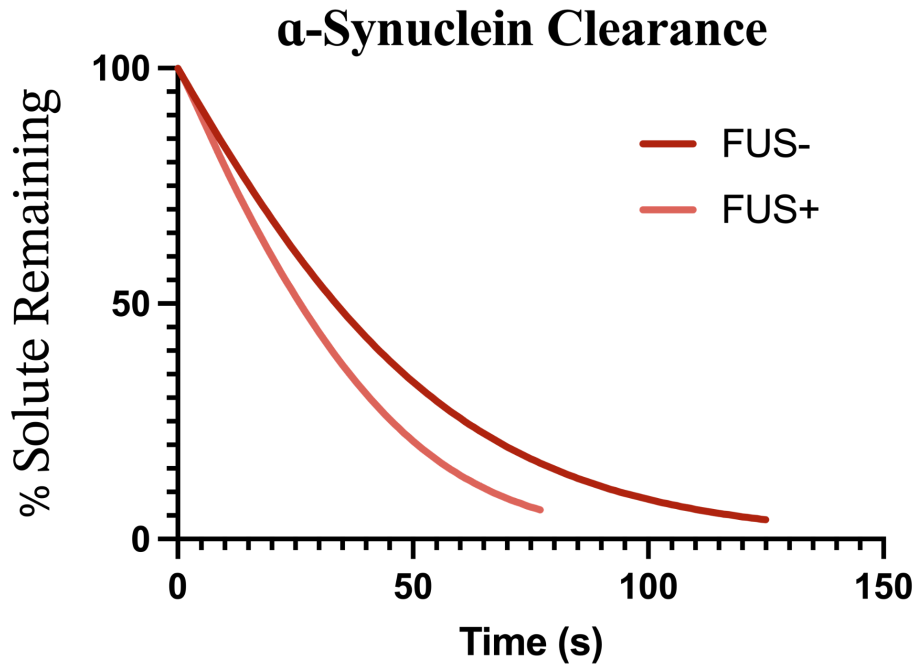


Figure 58. Rate of α -synuclein clearance with and without FUS

% Decrease in Clearance Duration for each Species

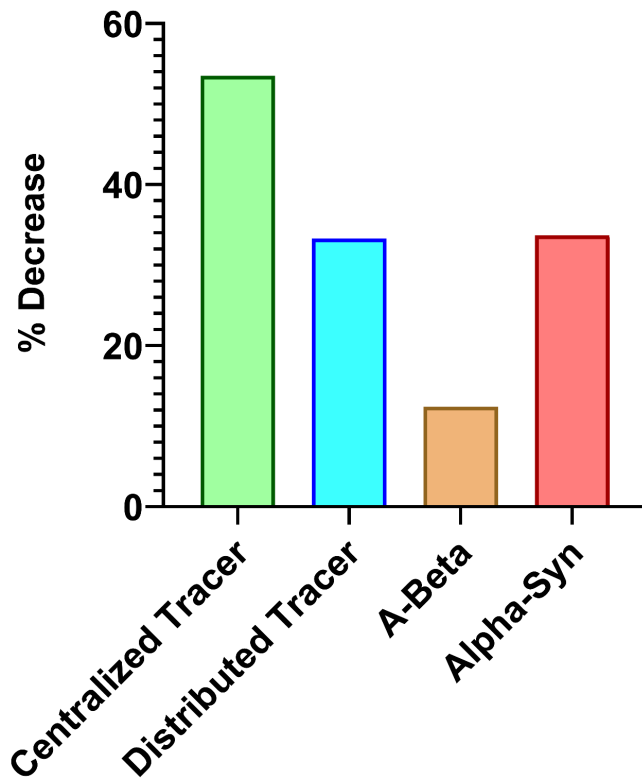


Figure 59. Percent decrease in FUS-enhanced solute clearance time for different species

Distributed Solute Model Flux Comparisons

The flux dynamics are again shown in figures 60-62 to highlight the effects of FUS for each species. Figure 63 shows the change in magnitude of these fluxes as well.

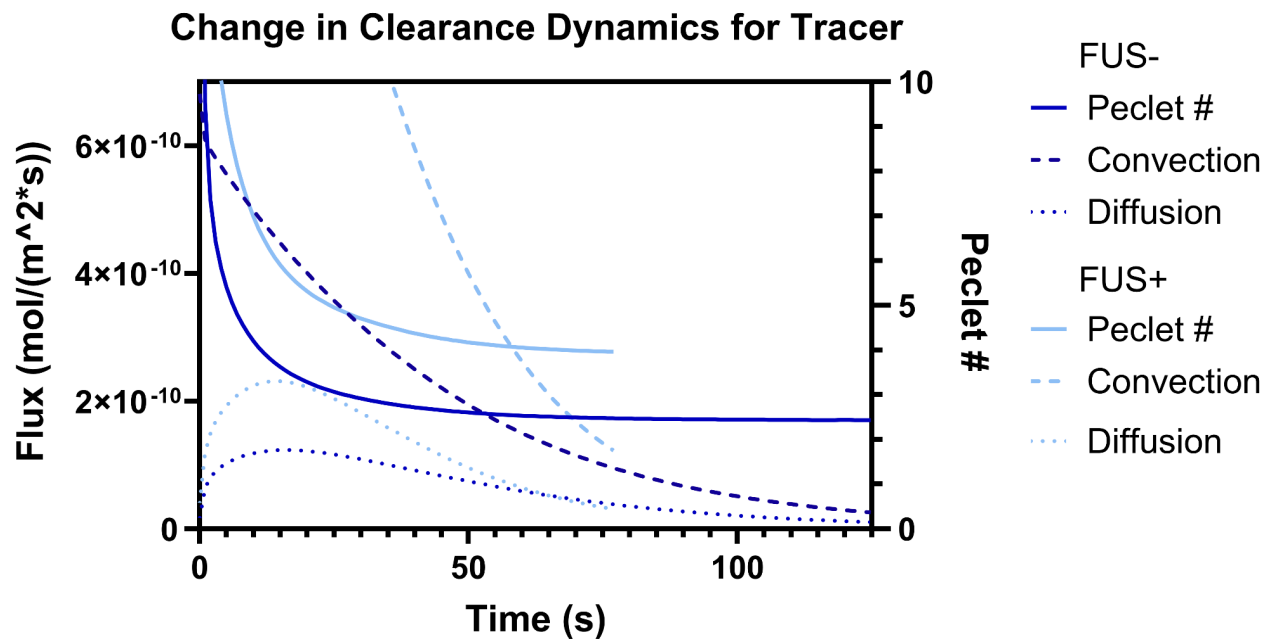


Figure 60. Contributions to tracer flux with and without FUS

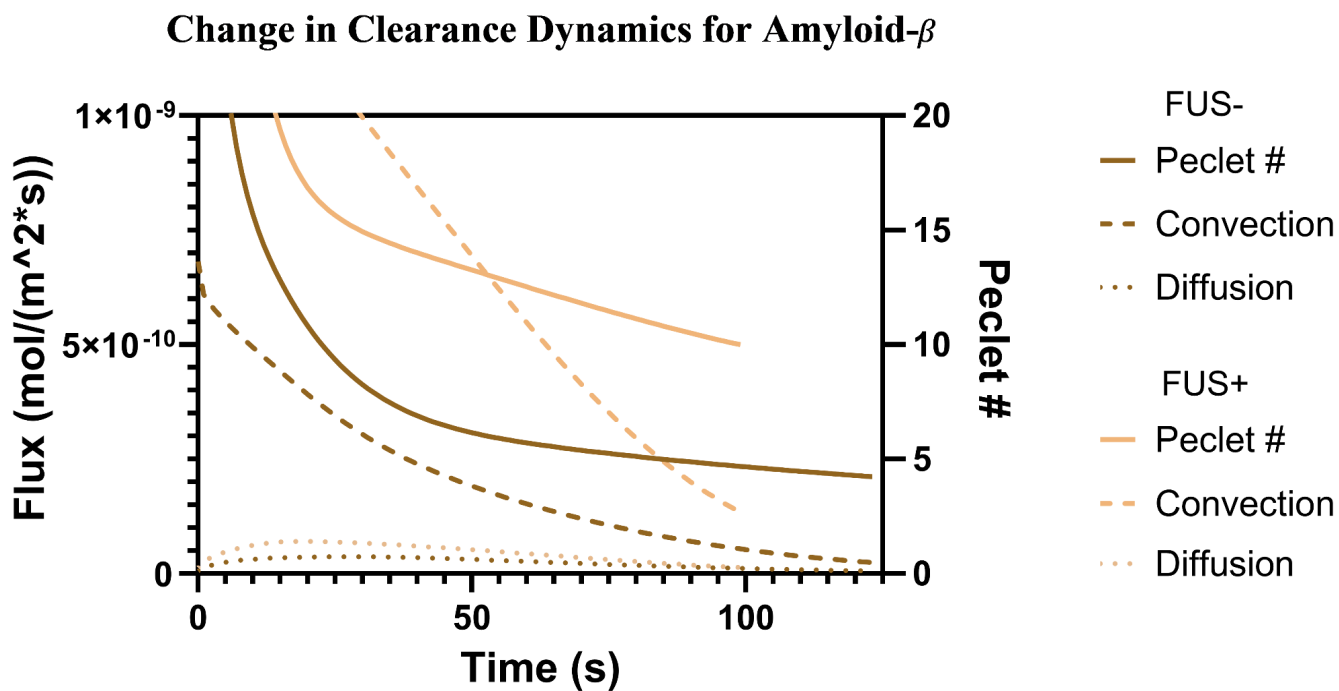


Figure 61. Contributions to amyloid- β flux with and without FUS

Change in Clearance Dynamics for α -Synuclein

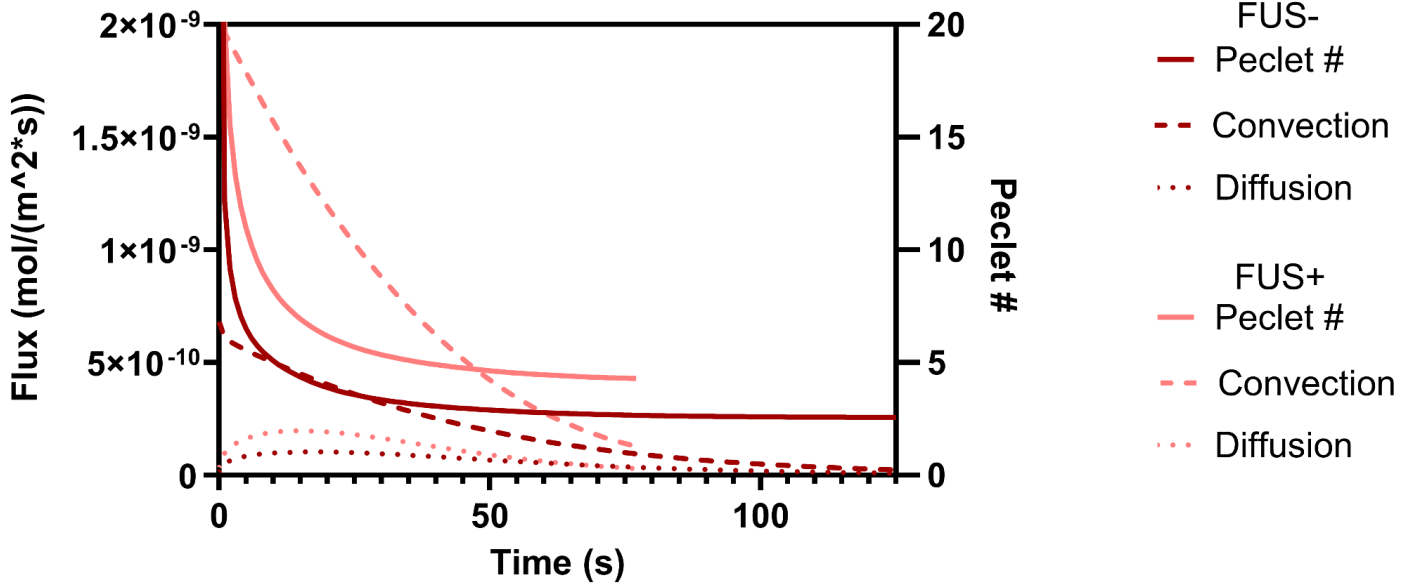


Figure 62. Contributions to α -synuclein flux with and without FUS.

FUS-mediated Changes in Species Flux

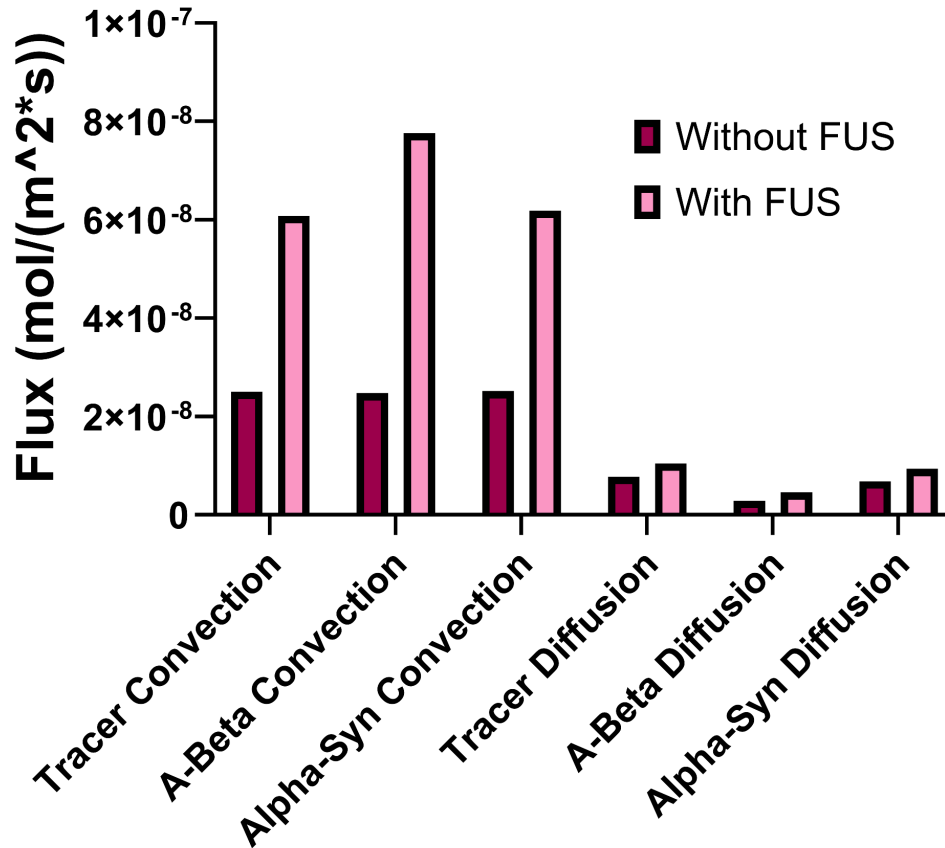


Figure 63. Fold changes in convective and diffusive flux for each species.

Discussion

The Effects of FUS

Across the board, FUS BBBO shortened the time needed for 95% of the initial mass to clear and increased the Péclet number. For the centralized tracer models, the size of the FUS focal region corresponded to the size of the effect, with the “Whole FUS” model clearing the fastest and the “No FUS” model clearing the slowest. Interestingly, the “PAS FUS” model cleared faster and experienced a higher Péclet number than the “PVS FUS” model, despite the exact same FUS focal volume for both models. This unexpected outcome could be related to the unique Péclet number seen in the “PAS FUS” model, which doesn’t stabilize at a certain value like the other models but instead continues increasing rapidly up until the simulation terminates. A possible explanation could be that the FUS-induced increase in perivascular space volume (~175%) had a larger effect on the periarterial side because this side is the source of the CSF, despite the PVS having an overall larger volume increase due to a larger initial volume. A larger PAS could mean more influx of CSF and more convection, whereas an increased PVS might simply increase the rate at which CSF flows through the parenchyma. In other words, perhaps the expanded PVS is bottlenecked by the amount of CSF the PAS can allow into the parenchyma, whereas the expanded PAS sets the rate of CSF flux that the PVS then accommodates. An additional explanation could be that FUS influences the pressure gradient that drives glymphatic CSF flow. On the PAS side, an increase fluid inlet and an increase in pressure could increase the rate of waste clearance. On the PVS side, it would follow that a fluid inlet and increased pressure would oppose, and thus less efficiently enhance, glymphatic flow. These insights were unexpected and could inform FUS targeting practices. Altogether, the data from this first set of models suggests that FUS enhances the rate of waste clearance by increasing the Péclet number, or the relative contribution of convection to mass transport. This is in direct agreement with the findings from Curley et al. (2020).

Different Solute Distributions

The “Whole FUS” centralized tracer model cleared in 46.5% of the amount of time with FUS BBBO as compared to without, while the distributed model cleared in 67% of the base time when FUS was present. This is promising insofar as it suggests that FUS BBBO might preferentially enhance the clearance of accumulated solute over dispersed solute. However, it is worth noting here that the initial masses are not equal. The initial *concentration* is held constant between models, not the mass. Hence, the equal distribution models have an overall larger initial mass. Regardless, this should not affect the magnitude of the FUS BBBO effects, especially because the rate of solute clearance decreases with less solute in a manner reminiscent of an exponential decay function. An explanation for why FUS might better enhance aggregated solutes is that, by greatly improving convection, more CSF flows directly down the pressure gradient, between the arteriole and venule, compared to peripheral paths. In the centralized models, this would lead to more rapid clearance, while in the distributed models, the solute on the periphery would take longer to clear. Overall, it is reassuring that the models suggest that FUS BBBO can shorten waste clearance to almost half the time in the worst case for various solutes. This finding is in agreement with the results of the Ye et al. (2023) and Lee et al. (2020) studies but adds to them by suggesting that aggregated, but still soluble, solutes located directly between vessels might be the most affected by FUS-enhanced glymphatic clearance.

Different Solutes

The solute characteristics were determined by each species’ measured diffusion coefficient (DC) in the mammalian brain parenchyma. The tracer had the highest DC, followed by α -synuclein, and finally by amyloid- β . This corresponds to a 160%, 200%, and 250% increase in the Péclet number respectively (Figs. 60-62). It also trends with a 33.3%, 33.7%, and 12.4% decrease in the time to clear solute (Fig 59). This data challenges the earlier notion that convection is the sole driver in FUS-enhanced solute clearance and instead suggests that the DC and diffusive flux play major roles in glymphatic waste clearance. Why would amyloid- β ,

with the largest proportional increase in convection, exhibit the smallest decrease in clearance time? The answer lies in Figure 63 and the relationship between a solute's ability to diffuse and convect. Diffusion coefficients are determined experimentally by measuring the amount of flux of a solute in a certain medium with a certain concentration gradient. Simply put, diffusion coefficients indicate how well a solute can diffuse. One might initially think of convection and diffusion as opposing processes, and indeed in many systems they are. Convection can create concentration gradients that increase in the same direction as flux, whereas diffusive flux always occurs down a concentration gradient. However, in order for a solute to advect, a certain degree of mixing is required to happen between the flowing solvent and the solute. This mixing process is mediated by diffusion, meaning that species that diffuse more efficiently will also mix with a convecting fluid more efficiently. This explains why the tracer and α -synuclein experienced more enhanced clearance with FUS. With larger DCs, they are better at diffusive mixing with the CSF and thus advect quickly out of the model. As can be seen in figures 60-62, these species demonstrated a notably larger increase in peak diffusive flux compared with amyloid- β . So how does amyloid- β have a larger increase in Péclet number, and why does figure 63 indicate that amyloid- β experienced more enhanced convective ($\sim 4x$ increase compared to $\sim 3x$) AND diffusive (1.6x increase compared to $\sim 1.3x$) flux than the other species? With a lower DC, amyloid- β mixes poorly with the CSF and convects less efficiently. This increases the simulation duration, which provides amyloid- β with more time to diffuse. Because glymphatic flow concentrates solute around the venule, diffusion will occur away from the perivenular space, opposite convection. This will increase the overall amount of diffusive flux. The model will continue to run until the convecting CSF carries that solute towards the venule, which will increase the overall amount of convective mass flux as well. This back-and-forth process of opposing convection and diffusion, which is shown in Figure 64 and is promoted by poor mixing, increases the overall amount of flux that occurs in the simulation without improving the clearance efficiency. Figure 65 shows an example of how the convection and diffusion flux profiles of a solute oppose one another for the FUS BBBO tracer model. Note that near the venule, diffusive flux points into the PVS because the CSF flowing therein acts as a diffusive sink.

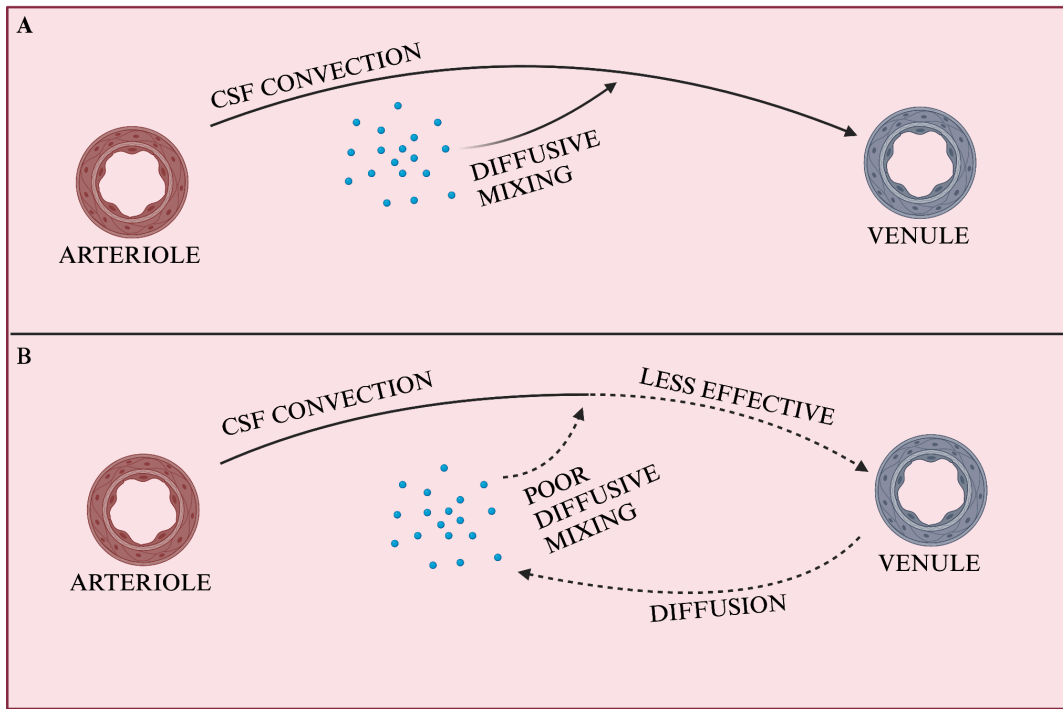


Figure 64. *A. Convection is enhanced by diffusion-mediated mixing of the solute with CSF. B. Species with low diffusivity mix poorly with CSF, which hinders convection and increases diffusive flux.*

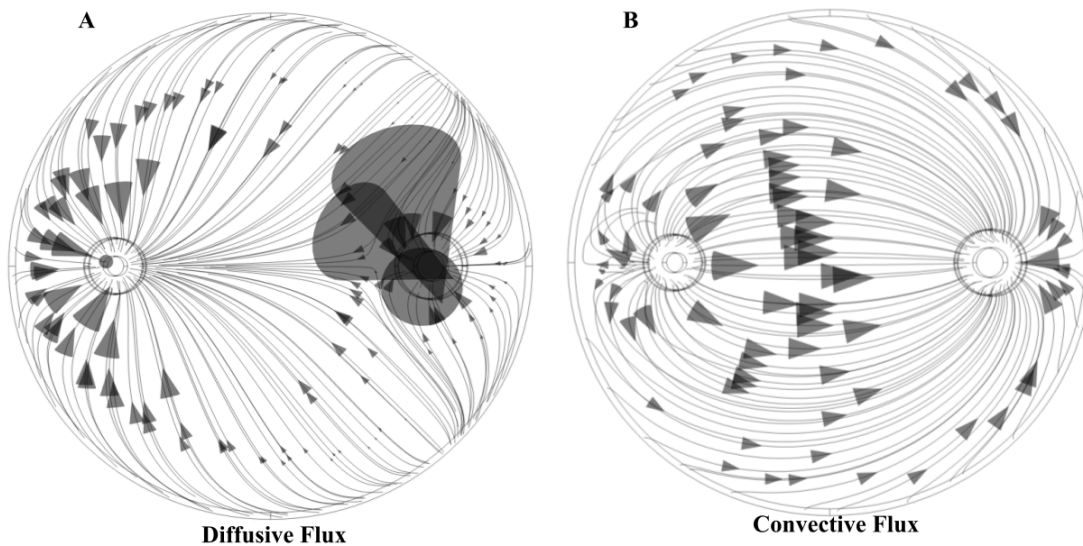


Figure 65. *A. Diffusive flux profile B. Convective flux profile.*

This unintuitive insight suggests that FUS will best enhance peak diffusion for solutes with a higher diffusion coefficient. This will improve mixing and minimize diffusive flux, thereby enhancing glymphatic clearance. A higher peak diffusion corresponds to better CSF mixing and not just diffusion towards a CSF “sink” in the perivenule space because studies have shown that an agent like Albumin ($DC= 1.6E-11 \text{ m}^2/\text{s}$) would take over 100 hours to diffuse through 1 cm of brain tissue, which is not efficient enough to maintain human brain

homeostasis.¹⁴ These conclusions provides support to existing models that challenge the notion that convection plays the main role in glymphatic transport (Jin et al. (2016), Asgari et al. (2016)), while also providing nuance to current models and studies that have demonstrated FUS-enhanced glymphatic waste clearance without determining a clear mechanism (Curley et al. (2020), Ye et al. (2023), Kedarasetti et al. (2022)).

This finding also suggests that less diffusive agents, like amyloid beta, might not depend on the glymphatic system as the primary mode of clearance. FUS only enhanced clearance of amyloid beta by ~10%, indicating that, even with a technology that augments this waste clearance system, solutes with low diffusivity likely depend on another mechanism to be cleared, such as enhanced microglial activation and phagocytosis.^{35,80} This notion is supported by the idea that a slower glymphatic clearance time increases the opportunities for microglia to surveil and phagocytose solutes, and by studies that have shown that amyloid beta and microglia colocalize in AD models.^{81,82} Interestingly, microglia have been shown to consistently aggregate with amyloid beta in perivascular spaces, which further suggests that microglia might compensate for solute-specific inefficiencies of the glymphatic system in disease contexts.⁸³ Likely, most pathological solutes depend on a combination of clearance mechanisms, including the glymphatics system, to varying degrees. This finding can shape the optimization of therapeutic strategies for various neurodegenerative diseases and adds to our understanding of brain homeostasis.

Model Novelty and Limitations

While there are many computational models of the glymphatics system, none provide comprehensive 3D pressure, velocity, and concentration flux profiles to the author's knowledge. Some individually explore pressure, concentration flux over time, 2D models of spatial convection, or flow velocities, but none integrate and visualize these data in a 3D format.^{50, 52,59, 70} Furthermore, there are currently no models that explore the effects of FUS BBBO on the glymphatics system. Therefore, this model provides insights that are entirely unique and could become foundational for future computational and *in vivo* studies.

This model has limitations. The most obvious is the model's simplistic geometry. No vessels are perfectly cylindrical or parallel, and if there are systemic effects of FUS on glymphatics, this model of a single arteriole-venule unit will fail to identify them. Another example of model limitations is that perivascular spaces are notably elliptical, not annular as modeled.^{6, 48, 71} Additionally, the assumption that BBBO fails to occur in the model vessels is a simplification because, with a large enough FUS amplitude, BBBO could theoretically occur in these vessels. However, this limitation is relatively minor because FUS BBBO has not been reported in vessels of this caliber. Simulating FUS BBBO in these vessels would also demand simulating blood flow and perhaps even the effects of vasoconstriction and vasodilation, both of which could doubtless have effects on glymphatic flow. Additionally, the heterogeneity of brain parenchyma is lumped into only a few parameters. Microglia, astrocytes, neurons, and other species in the neuropil would indeed affect mass transport. For instance, there is anisotropy along neuronal tracts, while my model assumes isotropy throughout the parenchyma.⁷² The diffusion coefficient of various solutes through brain microstructures, like the one micron-thick glia limitans, has not been measured *in vivo*. Therefore, only the DCs of the solutes in the parenchyma were used. Finally, this model is limited by a lack of consistency among *in vivo* studies. Parameters were collected from various mammals, and so might fail to capture true human glymphatics.

Although the model is indeed limited in many ways, the assumptions that are made are realistic and allow the investigation of the glymphatics system and the bioeffects of FUS. The insights produced by this study might otherwise have been very difficult or impossible to produce.

Future Directions

Excitement for the therapeutic potential of FUS for neurodegenerative disorders has been growing over the last decade.⁷³ Because the glymphatic system was first characterized *in vivo* in 2012, the combination of FUS and glymphatics is still in an incipient stage.⁶ Many publications on FUS for neurodegenerative disease focus on the

technology's ability to immunomodulate. Some studies, even ones as recent as 2022, claim that FUS's neurotherapeutic effects are primarily due to microglial activation without homage to the glymphatic system.^{31,35,74} However, many studies recognize the role that the glymphatic system plays in maintaining brain homeostasis, which is leading to the adoption of the glymphatic system as a central therapeutic target.^{9,75,76} The finding that the glymphatic system is primarily active during sleep has driven efforts to replicate the regulatory processes that occur during slow-wave sleep with different therapies.⁷⁷ This modeling project has indicated that FUS BBBO replicates those processes by increasing brain porosity and permeability. This could drive sleep-like glymphatic clearance even during wakeful states. FUS could be especially useful to address age-related risk factors for neurodegeneration related to impaired glymphatics such as chronic sleep deprivation and poor sleep quality. Ideally, this model could advance the field of biomedicine through the insights it has produced into the mechanisms behind glymphatic waste clearance and by increasing healthcare provider confidence in FUS as a therapeutic technology. The model also has exciting possibilities for future avenues of investigation.

First, the model could be further validated with *in vivo* experimentation. The model has already shown agreement with the current studies into FUS-enhanced glymphatics, as discussed earlier. Beyond this, the model's prediction should be directly compared to the actual rate of waste clearance in an animal model, as was done in the validation done by Ye et al. (2023). This would be accomplished by completing intracisterna magna tracer injections during MR imaging, and comparing the actual clearance time to the model's prediction.

Second, the model could be expanded to include a region of brain tissue that is larger than the FUS focal volume cross section. This would allow researchers to better understand the spatial effects of FUS, and would facilitate efforts to experimentally validate the model with MRI. Two-photon microscopy or other computational models of vascular orientation (such as Schreder et al. (2022)) could be used to create anatomical guides to scale up the model.

Finally, the model could be adapted to other neurovascular disorders, like Cerebral Cavernous Malformations (CCM) or glioblastoma. These efforts could accelerate the adoption of FUS for other clinical issues that FUS has already demonstrated benefits for in preclinical trials.^{15,78,79}

Conclusion

Altogether, this model suggests that FUS greatly improves waste clearance by increasing both diffusion and convection. These trends work together to increase solute mixing with the CSF in tandem with the rate of CSF flow from the arteriole to the venule. Solutes more centralized to the CSF flow profile and that have a higher DC tend to clear more rapidly due to increased convection and enhanced diffusive mixing. The magnitude of FUS effects corresponds to the size of the focal volume, with slightly greater effects for arterioles compared to venules. These could be instrumental insights for transforming FUS into a common therapeutic technology for neurodegenerative diseases.

References

1. Hong S, Van Kaer L. Immune privilege: keeping an eye on natural killer T cells. *J Exp Med*. 1999 Nov 1;190(9):1197-200. doi: 10.1084/jem.190.9.1197. PMID: 10544192; PMCID: PMC2195673.
2. Liao S, Padera TP (2013) Lymphatic function and immune regulation in health and disease. *Lymphat Res Biol* 11:136–143. doi:10.1089/lrb.2013.0012
3. Jessen, N.A., Munk, A.S.F., Lundgaard, I. et al. The Glymphatic System: A Beginner’s Guide. *Neurochem Res* 40, 2583–2599 (2015). <https://doi.org/10.1007/s11064-015-1581-6>
4. Tomas Bohr, Maiken Nedergaard, et al. The glymphatic system: Current understanding and modeling, *iScience*, Volume 25, Issue 9, 2022104987, ISSN 2589-0042, <https://doi.org/10.1016/j.isci.2022.104987>.
5. Wardlaw, J.M., Benveniste, H., Nedergaard, M. et al. Perivascular spaces in the brain: anatomy, physiology and pathology. *Nat Rev Neurol* 16, 137–153 (2020).
<https://doi.org/10.1038/s41582-020-0312-z>
6. Jeffrey J. Iliff et al. ,A Paravascular Pathway Facilitates CSF Flow Through the Brain Parenchyma and the Clearance of Interstitial Solutes, Including Amyloid β .*Sci. Transl. Med.*4,147ra111-147ra111(2012). DOI:10.1126/scitranslmed.3003748
7. Wolburg, H., Paulus, W. Choroid plexus: biology and pathology. *Acta Neuropathol* 119, 75–88 (2010).
<https://doi.org/10.1007/s00401-009-0627-8>
8. Johanson CE. *J Choroid Plexus–Cerebrospinal Fluid Circulatory Dynamics: Impact on Brain Growth, Metabolism, and Repair*. Totowa, NJ: Humana Press, 2008.
9. Plog BA, Nedergaard M. The Glymphatic System in Central Nervous System Health and Disease: Past, Present, and Future. *Annu Rev Pathol*. 2018 Jan 24;13:379-394.
<https://doi.org/10.1146/annurev-pathol-051217-111018>
10. Damkier, Helle H., Peter D. Brown, and Jeppe Praetorius. “Cerebrospinal Fluid Secretion by the Choroid Plexus.” *Physiological Reviews* 93, no. 4 (October 1, 2013): 1847–92.
<https://doi.org/10.1152/physrev.00004.2013>.

11. Martin Kaag Rasmussen, Humberto Mestre, and Maiken Nedergaard, Fluid transport in the brain, *Physiological Reviews* 2022 102:2, 1025-1151, <https://doi.org/10.1152/physrev.00031.2020>
12. Hablitz, Lauren M. et al., The glymphatics system, *Current Biology*, Volume 31, Issue 20, R1371 - R1375, <https://doi.org/10.1016/j.cub.2021.08.026>
13. Reddy OC, van der Werf YD. The Sleeping Brain: Harnessing the Power of the Glymphatic System through Lifestyle Choices. *Brain Sci.* 2020 Nov 17;10(11):868. doi: 10.3390/brainsci10110868. PMID: 33212927; PMCID: PMC7698404.
14. Maiken Nedergaard, Garbage Truck of the Brain, *Science* 340, 1529-1530 (2013), <https://doi.org/10.1126/science.1240514>
15. Catherine M. Gorick, Natasha D. Sheybani, Richard J. Price et al., Applications of focused ultrasound-mediated blood-brain barrier opening, *Advanced Drug Delivery Reviews*, Volume 191, 2022, 114583, ISSN 0169-409X, <https://doi.org/10.1016/j.addr.2022.114583>.
16. Mark R. Schwartz, Anna C. Debski, Richard J. Price, Ultrasound-targeted nucleic acid delivery for solid tumor therapy, *Journal of Controlled Release*, Volume 339, 2021, Pages 531-546, ISSN 0168-3659, <https://doi.org/10.1016/j.jconrel.2021.10.010>.
17. Fisher, Delaney G., Khadijeh A. Sharifi, Ishaan M. Shah, Catherine M. Gorick, Victoria R. Breza, Anna C. Debski, Matthew R. Hoch, et al. "Focused Ultrasound Blood-Brain Barrier Opening Arrests the Growth and Formation of Cerebral Cavernous Malformations." *bioRxiv*, January 1, 2024, 2024.01.31.577810. <https://doi.org/10.1101/2024.01.31.577810>.
18. Ma, Xishun, Tongxia Li, Lizhen Du, and Tongliang Han. "Research and Progress of Focused Ultrasound in the Treatment of Alzheimer's Disease." *Frontiers in Neurology* 14 (2023). <https://www.frontiersin.org/journals/neurology/articles/10.3389/fneur.2023.1323386>.
19. Kelsie F. Timbie, Brian P. Mead, Richard J. Price, Drug and gene delivery across the blood-brain barrier with focused ultrasound, *Journal of Controlled Release*, Volume 219, 2015, Pages 61-75, ISSN 0168-3659, <https://doi.org/10.1016/j.jconrel.2015.08.059>.

20. Song KH, Harvey BK, Borden MA. State-of-the-art of microbubble-assisted blood-brain barrier disruption. *Theranostics* 2018; 8(16):4393-4408. doi:10.7150/thno.26869.
<https://www.thno.org/v08p4393.htm>
21. Hynynen, Kullervo, Nathan McDannold, Natalia Vykhodtseva, and Ferenc A. Jolesz. “Noninvasive MR Imaging–Guided Focal Opening of the Blood-Brain Barrier in Rabbits.” *Radiology* 220, no. 3 (September 1, 2001): 640–46. <https://doi.org/10.1148/radiol.2202001804>.
22. Little RC. *Physiology of the heart and circulation*. 3rd ed. Chicago: Year Book Medical Publishers. 1985:359
23. S. Dubey, S. Heinen, S. Krantic, J. McLaurin, D.R. Branch, K. Hynynen, & I. Aubert, Clinically approved IVIg delivered to the hippocampus with focused ultrasound promotes neurogenesis in a model of Alzheimer’s disease, *Proc. Natl. Acad. Sci. U.S.A.* 117 (51) 32691-32700,
<https://doi.org/10.1073/pnas.1908658117>
24. Xhima, K., Nabbouh, F., Hynynen, K., Aubert, I. and Tandon, A. (2018), Noninvasive delivery of an α -synuclein gene silencing vector with magnetic resonance–guided focused ultrasound. *Mov Disord.*, 33: 1567-1579. <https://doi.org/10.1002/mds.101>
25. Kelsie F Timbie, Umara Afzal, Abhijit Date, Clark Zhang, Ji Song, G. Wilson Miller, Jung Soo Suk, Justin Hanes, Richard J Price, MR image-guided delivery of cisplatin-loaded brain-penetrating nanoparticles to invasive glioma with focused ultrasound, *Journal of Controlled Release*, Volume 263, 2017, Pages 120-131, ISSN 0168-3659, <https://doi.org/10.1016/j.jconrel.2017.03.017>
26. Chun-Yao Wu et al., A preliminary study of Parkinson’s gene therapy via sono-magnetic sensing gene vector for conquering extra/intracellular barriers in mice, *Brain Stimulation*, Volume 13, Issue 3, 2020, Pages 786-799, ISSN 1935-861X, <https://doi.org/10.1016/j.brs.2020.02.024>
27. Ye, Byoung Seok, Kyung Won Chang, Sungwoo Kang, Seun Jeon, and Jin Woo Chang. “Repetitive and Extensive Focused Ultrasound–Mediated Bilateral Frontal Blood-Brain Barrier Opening for Alzheimer’s Disease,” January 10, 2025. <https://doi.org/10.3171/2024.8.JNS24989>.

28. Gao, M. et al., "Targeted mRNA Nanoparticles Ameliorate Blood–Brain Barrier Disruption Postischemic Stroke by Modulating Microglia Polarization | ACS Nano." <https://pubs.acs.org/doi/10.1021/acsnano.3c09817>.
29. Lipsman, N., Meng, Y., Bethune, A.J. et al. Blood–brain barrier opening in Alzheimer’s disease using MR-guided focused ultrasound. *Nat Commun* 9, 2336 (2018). <https://doi.org/10.1038/s41467-018-04529-6>
30. Abrahao, A., Meng, Y., Llinas, M. et al. First-in-human trial of blood–brain barrier opening in amyotrophic lateral sclerosis using MR-guided focused ultrasound. *Nat Commun* 10, 4373 (2019). <https://doi.org/10.1038/s41467-019-12426-9>
31. A. R. Kline-Schoder, S. Chintamen, V. Menon, S. G. Kernie and E. E. Konofagou, "Focused-ultrasound blood-brain barrier opening promotes neuroprotective microglia," 2022 IEEE International Ultrasonics Symposium (IUS), Venice, Italy, 2022, pp. 1-3, doi: 10.1109/IUS54386.2022.9958101.
32. Colleen T. Curley et al., Augmentation of brain tumor interstitial flow via focused ultrasound promotes brain-penetrating nanoparticle dispersion and transfection. *Sci. Adv.*6, eaay1344(2020). DOI:10.1126/sciadv.aay1344
33. D. Ye, S. Chen, Y. Liu, C. Weixel, Z. Hu, J. Yuan, & H. Chen, Mechanically manipulating glymphatic transport by ultrasound combined with microbubbles, *Proc. Natl. Acad. Sci. U.S.A.* 120 (21) e2212933120, <https://doi.org/10.1073/pnas.2212933120> (2023).
34. Lee, Y., Choi, Y., Park, E.J. et al. Improvement of glymphatic–lymphatic drainage of beta-amyloid by focused ultrasound in Alzheimer’s disease model. *Sci Rep* 10, 16144 (2020). <https://doi.org/10.1038/s41598-020-73151-8>
35. Jessica F. Jordão, Isabelle Aubert et al., Amyloid- β plaque reduction, endogenous antibody delivery and glial activation by brain-targeted, transcranial focused ultrasound, *Experimental Neurology*, Volume 248, 2013, Pages 16-29, ISSN 0014-4886, <https://doi.org/10.1016/j.expneurol.2013.05.008>.
36. Meng, Y., Abrahao, A., Heyn, C.C., Bethune, A.J., Huang, Y., Pople, C.B., Aubert, I., Hamani, C., Zinman, L., Hynynen, K., Black, S.E. and Lipsman, N. (2019), Glymphatics Visualization after Focused

Ultrasound-Induced Blood–Brain Barrier Opening in Humans. *Ann Neurol*, 86: 975-980.

<https://doi.org/10.1002/ana.25604>

37. Schreder Helena E., Liu Jia, Kelley Douglas H., Thomas John H. and Boster Kimberly A. S. 2022A hydraulic resistance model for interstitial fluid flow in the brain *J. R. Soc. Interface*.1920210812, <http://doi.org/10.1098/rsif.2021.0812>
38. Kedarasetti, R.T., Drew, P.J. & Costanzo, F. Arterial vasodilation drives convective fluid flow in the brain: a poroelastic model. *Fluids Barriers CNS* 19, 34 (2022). <https://doi.org/10.1186/s12987-022-00326-y>
39. Teixeira, Ana Margarida, and Pedro Martins. “A Review of Bioengineering Techniques Applied to Breast Tissue: Mechanical Properties, Tissue Engineering and Finite Element Analysis.” *Frontiers in Bioengineering and Biotechnology* 11 (2023). <https://www.frontiersin.org/journals/bioengineering-and-biotechnology/articles/10.3389/fbioe.2023.1161815>.
40. Boccaccio A, Ballini A, Pappalettere C, Tullo D, Cantore S, Desiate A. Finite element method (FEM), mechanobiology and biomimetic scaffolds in bone tissue engineering. *Int J Biol Sci*. 2011 Jan 26;7(1):112-32. doi: 10.7150/ijbs.7.112. PMID: 21278921; PMCID: PMC3030147.
41. Larrabee, W.F., Jr. (1986), A finite element model of skin deformation. I. Biomechanics of skin and soft tissue: A review. *The Laryngoscope*, 96: 399-405. <https://doi.org/10.1288/00005537-198604000-00012>
42. El-Bouri, W. K. and Payne, S. J. (2016), A statistical model of the penetrating arterioles and venules in the human cerebral cortex. *Microcirculation*, 23: 580–590. doi: 10.1111/micc.12318
43. Kyrtos CR, Baras JS (2015) Modeling the Role of the Glymphatic Pathway and Cerebral Blood Vessel Properties in Alzheimer’s Disease Pathogenesis. *PLOS ONE* 10(10): e0139574. <https://doi.org/10.1371/journal.pone.0139574>
44. Kedarasetti, R.T., Drew, P.J. & Costanzo, F. Arterial vasodilation drives convective fluid flow in the brain: a poroelastic model. *Fluids Barriers CNS* 19, 34 (2022). <https://doi.org/10.1186/s12987-022-00326-y>

45. Wilson DF, Matschinsky FM. Cerebrovascular Blood Flow Design and Regulation; Vulnerability in Aging Brain. *Front Physiol.* 2020 Oct 16;11:584891. doi: 10.3389/fphys.2020.584891. PMID: 33178048; PMCID: PMC7596697.
46. Schain, Aaron J., Agustin Melo-Carrillo, Andrew M. Strassman, and Rami Burstein. "Cortical Spreading Depression Closes Paravascular Space and Impairs Glymphatic Flow: Implications for Migraine Headache." *The Journal of Neuroscience* 37, no. 11 (March 15, 2017): 2904. <https://doi.org/10.1523/JNEUROSCI.3390-16.2017>.
47. Shih AY, Driscoll JD, Drew PJ, Nishimura N, Schaffer CB, Kleinfeld D. Two-Photon Microscopy as a Tool to Study Blood Flow and Neurovascular Coupling in the Rodent Brain. *Journal of Cerebral Blood Flow & Metabolism.* 2012;32(7):1277-1309. doi:10.1038/jcbfm.2011.196
48. Mestre, H., Tithof, J., Du, T. et al. Flow of cerebrospinal fluid is driven by arterial pulsations and is reduced in hypertension. *Nat Commun* 9, 4878 (2018). <https://doi.org/10.1038/s41467-018-07318-3>
49. Asgari, M., de Zélicourt, D. & Kurtcuoglu, V. Glymphatic solute transport does not require bulk flow. *Sci Rep* 6, 38635 (2016). <https://doi.org/10.1038/srep38635>
50. Vinje V, Eklund A, Mardal KA, Rognes ME, Støverud KH. Intracranial pressure elevation alters CSF clearance pathways. *Fluids Barriers CNS.* 2020 Apr 16;17(1):29. doi: 10.1186/s12987-020-00189-1. PMID: 32299464; PMCID: PMC7161287.
51. Daniel L. Adams, Valentina Piserchia, John R. Economides, Jonathan C. Horton, Vascular Supply of the Cerebral Cortex is Specialized for Cell Layers but Not Columns, *Cerebral Cortex*, Volume 25, Issue 10, October 2015, Pages 3673–3681, <https://doi.org/10.1093/cercor/bhu221>
52. Jin BJ, Smith AJ, Verkman AS. Spatial model of convective solute transport in brain extracellular space does not support a "glymphatic" mechanism. *J Gen Physiol.* 2016 Dec;148(6):489-501. doi: 10.1085/jgp.201611684. Epub 2016 Nov 11. PMID: 27836940; PMCID: PMC5129742.
53. Syková, Eva, and Charles Nicholson. "Diffusion in Brain Extracellular Space." *Physiological Reviews* 88, no. 4 (October 1, 2008): 1277–1340. <https://doi.org/10.1152/physrev.00027.2007>.

54. Levin, VA, JD Fenstermacher, and CS Patlak. "Sucrose and Inulin Space Measurements of Cerebral Cortex in Four Mammalian Species." *American Journal of Physiology-Legacy Content* 219, no. 5 (November 1, 1970): 1528–33. <https://doi.org/10.1152/ajplegacy.1970.219.5.1528>.
55. Nicholson, C, Phillips, J M, (1981), Ion diffusion modified by tortuosity and volume fraction in the extracellular microenvironment of the rat cerebellum.. *The Journal of Physiology*, 321 doi: 10.1113/jphysiol.1981.sp013981.
56. Koch, T., Vinje, V. & Mardal, KA. Estimates of the permeability of extra-cellular pathways through the astrocyte endfoot sheath. *Fluids Barriers CNS* 20, 20 (2023).
<https://doi.org/10.1186/s12987-023-00421-8>
57. Waters J. The concentration of soluble extracellular amyloid- β protein in acute brain slices from CRND8 mice. *PLoS One*. 2010 Dec 29;5(12):e15709. doi: 10.1371/journal.pone.0015709. PMID: 21209950; PMCID: PMC3012091.
58. Mathiisen, T.M., Lehre, K.P., Danbolt, N.C. and Ottersen, O.P. (2010), The perivascular astroglial sheath provides a complete covering of the brain microvessels: An electron microscopic 3D reconstruction. *Glia*, 58: 1094-1103. <https://doi.org/10.1002/glia.20990>
59. Daversin-Catty C, Vinje V, Mardal KA, Rognes ME. The mechanisms behind perivascular fluid flow. *PLoS One*. 2020 Dec 29;15(12):e0244442. doi: 10.1371/journal.pone.0244442. PMID: 33373419; PMCID: PMC7771676.
60. Tithof, J., Kelley, D.H., Mestre, H. et al. Hydraulic resistance of periarterial spaces in the brain. *Fluids Barriers CNS* 16, 19 (2019). <https://doi.org/10.1186/s12987-019-0140-y>
61. Vinje V, Bakker ENTP, Rognes ME. Brain solute transport is more rapid in periarterial than perivenous spaces. *Sci Rep*. 2021 Aug 9;11(1):16085. doi: 10.1038/s41598-021-95306-x. PMID: 34373476; PMCID: PMC8352970.
62. I.G. Bloomfield, I.H. Johnston, L.E. Bilston; Effects of Proteins, Blood Cells and Glucose on the Viscosity of Cerebrospinal Fluid. *Pediatr Neurosurg* 1 May 1998; 28 (5): 246–251.
<https://doi.org/10.1159/000028659>

63. Levin E, Muravchick S, Gold MI. Density of normal human cerebrospinal fluid and tetracaine solutions. *Anesth Analg*. 1981 Nov;60(11):814-7. PMID: 7197494.
64. Lea-Banks H, Meng Y, Wu SK, Belhadjhamida R, Hamani C, Hynynen K. Ultrasound-sensitive nanodroplets achieve targeted neuromodulation. *J Control Release*. 2021 Apr 10;332:30-39. doi: 10.1016/j.jconrel.2021.02.010. Epub 2021 Feb 16. PMID: 33600879; PMCID: PMC8089063.
65. David S. Hersh, Ben A. Nguyen, Jimena G. Dancy, Arjun R. Adapa, Jeffrey A. Winkles, Graeme F. Woodworth, Anthony J. Kim, Victor Frenkel, Pulsed ultrasound expands the extracellular and perivascular spaces of the brain, *Brain Research*, Volume 1646, 2016, Pages 543-550, ISSN 0006-8993, <https://doi.org/10.1016/j.brainres.2016.06.040>
66. Yong, Y., Cai, Y., Lin, J. et al. Advancement in modulation of brain extracellular space and unlocking its potential for intervention of neurological diseases. *Med-X* 2, 6 (2024). <https://doi.org/10.1007/s44258-024-00021-7>
67. Tian Yuan, Li Shen, Daniele Dini, Porosity-permeability tensor relationship of closely and randomly packed fibrous biomaterials and biological tissues: Application to the brain white matter, *Acta Biomaterialia*, Volume 173, 2024, Pages 123-134, ISSN 1742-7061, <https://doi.org/10.1016/j.actbio.2023.11.007>
68. Valdez MA, Fernandez E, Matsunaga T, Erickson RP, Trouard TP. Distribution and Diffusion of Macromolecule Delivery to the Brain via Focused Ultrasound using Magnetic Resonance and Multispectral Fluorescence Imaging. *Ultrasound Med Biol*. 2020 Jan;46(1):122-136. doi: 10.1016/j.ultrasmedbio.2019.08.024. Epub 2019 Oct 2. PMID: 31585767; PMCID: PMC6937597.
69. Nath S, Meuvis J, Hendrix J, Carl SA, Engelborghs Y. Early aggregation steps in alpha-synuclein as measured by FCS and FRET: evidence for a contagious conformational change. *Biophys J*. 2010 Apr 7;98(7):1302-11. doi: 10.1016/j.bpj.2009.12.4290. PMID: 20371330; PMCID: PMC2849099.
70. Esmaeil Davoodi-Bojd, Guangliang Ding, Li Zhang, Qingjiang Li, Lian Li, Michael Chopp, ZhengGang Zhang, Quan Jiang, Modeling glymphatic system of the brain using MRI, *NeuroImage*, Volume 188, 2019, Pages 616-627, ISSN 1053-8119, <https://doi.org/10.1016/j.neuroimage.2018.12.039>.